ORNL/Sub--79-07862/02

DE91 014979

MIT Research Report

MATERIAL PROPERTY DEVELOPMENT FOR REFRACTORIES

May 1990

Research sponsored by the U.S. Department of Energy,
Office of Fossil Energy
Advanced Research and Technology Development, Materials Program

Report Prepared by

SOOBONG SHIN and ORAL BUYUKOZTURK

Massachusetts Institute of Technology
Department of Civil Engineering
Cambridge, Massachusetts 02139

under

Subcontract 19K-078620

for

OAK RIDGE NATIONAL LABORATORY
Oak Ridge, Tennessee 37831

managed by

MARTIN MARIETTA ENERGY SYSTEMS, INC.

for the

U.S. DEPARTMENT OF ENERGY
under Contract No. DE-AC05-84OR21400

Abstract

The analysis and design of refractory linings are difficult due to the complexity of their material behaviors. Previous work at the Massachusetts Institute of Technology provided (1) material and system modeling of the behavior of refractory lining, which can be implemented into a finite element computer program, and (2) material data-base from experiments, which would be useful for users, designers, and manufacturers. The objectives of the current research is to expand and refine the material data-base by characterizing the short-term thermomechanical behaviors of refractories, with a focus on candidate materials for slagging coal gasifier linings.

The selected material for the testing were dense brick, dense castable, insulating castable, and insulting firebrick refractories. The high temperature testing system and related problems to the tests are reviewed. A test program was established to characterize the thermomechanical behaviors. Those include monotonic compressive loading tests at constant elevated temperature, and short-term constant compressive load tests at predetermined constant temperature levels. For the dense brick, castable refractories, a transition temperature is observed at roughly equal to $T_M/2$ (where T_M is the melting temperature). In monotonic tests at temperatures below the transition one, linear elastic deformations are observed with brittle fracture. For castable refractories, between 0.3-0.5 T_M a small amount of stress-softening is observed. For temperatures above transition a significant non-linearity is observed in the post-peak region. For the insulating firebrick, a perfect elastic-plastic behavior without transition temperature is observed under monotonic loading at elevated temperatures. Constant load tests at predetermined constant temperature levels indicate that creep is a major factor in non-linear deformations above the transition temperature. All the obtained thermomechanical properties are summarized in Appendix A.

A new model for predicting creep behavior at elevated temperatures is proposed. The proposed model shows good agreement with test data over the temperature and load ranges tested.

Acknowledgements

The work described in this thesis was partially sponsored by the U.S. Department of Energy, Fossil Energy AR & TD Materials Program, DOE/FE AA 15 10 10 0, subcontract 19X-078620, Work Breakdown Structure Element, MIT-3.

The authors express their sincere appreciation to R. R. Judkins, R.A. Bradley and P. T. Carlson of Oak Ridge National Laboratory for their interest in this work and for their support.

This report originally formed the thesis of Mr. S. Shin, submitted to the Department of Civil Engineering in partial fulfillment of the requirements of the degree of Master of Science at the Massachusetts Institute of Technology, supervised by Professor O. Buyukozturk.

Contents

Titlepage 2

Abstract 3

Acknowledgements 4

Contents 5

List of Figures 9

List of Tables 13

1 INTRODUCTION 14

1.1 BACKGROUND 14

1.2 REVIEW OF PREVIOUS WORK AT MIT 15

1.3 CURRENT RESEARCH OBJECTIVES AND APPROACHES 17

1.4 DOCUMENT ORGANIZATION 18

2 LINING SYSTEMS AND MATERIALS FOR COAL GASIFIERS 20

2.1 LINING SYSTEMS OF HIGH TEMPERATURE VESSELS 20

2.1.1 System Configurations 20

2.1.2 Operating Conditions 21

2.1.3 Failure Mechanisms 24

2.1.4 Candidate Materials 25
2.2 BEHAVIOR OF LINING MATERIALS AT HIGH TEMPERATURE . . 27
2.2.1 Environmental Effects on the Behavior of Refractories 27
2.2.2 Thermomechanical Behavior of Refractories 29
2.2.3 Thermophysical Properties of Refractories 31

3 TESTING 36
3.1 EQUIPMENT FOR HIGH TEMPERATURE TESTING 36
3.1.1 Furnace and Temperature Controller 37
3.1.2 Retort System 40
3.1.3 Data Acquisition and Control System 43
3.2 TEST PROGRAM 43
3.2.1 Selection of Materials 43
3.2.2 Preparation of Specimens 45
3.2.3 Thermomechanical Testing Programs 46
3.3 PROBLEMS RELATED TO THE TESTING 50
3.3.1 Introduction 50
3.3.2 Problems in the Preparation of Specimens 52
3.3.3 Problems in Test Machine 56
3.3.4 Problem in Data Interpretation 58

4 HIGH-ALUMINA AND HIGH-CHROMIA DENSE BRICK MATERIALS 62
4.1 SYNOPSIS 62
4.2 THERMOMECHANICAL BEHAVIOR UNDER MONOTONIC UNIAXIAL COMPRESSIVE LOADS AT CONSTANT TEMPERATURES . . . 63
4.3 BEHAVIOR UNDER CONSTANT COMPRESSIVE LOADS AT CONSTANT TEMPERATURES 77
4.3.1 Effects of temperature on the Thermomechanical Behavior Under Constant Compressive Loads 77
4.3.2 Deformation Mechanism 83

5 HIGH-ALUMINA DENSE CASTABLE MATERIAL 87

5.1 SYNOPSIS 87
5.2 THERMOMECHANICAL BEHAVIOR UNDER MONOTONIC UNIAXIAL COMPRESSIVE LOADS AT CONSTANT TEMPERATURES . . . 87
5.3 BEHAVIOR UNDER CONSTANT COMPRESSIVE LOADS AT CONSTANT TEMPERATURES 95

6 INSULATING CASTABLE MATERIAL 101
6.1 SYNOPSIS 101
6.2 BEHAVIOR UNDER MONOTONIC COMPRESSIVE LOADS AT CONSTANT TEMPERATURES 101
6.3 BEHAVIOR UNDER CONSTANT COMPRESSIVE LOADS AT CONSTANT TEMPERTURES 109

7 INSULATING FIRE-BRICK MATERIAL 115
7.1 SYNOPSIS 115
7.2 BEHAVIOR UNDER MONOTONIC COMPRESSIVE LOADS AT CONSTANT TEMPERATURES 115

8 MODELING OF CREEP BEHAVIOR 122
8.1 CREEP BEHAVIOR OF REFRACTORIES AT HIGH TEMPERATURE 122
8.2 REVIEW OF AVAILABLE CREEP MODELS FOR HIGH TEMPERATURE SYSTEMS 133
8.2.1 General Formulations 133
8.2.2 Discussion on Incompressibility of Creep 138
8.3 A GENERALIZED CREEP MODEL FOR HIGH TEMPERATURE SYSTEMS 139
8.3.1 Desirable Requirements For A Creep Model of Refractory Materials 139
8.3.2 Development of A Generalized Creep Model 140
8.3.3 Discussion 145

9 SUMMARY, CONCLUSIONS, AND RECOMMENDATIONS 158
9.1 SYNOPSIS 158

9.2 SUMMARY OF THE PRESENT RESEARCH 158
9.3 CONCLUSIONS 160
9.3.1 Properties of Dense Brick Refractories (CPS-90A-10C and CPS-82C-18M) 161
9.3.2 Properties of Castable Refractories (DC-95A-5Ca and IC-55A-36S) 162
9.3.3 Properties of Insulating Firebrick (IB-39A-44S) 163
9.3.4 Modeling of Creep Behavior 163
9.4 RECOMMENDATIONS FOR FUTURE RESEARCH 163

REFRENECES **165**

APPENDIX **170**

A MATERIAL DATA-BASE OF REFRACTORIES 170
A.1 MATERIAL DATA-BASE OF DENSE BRICKS (CPS-90A-10C & CPS-82C-18M) 171
A.2 MATERIAL DATA-BASE OF DENSE CASTABLE DC-95A-5Ca 179
A.3 MATERIAL DATA-BASE OF INSULATING CASTABLE IC-55A-36S . 183
A.4 MATERIAL DATA-BASE OF INSULATING FIREBRICK IB-39A-44S . 187

List of Figures

2-1 High Temperature Monolithic Linings (Tseng, 1982) 22
2-2 High Temperature Brick Linings (Chen, 1984) 23
2-3 Typical Uniaxial Strength vs. Temperature Curves of Refractories. 30
2-4 Thermal Conductivity vs. Temperature Curves of a Dense and an Insulating Refractory Concretes (Babcock & Wilcox, 1981) 33
2-5 Thermal Expansion vs. Temperature Curves of Castables during Initial Heat-up (Babcock & Wilcox, 1981) 34

3-1 Sketch of the Major Components of the Thermomechanical Testing System 38
3-2 Picture of the Major Components of the Thermomechanical Testing System 39
3-3 Retort Assembly for Application of Compressive Loads at High Temperatures 41
3-4 Picture of the Furnace and Retort System for High Temperatures 42
3-5 Behavior of a Cylinder under Uniaxial Compressive Loading (Kotsovos, 1983; Van Mier, 1984) 47
3-6 Coring Equipments and a Cylindrical Specimen Cored out of a Brick . . 48
3-7 Strength Values at Different Coring Speeds 54
3-8 Stress-strain Curves at Different Coring Speeds 55
3-9 Boundary Conditions in the Testing of Material Stress-strain Response (Van Mier, 1984) 57
3-10 Zero-correction for Stress-strain Curves (Van Mier, 1984) 60

4-1 Stress-strain curves for CPS-90A-10C at different temperature levels and a constant displacement rate of 7.218×10^{-5} in/sec 64
4-2 Stress-strain curves for CPS-82C-18M at differernt temperature levels and a constant displacement rate of 7.218×10^{-5} in/sec 65
4-3 Strength Variation with Temperature for CPS-82C-18M 67
4-4 Strength Variation with Temperature for CPS-90A-10C 68
4-5 Initial Stiffness Variation with Temperature for CPS-82C-18M 70
4-6 Initial Stiffness Variation with Temperature for CPS-90A-10C 71
4-7 Variation of the Associated Peak Strain with Temperature for CPS-90A-10C 73
4-8 Variation of the Associated Peak Strain with Temperature for CPS-82C-18M 74
4-9 Variation of Toughness Measure with Temperature for CPS-82C-18M . . 75
4-10 Variation of Toughness Measure with Temperature for CPS-90A-10C . . 76
4-11 Creep Strains for CPS-90A-10C at Different Temperature and Load Levels 78

4-12 Variation of the Log of the Creep Strain-rate at Different Temperature and Load Levels for CPS-90A-10C 79
4-13 Creep Strains for CPS-82C-18M at Different Temperature and Load Levels 80
4-14 Variation of the Log of the Creep Strain-rate at Different Temperature and Load Levels for CPS-82C-18M 81
4-15 Creep Strains for CPS-90A-10C at the Same Temperature and Final Load Level, but Different Load Histories 82
4-16 Deformation Mechanism Map for CPS-90A-10C (Tamer and Buyukozturk, 1988) 85
4-17 Deformation Mechanism Map for CPS-82C-18M (Tamer and Buyukozturk, 1988) 86

5-1 Stress-strain Curves for DC-95A-5Ca at Different Temperature Levels and a Constant Displacement Rate of 7.218×10^{-5} in/sec. 89
5-2 Strength Variation with Temperature for DC-95A-5Ca 91
5-3 Variation of the Associated Peak Strain with Temperature for DC-95A-5Ca 92
5-4 Variation of Initial Stiffness with Temperature for DC-95A-5Ca 93
5-5 Vaiation of Toughness with Temperature for DC-95A-5Ca 94
5-6 Creep Strains for DC-95A-5Ca at Different Temperatures under the Constant Stress Levels 96
5-7 Variation of the Log of the Creep Strain-rate at Different Temperatures under the Constant Stress Levels 97
5-8 Creep Strains for DC-95A-5Ca under Different Stresses at Constant Temperature Level 99
5-9 Variation of the Log of the Creep Strain-rate under Different Stresses at Constant Temperature Level 100

6-1 Stress-strain Curves for IC-55A-36S at Different Temperature Levels and a Constant Displacement Rate of 7.218×10^{-5} in/sec. 103
6-2 Strength Variation with Temperature for IC-55A-36S 105
6-3 Variation of the Associated Peak Strain with Temperature for IC-55A-36S 106
6-4 Variation of Initial Stiffness with Temperature for IC-55A-36S 107
6-5 Vaiation of Toughness with Temperature for IC-55A-36S 108
6-6 Creep Strains for IC-55A-36S at Different Temperatures under the Constant Stress Levels 111
6-7 Variation of the Log of the Creep Strain-rate at Different Temperatures under the Constant Stress Levels 112
6-8 Creep Strains for IC-55A-36S under Different Stresses at Constant Temperature Level 113
6-9 Variation of the Log of the Creep Strain-rate under Different Stresses at Constant Temperature Level 114

7-1 Stress-strain Curves for IB-39A-44S at Different Temperature Levels and a Constant Displacement Rate of 7.218×10^{-5} in/sec 118
7-2 Simplified Stress-strain Curves for IB-39A-44S of Fig. 7.1 119
7-3 Strength Variation with Temperature for IB-39A-44S 120
7-4 Variation of the Initial Stiffness with Temperature for IB-39A-44S 121

8-1 Hoop, Axial and Radial Stresses in the Center of the Dense Component with an 8 Hour Hold Period (Pike et al., 1980) 124
8-2 A Typical Creep Curve 125
8-3 Larson-Miller Plot for Creep Rupture Time (t_f) 127
8-4 Power-law Creep by Dislocation Climb (Frost and Ashby, 1982) 128
8-5 Graphical Illustration of the Climb-Glide Sequence (Ashby and Jones, 1980) 129
8-6 Power-law Breakdown (Frost and Ashby, 1982) 130
8-7 Dynamic Recrystallization of Power-law Creep (Frost and Ashby, 1982) . 130
8-8 Mechanisms of Diffusional Creep (Ashby and Jones, 1980) 131
8-9 Diffusional Flow by Diffusional Transport Through and Round the Grains (Frost and Ashby (1982) 131
8-10 A Deformation Mechanism Map at Different Stresses and Tempeartures . 132
8-11 Experimental Comparison of Time- and Strain-hardening Theories (Boyle and Spence, 1983) 136
8-12aTwo Series of Kelvin Model (Pike et al., 1980) 137
8-12bModified Visco-elastic Model (Tseng and Buyukozturk, 1982) 137
8-12cBurger-body Model 137
8-13aVariation of Creep Strain Rate with Temperature (Ashby and Jones, 1980) 141
8-13bVariation of Creep Strain Rate with Stress (Ashby and Jones, 1980) . . . 141
8-14 Calculation of Activation Energy 'Q' from Arrehnius Plot for the Dense Brick Refractory CPS-90A-10C 146
8-15 Calculation of Stress Exponent 'n' from Arrehnius Plot for the Dense Brick Refractory CPS-90A-10C 147
8-16 Comparison of the Proposed Model with a Creep Test Data of the Dense Brick Refractory CPS-90A-10C 148
8-17 Calculation of Activation Energy 'Q' from Arrehnius Plot for the Dense Castable Refractory DC-95A-5Ca 149
8-18 Calculation of Stress Exponent 'n' from Arrehnius Plot for the Dense Castable Refractory DC-95A-5Ca 150
8-19 Comparison of the Proposed Model with a Creep Test Data of the Dense Castable Refractory DC-95A-5Ca under Constant Stress (4.5 ksi) 151
8-20 Comparison of the Proposed Model with a Creep Test Data of the Dense Castable Refractory DC-95A-5Ca under Constant Temperature (1500°F) 152
8-21 Calculation of Activation Energy 'Q' from Arrehnius Plot for the Insulating Castable Refractory IC-55A-36S 153

8-22 Calculation of Stress Exponent 'n' from Arrehnius Plot for the Insulating Castable Refractory IC-55A-36S 154
8-23 Comparison of the Proposed Model with a Creep Test Data of the Insulating Castable Refractory IC-55A-36S under Constant Stress (4.5 ksi) . 155
8-24 Comparison of the Proposed Model with a Creep Test Data of the Insulating Castable Refractory IC-55A-36S under Constant Temperature (1500°F) 156

List of Tables

3.1 Properties of Selected Materials for Thermomechanical Testing 44

8.1 Parameters of the Proposed Creep Model Obtained for Each Material . . 157

APPENDIX **170**

A.1 Constant Temperature, Monotonic-Displacement Uniaxial Compression Tests for Material CPS-90A-10C 172
A.2 Variation of Short-term Creep Strain Rate of Material CPS-90A-10C . . 173
A.3 Constant Load Tests at Varying Temperatures of Material CPS-90A-10C 173
A.4 Thermophysical Properties of Material CPS-90A-10C 174
A.5 Constant Temperature, Monotonic-Displacement Uniaxial Compression Tests for Material CPS-82C-18M 176
A.6 Variation of Short-term Creep Strain Rate of Material CPS-82C-18M . . 177
A.7 Thermal Cycling at Zero Load, followed by Monotonic-Displacement Uniaxial Compressive Load Tests 177
A.8 Thermophysical Properties of Material CPS-82C-18M 178
A.9 Constant Temperature, Monotonic Displacement Uniaxial Compression Tests for Material DC-95A-5Ca 180
A.10 Variation of Short-term Creep Strain Rate of Material DC-95A-5Ca . . . 181
A.11 Cold Modulus of Rupture and Cold Crushing Strength 181
A.12 Thermophysical Properties of Material DC-95A-5Ca 182
A.13 Constant Temperature, Monotonic Displacement Uniaxial Compression Tests for Material IC-55A-36S 184
A.14 Variation of Short-term Creep Strain Rate of Material IC-55A-36S 185
A.15 Hot Modulus of Rupture of IC-55A-36S 185
A.16 Linear Shrinkage of IC-55A-36S 185
A.17 Themophysical properties of Material IC-55A-36S 186
A.18 Constant Temperature, Monotonic-Displacement Uniaxial Compression Tests for Material IB-39A-44S 188
A.19 Thermophysical Properties of Material IB-39A-44S 189

Chapter 1

INTRODUCTION

1.1 BACKGROUND

Refractory concrete linings at high temprature are used in many industrial factories such as fossil power plants, coal gasification plants (Bakker and Stringer, 1981; Bakker et al., 1984; Chen and Buyukozturk, 1984; Kennedy, 1979), petroleum refinery units (Crowley and Johnson, 1972; Crowley, 1984; Gilchrist, 1977; Wygant and Bulkley, 1954), blast furnace (ISI, 1968), steel convertors, metal smelting and refinery industry (Huggett, 1966; McGannon, 1964), boilers, petrochemical plants, steam-raising plants, ammonia plants, incinerators, and cement kilns. Typical refractory concrete linings for these vessels consist of an outside steel shell and layers of refractories. The linings are usually composed of a dense layer next to the hot face and a layer of insulating material next to the steel shell. The linings can be either monolithic or composed of bricks that are jointed together using a mortar material. Cooling systems can be used to keep the shell temperature at certain predetermined levels.

Refractory linings are used to protect the steel shell from the extremely severe process environments. The operating conditions include a combination of high temperature, high pressure, mechanical and thermal cyclic loads, corrosive gases, and molten by-products that run down the walls of the gasifiers. These environments lead to the complex

situations of stresses and strains in linings and finally to the failure of the refractory lining systems. The failure modes can be generally categorized as: (1) cracking, spalling, and joint failure due to thermal gradients, shrinkage, and creep, and (2) material degradation and mass loss due to corrosion attack by the slags and gases.

The analysis and design of refractory linings are difficult due to the complexity of their material behaviors. The thermal and mechanical properties of refractory linings are dependent on temperature and applied stresses, and refractory materials have relatively low resistance to tension. In order to achieve a safe design, a thorough understanding of the behavior of the lining systems is required. Such a behavioral understanding includes the refractory material behavior with respect to the effects of monotonic and cyclic mechanical properties, elevated temperatures and thermal cyclings, environmental interactions with slags and process gases, and history of thermomechanical loadings. There is a lack of thermomechanical data on the behavior of the refractory materials in the processing environments, requiring further development of a comprehensive set of materials data-bases.

1.2 REVIEW OF PREVIOUS WORK AT MIT

Previous MIT work can be divided into two categories globally; (1) material and system modeling of the behaviors of refractory linings (Pike et al., 1980; Tseng and Buyukozturk, 1982; Buyukozturk and Shareef, 1983; Chen and Buyukozturk, 1984), and (2) experiments of selected high-alumina and high-chromia dense refractory bricks manufactured by sintering, hot-pressing, or fusion-casting under elevated temperature and/or slag-impregnated conditions (Tamer and Buyukozturk, 1988).

Constitutive models basically included temperature-dependent material properties to represent the material behaviors. The temperature effect was introduced by scaling the stress-strain curves at different levels, with respect to the peak stress and the associated

axial peak strain. For accurate predictions of the temperature distribution through the vessel walls, a transient heat transfer analysis capability was developed with the adoption of a finite difference solution scheme. Emphasis was placed on the development of a time-independent constitutive model to predict the material response to multiaxial, non-proportional and cyclic loads. In addition, several time-dependent creep models were developed because of the importance of the creep behavior at high temperature. A conductivity model for cracked media, and polynomial representations of the thermophysical and thermomechanical properties were proposed by Tseng and Buyukozturk (1982). The developed material models and the heat transfer analysis capability were incorporated into a finite element program for three dimensional nonlinear analysis of refractory linings on heat-up and cool-down cycles. A predictive corrosion model was proposed to study the long-term corrosion process of lining systems (Chen and Buyukozturk, 1984). Based on this model, sensitivity studies were performed to identify the important factors characterizing the long-term behavior of the linings. Using the finite element program, the thermomechanical behavior of linings with various material combinations, lining geometries, and heating schemes were studied. Based on the findings from the thermomechanical and corrosion analysis, tentative recommendations were made for the design and operation of lining systems.

A test program of selected dense refractory bricks was conducted. The general objectives of the program were:

1. to characterize the compressive behavior of refractories at high temperature in coal gasifier environments,

2. to relate the macroscopic deformation and fracture behavior to the microstructural properties, and

3. to develop a comprehensive material data-base, to be used in studying the thermomechanical behavior of brick-mortar lining systems.

The scope of the testing program consisted of short-term uniaxial monotonic and cyclic mechanical load tests at room and predetermined elevated temperatures, and constant load tests under constant or varying temperatures. Relating materials with different compositions of alumina and also with different manufacturing processes were tested. A high temperature thermomechanical testing facility under controlled gas environments was developed at MIT.

1.3 CURRENT RESEARCH OBJECTIVES AND APPROACHES

The general objectives of the current research are:

1. to develop a limited material data-base that can be used by refractory designers, users, and manufacturers.

2. to develop a refined model for predicting creep behavior of refractories at elevated temepratures.

The material properties of interest can be divided into two main categories: thermophysical and thermomechanical properties. The thermophysical properties of interest include thermal conductivity, the density and specific heat, and the coefficient of thermal expansion. The effect of different temperature levels on the mentioned thermophysical properties is important. Thermomechanical properties include (1) the time-independent stress-strain response of the material subject to different monotonic and cyclic mechanical loadings under predetermined constant temperatures, and (2) the time-dependent material behavior subject to short-term and long-term constant mechanical loadings under predetermined constant or increasing temperatures.

The current research program concentrates on obtaining necessary data on the short-term comprehensive behavior of refractories. The approach for this reserach may be summarized in the following steps:

1. Perform a literature survey on standard testing methods for the thermomechanical and thermophysical properties of refractories. Review existing material properties and relevant material models. Establish specific test procedures, and test the method of instrumentations.

2. Identify a candidate material for each category including dense brick, dense castable, insulating castable, and insulating brick.

3. (a) Perform short-term uniaxial monotonic tests on each category of refractory materials at predetermined constant temperature in the range of 70°F to 2400°F.

   (b) Perform short-term uniaxial constant compressive load tests on each category of refractory materials at predetermined constant temperature levels in the range of 70°F to 2400°F. The constant stresses are between 40% and 75% of compressive strength of the refractories.

4. Collect the thermomechanical data from the above-mentioned tests. Collect modulus of rupture data at room and elevated temperatures, and thermophysical data from the literature. Assemble the acquired data in a material data-base as graphs and tables in a form to be used by designers and manufacturers of high temperature vessels.

5. Evaluate all obtained data in view of modeling of the material behavior of refractories.

1.4 DOCUMENT ORGANIZATION

The list of figures and tables are located before Chapter 1. In Chapter 1, brief reviews of background and previous MIT work are presented. Current research objectives and approaches are also summarized.

A review of previous work on lining systems and materials for coal gasifiers is given in Chapter 2. System configurations, operating conditions, failure mechanisms, and candidate materials are reviewed at first. The behavior of lining materials at high temperature under compressive loadings is reviewed next.

Chapter 3 describes the current test program. The equipment built for high temperature systems is reviewed first. The test program is presented with selection of materials, preparation of specimens, and thermomechanical testing programs. Finally, problems related to the test are discussed.

The results from the thermomechanical tests and the discussion of the behaviors are presented in Chapter 4, 5, 6, and 7 for dense brick, dense castable, insulating castable, and insulating firebrick refractories, respectively. Compression tests at elevated temperatures consist of monotonic and short-term creep uniaxial compressive loading tests at constant or increasing temperatures.

In Chapter 8 a constitutive model for predicting the creep behavior at elevated temperatures is proposed. General creep behavior of refractories at high temperature is reviewed first. Some available creep models for high temperature systems are reviewed next. A generalized creep model is proposed after checking the desirable requirements finally.

Chapter 9 presents the summary, conclusions, and some recommendations for future work.

The references are included after Chapter 9.

The material data-base is presented in Appendix A.

Chapter 2

LINING SYSTEMS AND MATERIALS FOR COAL GASIFIERS

2.1 LINING SYSTEMS OF HIGH TEMPERATURE VESSELS

2.1.1 System Configurations

Gasification vessels, in which coal is converted to combustible gas, are usually cylindrical in shape, from 100 to 250 feet in height, and 15 to 60 feet in diameter. The vessels are composed of outside steel shell and refractory linings. The main purposes of the refractory linings are to maintain and improve the thermal efficiency of the system, and to protect the steel shells from high temperature and severe environments. The linings are either made of monolithic refractory castables (Fig. 2.1), or refractory bricks jointed together using a mortar material (Fig. 2.2). The refractory linings are usually composed of a dense layer next to the hot face and an insulating layer between the dense layer and the steel shell. The refractory linings are subjected to heat flux at the interior(hot face) and generally cooled from the exterior. Cooling sytems are frequently used to keep the shell temperature at a certain predetermined level to make the corrosive agents on the

shell inactive, and to reduce the hot-face temperature. The dense layer, which is in direct contact with the process environments, must be resistant to high temperature, corrosion, erosion, and abrasion. Therefore, the dense layer materials must have high thermal conductivity, better thermo-mechanical properties, and thermal shock resistance. The insulating refractory layer, which has a relatively low coefficient of thermal expansion and a low heat capacity, reduces the shell temperature and increases the thermal efficiency of the system. A compressive material layer can be used between the steel shell and the refractory linings to relieve some of the stresses caused by the lining expansion at high temperatures. In the case of monolithic linings, steel anchors extending from the steel shell into the refractory linings are usually used to enhance the integrity of the system. In the case of brick linings, the bricks are jointed together using mortar material.

2.1.2 Operating Conditions

In slagging coal gasifiers, the operating conditions are extreme (Bakker and Stringer, 1981; Crowley, 1975). Generally, the range of operating temperatures in slagging gasifiers is 2400°F - 3300°F (1315°C - 1816°C). Ash is present as molten slag that runs down the walls of the gasifiers, and that is corrosive to the linings. Gas pressures in the gasifiers usually range from atmospheric to 1000 psi. Gases consist of H_2O (steam), H_2, CO, CO_2 and small amounts of CH_2, N_2, NH_3, and H_2S. A typical value of the partial oxygen pressure during operation is $10^{-8}atm(10^{-3}Pa)$. Reducing gases, primarily H_2 or CO, will attack silica-containing refractories at low pressures and high temperatures, whereas steam and CO_2 are aggressive at high pressures and high temperatures. At reducing atmosphere, ash, which contains iron, is more corrosive to alumina-silica refractories than it is in an oxidizing atmosphere of the same temperature. Magnesia, on the other hand, may dissolve relatively large amounts of ferrous oxide in a reducing atmosphere without apparent damage. High pressure (1000 psi) steam-rich atmospheres tend to accelerate refractory deterioration. Lower pressures (0 - 100 psi) favor attack by hydrogen-rich

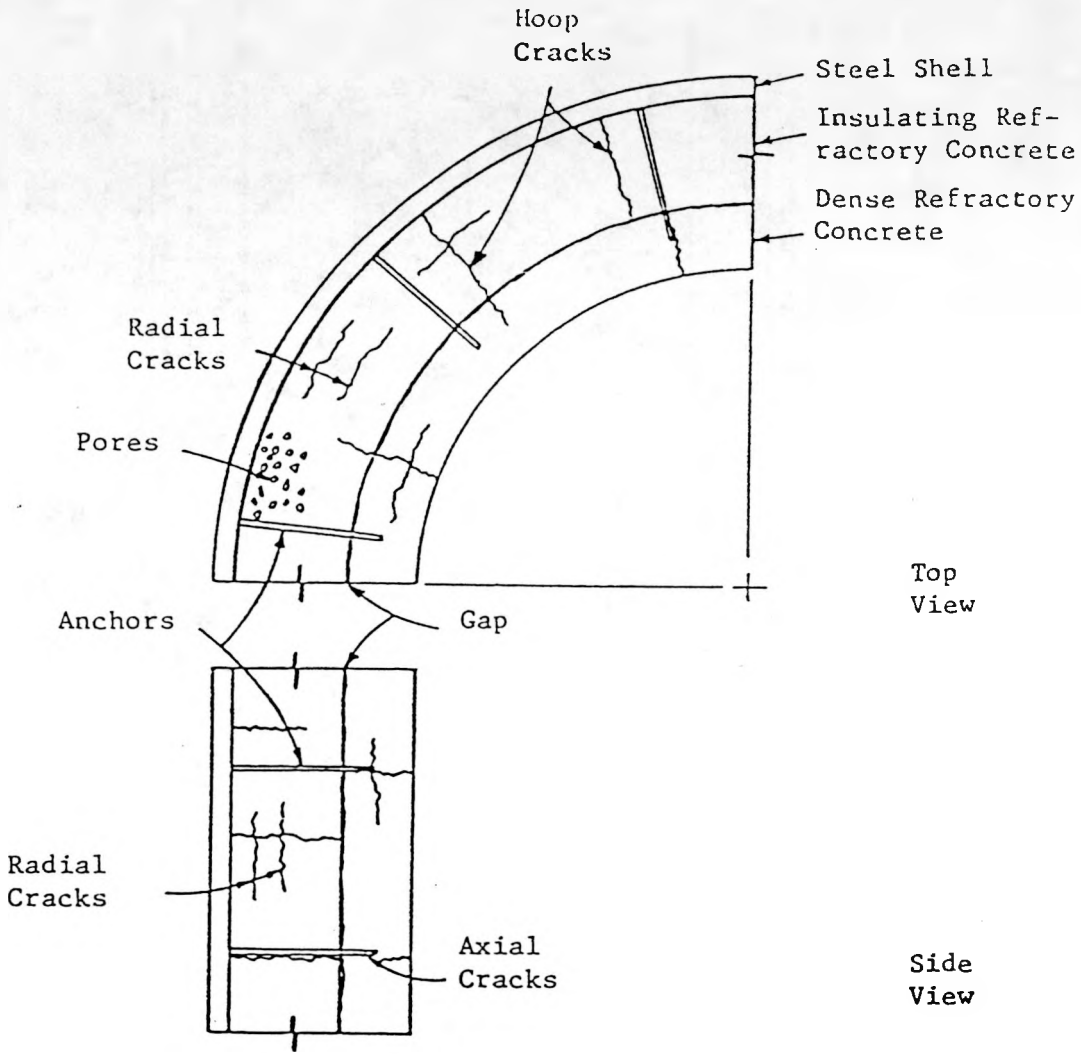

Figure 2-1: High Temperature Monolithic Linings (Tseng, 1982)

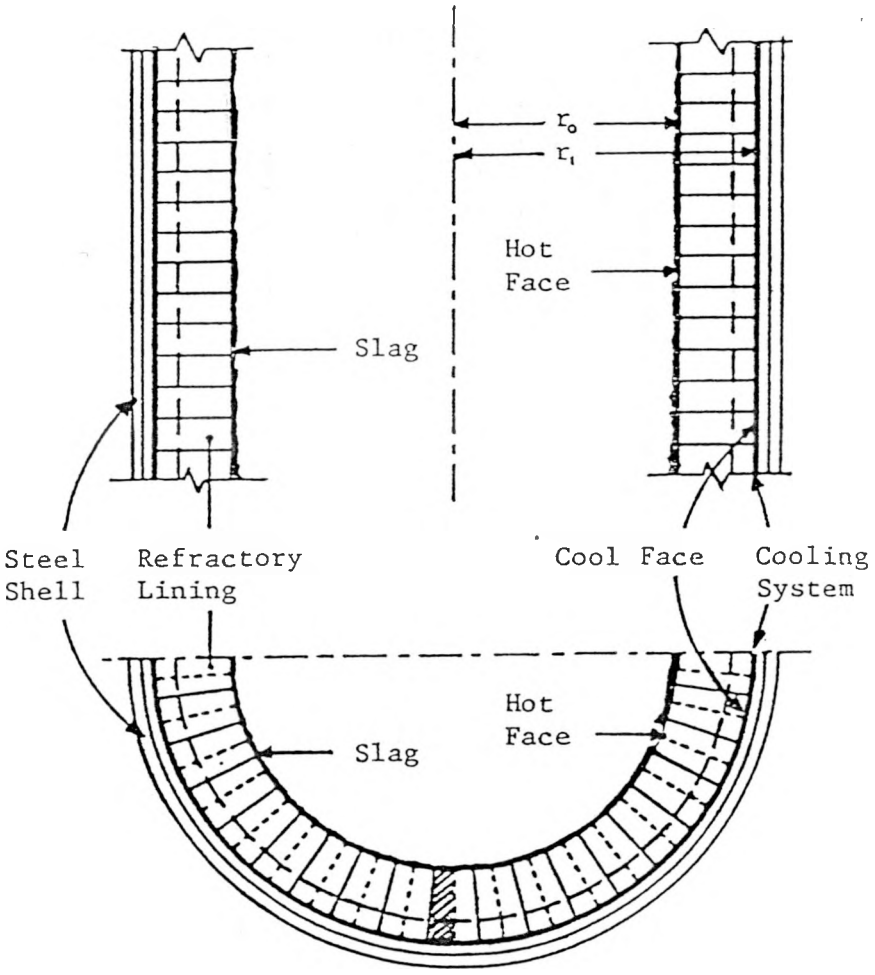

Figure 2-2: High Temperature Brick Linings (Chen, 1984)

atmospheres (Bortz et al., 1982).

Controlled heating and cooling rates are critical in protecting the refractory linings from serious failure environments. If the initial heat-up is too fast, the free water will form steam(H_2O), and the refractory concrete can literally be blasted apart with explosive force. It is evidenced by deep and widespread spalling. Therefore, during the initial heat-up, no direct flame should impinge upon the refractory materials. Rapid cooling of the hot-face also cause damage. Some finding of the study on heating rate are discussed with different heating rates (10°F/hr, 100°F/hr, and 1000°F) by Tseng and Buyukozturk (1982). In the case of slow heating (10°F/hr), hoop cracks occured in the dense component at intermediate temperature levels. In the case of rapid heating (100°F/hr), extensive radial cracks and hoop cracks occurred in the dense component during heat-up. The intermediate heating rate (100°F/hr) results in only slight radial cracks around the center of the dense component during heat-up. In this case, the first cracking in the lining occurred at hot-face temperatures higher than those for the other two cases. The usual rate for heating up the lining systems is recommended to be less than 250°F/hr (Tamer and Buyukozturk, 1988).

2.1.3 Failure Mechanisms

Several different failure mechanisms exist in lining systems. Generally, two different categories of failure may be observed:

1. by degradation of the mechanical properties of refractories at elevated temperatures through cracking, spalling and joint failure due to thermal attack and creep rupture, and

2. by disintegration of the refractories due to corrosion and erosion attack by gases and slags.

The large temperature differences across the lining thickness and the consistency of temperature through a long time process period raise a critical stress combination of tensile, compressive, and shear stresses in the linings. Such critical stress states may cause cracking, spalling problems, and the failure of joints between bricks in the case of brick systems. Furthermore, heat accumulation through the reduction in thermal conductivity due to hot slag penetration at locations of the cracks may accelerate the deterioration of the linings, eventually leading to the failure of the vessel shell. Molten slag attacks all refractories presently used in slagging coal gasifiers unless they are water-cooled to form a protective layer of frozen slag on the surface. Rapid cyclic temperature differentials create thermal stresses, which cause deterioration of the refractory materials. Other stresses, such as dead or live loads, can accelerate the deterioration frequently occurring in the form of creep cracks of spalling. Thermal stresses in the lining are one cause of spalling. Thermal stresses are particularly important at low temperatures during heat-up when the refractories are relatively brittle and when the maximum thermal gradients occur (Bortz et al., 1982).

Gaseous corrosion of high temperature refractory materials can occur at temperatures as low as 1350°F. Silicon carbide is subject to deterioration in oxidizing atmospheres at this temperature. Dust or particulate matter, contained in high velocity fluids and gases, can erode refractory materials by slowly degrading the exposed surface. Refractory surfaces can also be abraded by the rubbing and scouring action of moving solids. Erosion and abraison, however, are normally not major problems in slagging gasifiers since most refractories are inherently abrasion resistant and velocities in gasifiers are normally low except possibly in localized areas.

2.1.4 Candidate Materials

Since the lining systems of coal gasifiers experience very severe environmental conditions during operation, a selection of optimum materials is mandatory. The candidate materials

for high temperature applications are refractories. Refractoriness is usually defined as the capability of maintaining a desired degree of chemical and physical identity at high temperatures and in the environments of use (Budnikov, 1964). The main types of refractory materials are: refractory castables, plastic refractories, refractory ceramics, refractory fibres, and refractory metals (Crowley, 1984).

The most important factors to be considered in the selection of refractories under the processing environments over 2300°F are thermal cycling, process atmospheric corrosion, and for some processes, corrosion by ash slags. Erosion is a function of operating conditions and must be considered in design but generally does not govern a design. Spalling is not normally a function of normal operating conditions but is of concern to designers, refractory manufacturers, and operators. Shrinkage and creep at all temperatures up to the operating temperature must be as small as possible. The linear shrinkage should preferably be less than 0.1%. Desired maximum creep rates are less well defined. The thermal expansion should also be low, as most of the lining stress is generated by thermal expansion (Bakker, 1982).

In general two types of refractory materials have been used in slagging gasifiers: high alumina and high chromia refractories (Bakker and Stringer, 1981; McGee, 1984; Sweeney and Cross, 1982). The high-alumina refractories are known for their good resistance to thermal shock (Bandyopadhyay et al., 1983), while the high-chromia refractories are known for their good corrosion resistance (Bakker et al., 1984; Bonnare et al., 1980; Kennedy 1980; Washburn, 1982). Candidate materials may be selected based on their service temperatures and chemical compositions. The selection of proper lining materials and the design of the lining systems for high temperature, high corrosion environments require a thorough understanding of the behavior of lining materials.

2.2 BEHAVIOR OF LINING MATERIALS AT HIGH TEMPERATURE

2.2.1 Environmental Effects on the Behavior of Refractories

Since the matrix of most refractory concretes is extremely fine, it reacts quite readily with gases which may be present in the furnace such as CO, CO_2, and steam, especially at elevated pressures. This can lead to the formation of different compounds such as calcium carbonate or formate, Boehmite (AH), the high pressure hydrated calcium aluminate ($C_4A_3H_3$), and Anorthite (CAS_2) [1] (Bakker, 1982). The main components that were found to affect the refractory behavior are hydrogen (H_2) and carbon monoxide (CO). A hydrogen rich atmosphere was found to raise significantly the thermal conductivity of porous refractories. This effect was even more pronounced at high pressures (Wygant and Crowley, 1958). It was found that the effects of steam dominate the effects of CO (Brown, 1983), and that in a high-Btu gas atmosphere at 500°C, and 1000 psi, conditions exist such that CO decomposition may occur. Iron (Fe) was found to accelerate CO decomposition, and on the other hand the introduction of H_2S suppresses carbon formation in refractories.

In a coal gasification atmosphere at 500-1000 psi, Boehmite, calcite, and, less frequently, calcium formate are formed at temperatures below about 300°C. The formation of Boehmite markedly increases the strength of all concretes regardless of the aggregate used. The strength increase is related to the amount of Boehmite formed, which in its turn depends on the degree of steam saturation of the gas mixture. At temperatures above 300°C Boehmite starts to decompose. Complete decomposition has occurred at around 500°C. In low silica, high alumina concretes, like refractory bricks, this leaves $C_4A_3H_3$ and CA as the principal bonding phases and generally results in a decrease in

[1] Here, A, C, H, and S represent Al_2O_3, CaO, H_2O, and SiO_2, repectively.

strength. The actual strength loss depends on the heat-up and cool-down schedules used, but at atmospheres of 500°C is generally about 25% less than the strength of similiar samples fired in air. Thus, no catastropic loss in strength occurs. Refractory concretes containing silica or silicates, such as calcined clay base products like refractory castables, generally show a significant increase in strength after exposure to coal gas environments or high pressure steam at 500-1000°C, as compared to similar samples fired in air.

Alkali attack, which is another potential long-term failure mode for gasifier refractories, appears to be a more serious problem for high alumina refractories than for medium alumina refractories. In coal gasification vessels the alkalies can result in incipient melting of the hot face due to alkali fluxing, and surface washout by dissolution of alkali compounds. Alkali attack on refractories was found to be accelerated by the presence of silica and vandium compounds and enhanced by high porosity and surface area. In order to retard the alkali attack, one suggestion was to maximize the maturity of the bonding phase to develop a strong ceramic bond (Gentile et al., 1987).

Data on mechanical properties of refractory castables at high temperatures are quite limited due to the complex nature of refractory castables compared with refractory bricks. In use, the castable is cured and then fired from only one side so that a temperature gradient exists through the material. Thus, if the temperature is high enough, the hot face will have a ceramic bond; the cold face will retain the original hydraulic bond; and the interior will have a mixture of both bond types. The variation in bonding causes a variation in thermal conductivity, elastic modulus, strength, density, and other properties. In contrast, a refractory brick is already fired so that a uniform ceramic bond exists throughout the material in service temperature.

2.2.2 Thermomechanical Behavior of Refractories

The thermomechanical behavior is temperature, load history and time dependent. For the analysis of the lining systems, the required thermomechanical properties are basically:

1. multiaxial stress-strain relationships of materials at elevated temperatures,

2. creep properties under different stress and temperature levels, and

3. shrinkage properties.

With regard to time effects, such mechanical properties can be conveniently decoupled into:

1. time-independent or instantaneous constitutive behavior, and

2. time-dependent creep behavior.

In the time-independent behavior, the associated properties such as strength, strain at the peak stress, and elastic modulus can be represented as polynomial equations depending on temperature. In the time-dependent behavior, a creep model should be able to follow varying stress and unloading conditions.

Strength of the refractories is nonlinear through the wall, depending on the temperature gradient and final hot and cold face temperature. Typical uniaxial strength-temperature curves are shown in Fig. 2.3. The effect of this strength variation could have drastic effects on the ability of the refractory lining to withstand its own dead load and its ability to resist the thermal loads to the differential thermal expansion and shrinkage during initial firing. Hot strengths are as good as, or better than, cold strength until heated to the pyroplastic point, where one or a combination of ingredients in refractories starts to vitrify and becomes glassy, or softens (ACI, 1979).

The behavior of refractories at high temperatures can be categorized in three different regions (Evans and Langdon, 1976). At relatively low temperature, the behavior of the

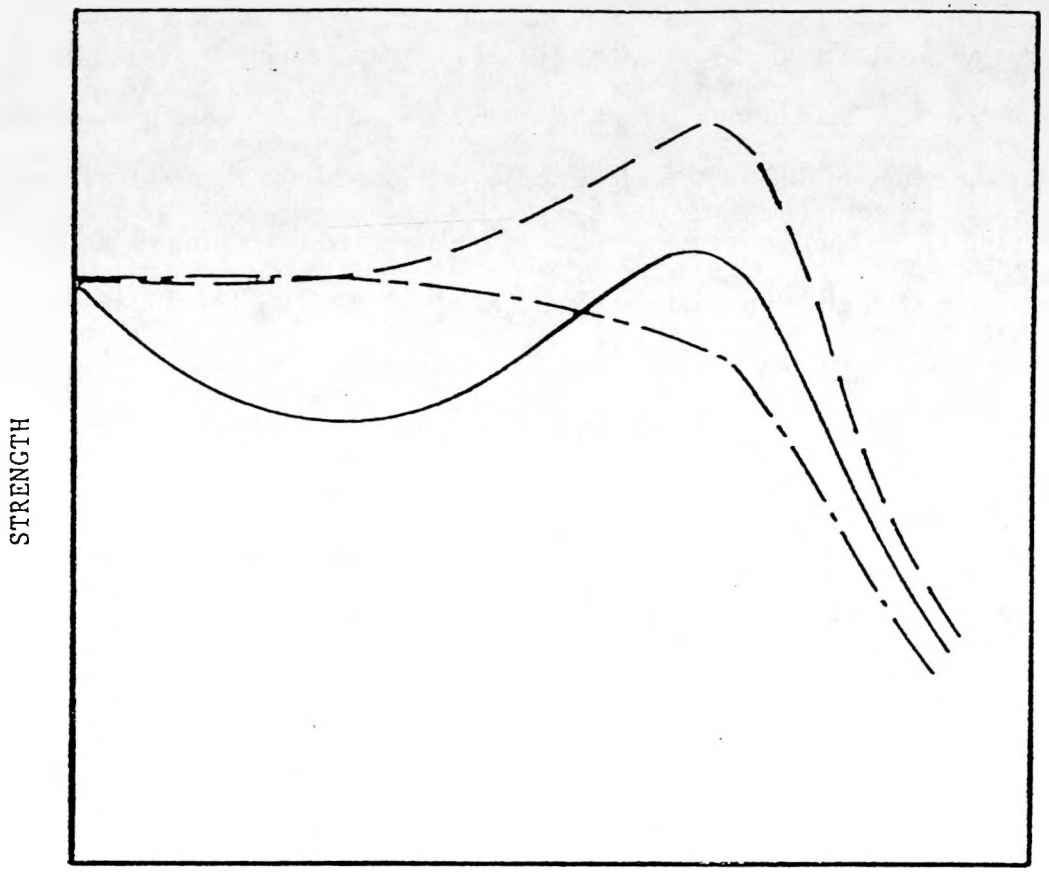

Figure 2-3: Typical Uniaxial Strength vs. Temperature Curves of Refractories.

material is brittle and only a small decrease in strength is observed with temperature. The intermediate temperature region exhibits a 'deformation assisted brittle fracture', where the material strength decreases faster with temperature. At relatively high temperatures a ductile behavior is observed.

A review of McCullough and Rigby (1971) reported two kinds of variation of strength with temperature for alumina refractory concretes: (1) a decrease in strength, levelling off over the range of 400-1000°C, followed by an increase of strength with temperature above 1100°C, and (2) an increase in strength at temperatures around 200°C followed by a decrease in strength to a minimum value at about 1200°C. The increase in strength of refractories was attributed to the formation of a ceramic bond which began to form at about 1125°C. An increase in compressive strength for both dense and insulating refractory concretes for temperature in the range of 1100°F-1500°F was reported (Tseng and Buyukozturk, 1982). A monotonic decrease in compressive strength for dense ceramics for elevated temperatures was also investigated (Tamer and Buyukozturk, 1988).

Test results for MOR (modulus of rupture) showed almost the same trend as those for compressive strength at elevated temperatures. Tests on alumina-silica showed a small decrease in MOR from room temperature to about 1500°F (Miller and Davies, 1966). From 1500°F to about 2000°F an increase in MOR with temperature was observed. At temperatures higher than 2000°F a rapid drop in MOR was observed. Similar results have also been observed by other researchers (Folk and Bohling, 1968; Clarke, 1983).

2.2.3 Thermophysical Properties of Refractories

The thermophysical properties of lining materials are generally temperature dependent. For the analysis of the refractory linings, the following thermophysical properties of the lining materials are required:

1. thermal conductivity (k_s), thermal diffusivity ($k_s/\rho C_p$),

2. density (ρ) and specific heat (C_p), and

3. coefficient of thermal expansion (α).

Researches have shown that there is a significant difference between thermal conductivities of refractory castables fired at constant temperature and fired in a temperature gradient (Ruh and Renkey, 1963). This difference reflects a difference in the degree of bonding which should cause similar differences in mechanical properties. Therefore, thermal conductivity in refractories may be defined as a function of temperature and bonding condition. Typical thermal conductivity - temperature curves are shown in Fig. 2.4. This figure describes the different values of thermal conductivity in heating and cooling processes. Dense refractories are required to have higher thermal conductivity than insulating refractories because dense refractories are directly contacted with hot temperature and severe environments. Thermal conductivity of the materials under process conditions is generally different from those provided by laboratory tests. This is mainly because the gases in the process environments are different from those in the tests, and the degradation of the materials (cracking, etc.) during the process cycles may produce different void volume (Tseng and Buyukozturk, 1982). The increase in the thermal conductivity would result in higher shell temperatures, and as a result additional cracks in the lining may form.

A nonlinear thermal expansion through the thickness of the refractory is produced due to the physical changes in the refractory as well as due to temperatrure changes. In the latter case expansion increases slightly with rising temperature. Thus, there is not only a difference in expansion due to the temperature gradient through the refractory but also due to the fact that the bonding mechanism is different. Three different bonding zones have been observed corresponding to temperature levels consistent with: (1) maintenance of hydrate material, (2) loss of chemically combined water, and (3) development of a ceramic bond. Typical thermal expansion - temperature curves for refractory castables

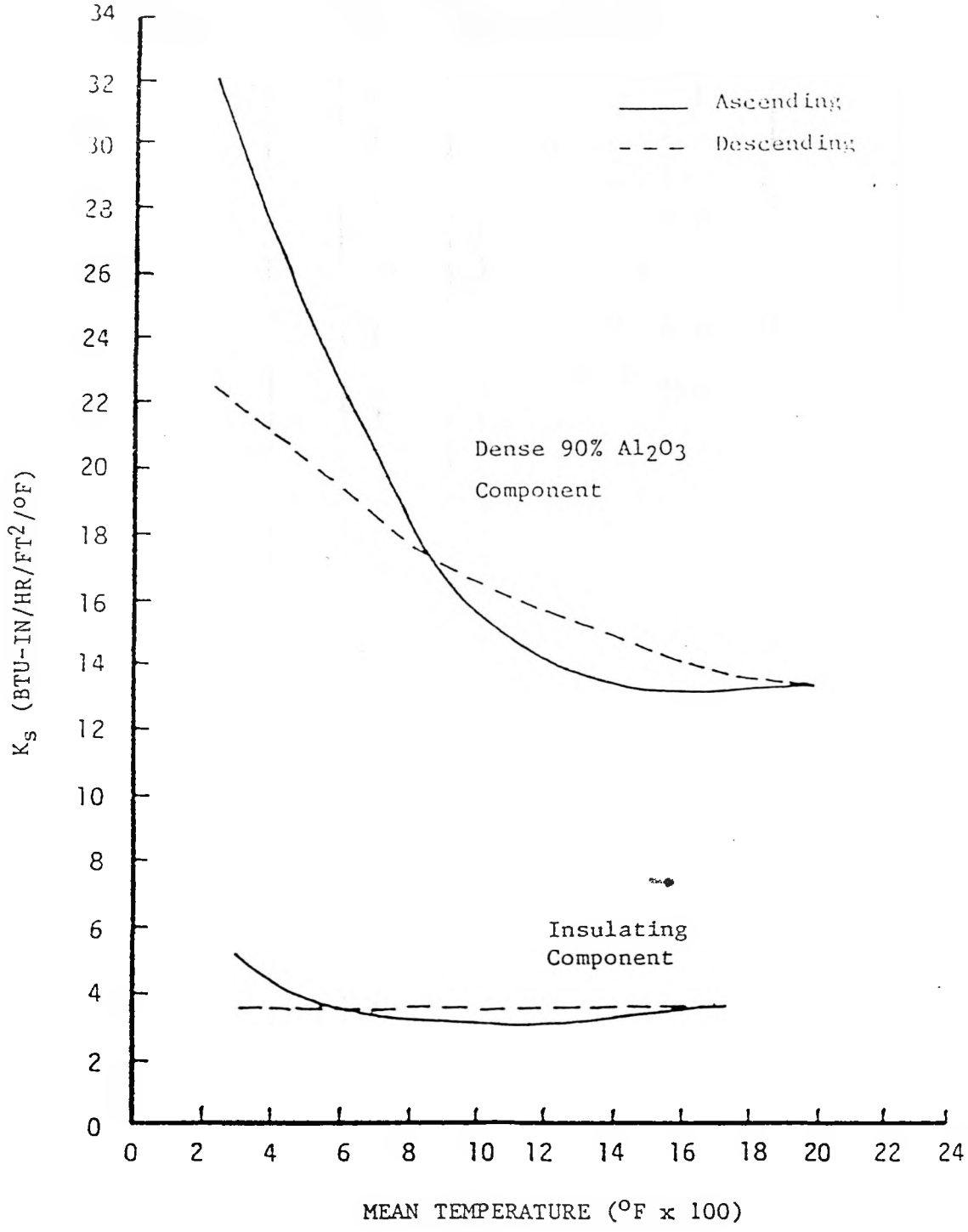

Figure 2-4: Thermal Conductivity vs. Temperature Curves of a Dense and an Insulating Refractory Concretes (Babcock & Wilcox, 1981)

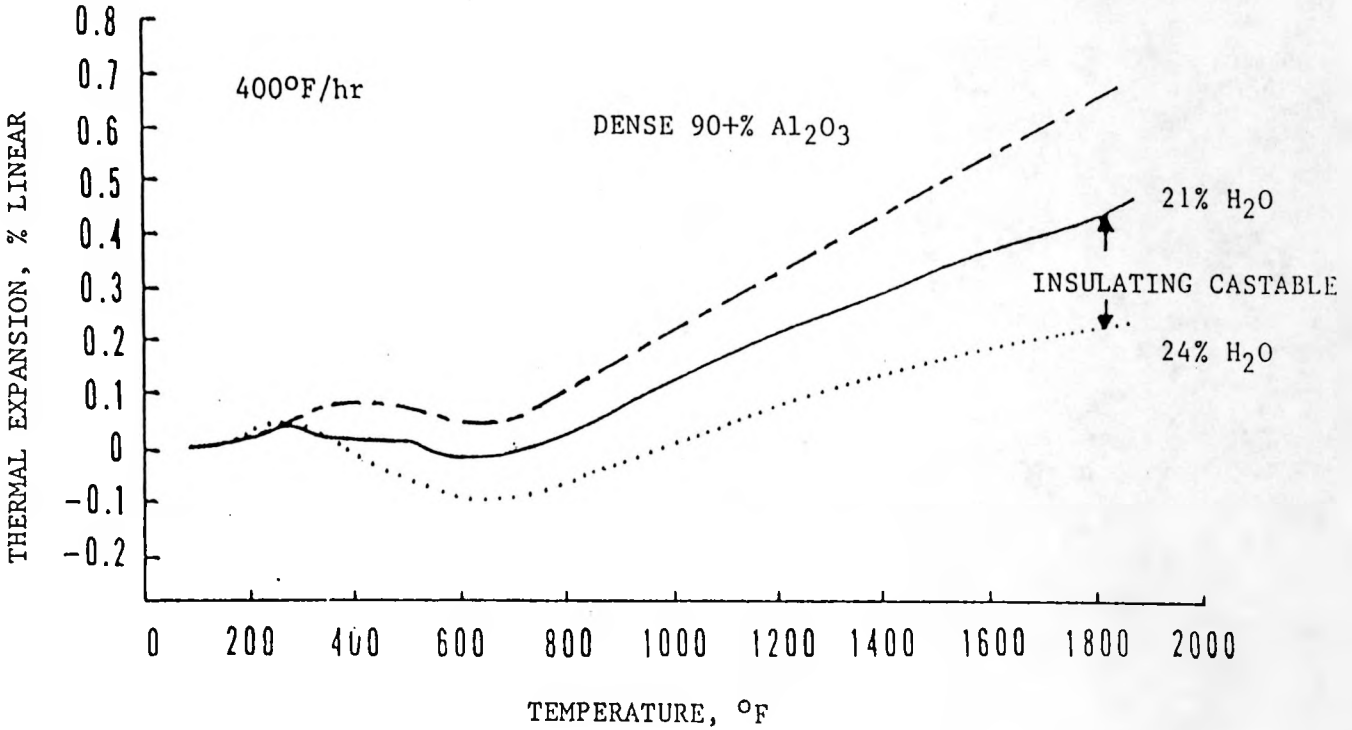

Figure 2-5: Thermal Expansion vs. Temperature Curves of Castables during Initial Heat-up (Babcock & Wilcox, 1981)

are drawn in Fig. 2.5 with 400°F/hr heating rate. The dense refractory castable shows larger thermal expansion with the temperature increase.

Chapter 3

TESTING

3.1 EQUIPMENT FOR HIGH TEMPERATURE TESTING

Test equipment was designed and built to test materials under compressive or flexural, monotonic, constant or cyclic mechanical loads, in room or elevated temperatures, in air or controlled gas environments. Tests under controlled gas environments are not included in the present research. Those are well explained by Tamer and Buyukozturk (1988). The general requirements for this system are:

- application of prescribed monotonic and cyclic compressive load histories at predetermined constant temperature levels,
- temperatures ranging from room temperature up to 2800°F with an accuracy of ± 5°F at 2800°F,
- maximum mechanical load capacity of 50,000 lbs. with noise (i.e. percentage error) levels not to exceed 0.3%,
- loading rams and heating elements able to resist action of melting products, and
- automated data acquisition and control.

The main system components, shown in Fig. 3.1 and Fig. 3.2, are 100 kips mechanical loading frame (from Manufactured Test Systems, MTS), a 2800°F high temperature furnace (from Applied Test Systems, ATS) with a microprocessor (from LFE Corporation) to apply mechanical loads at high temperatures, and a data acquisition (IBM XT and Fluke 2400B) and control system (PDP-11).

3.1.1 Furnace and Temperature Controller

Main considerations in the choice of the high temperature furnace are the dimensions and the shape of the heat zone, temperature uniformity around the specimen, and heating elements that would be inert to the maximum testing temperature. The temperature controller had to be accurate and flexible enough to prescribe different temperature histories. A split-type furnace with sdilicon carbide(SiC) resistance heating elements and a maximum operating temperature of 2800°F was selected. It is cylindrical with a 16 inch outside diameter and a 24 inch height. The shell length is 16 inch long, and is protected by one layer of insulation. The heat zone is circular with an 8 inch diameter and a 10 inch height. The heat zone shape and dimensions were chosen in order to insure temperature uniformity around a cylindrical specimen that is 2 inches in diameter and 6 inches long (These dimensions represent the maximum specimen for which the system was designed). In order to check for temperature uniformity, three thermocouple ports were provided at the furnace's center, and at 1.5 inches from the center on either side. Heating elements are made of silicon carbide and are arranged in a circular manner around the furnace's center. The heating elements are connected in series by cables outside the furnace's shell. Both ends of the furnace have 4 inch bore holes to allow access for the muffle tube and retort loading assembly. The selected temperature control system can prescribe variable heat-up and cool-down rates, and different soak periods. The microprocessor has built-in capabilities for thermal cycling, up to 252 cycles, with up to 8 different ramp and soak periods per cycle. The temperature controller is connected to a chromel-alumel (nickel-

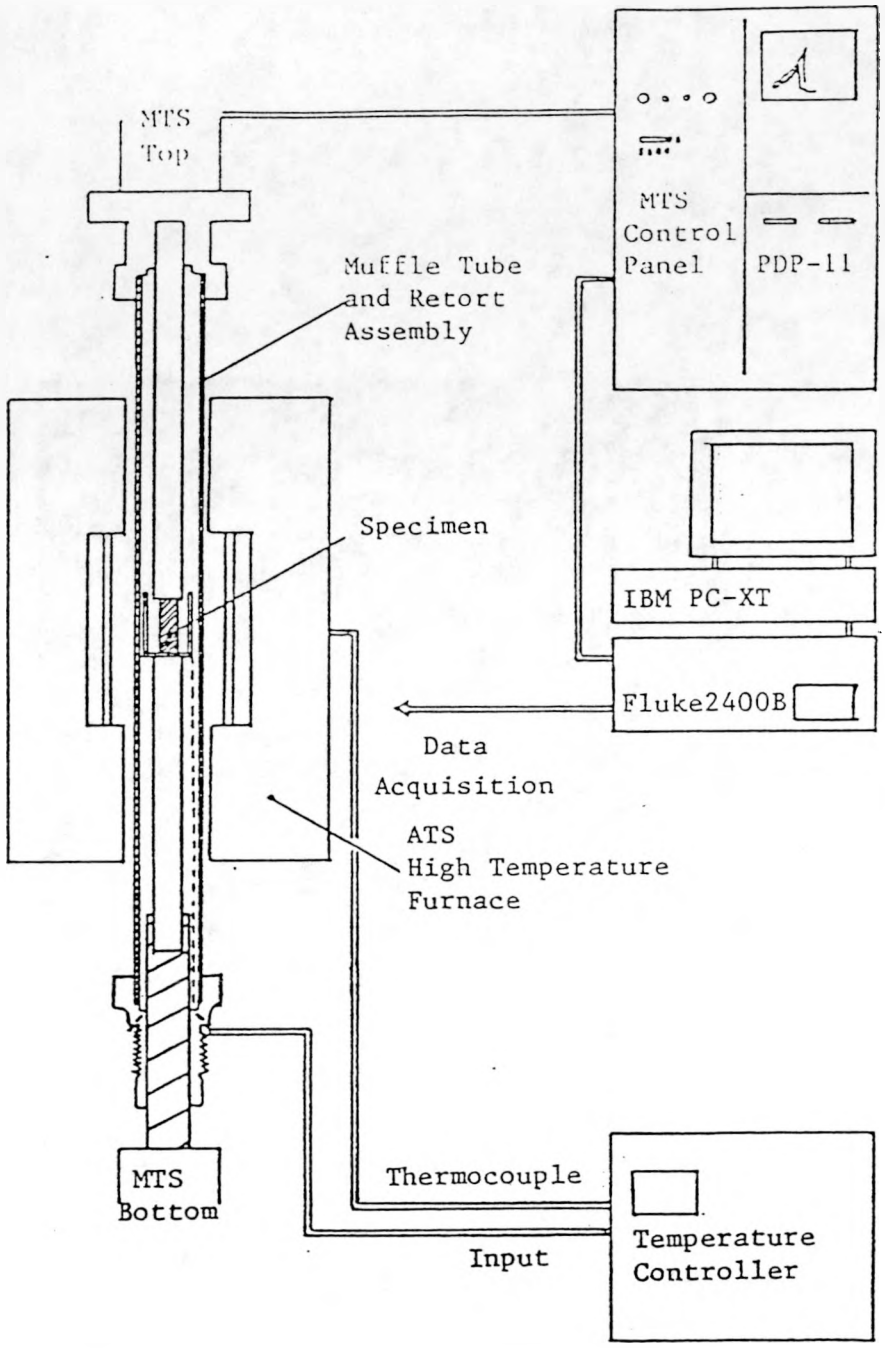

Figure 3-1: Sketch of the Major Components of the Thermomechanical Testing System

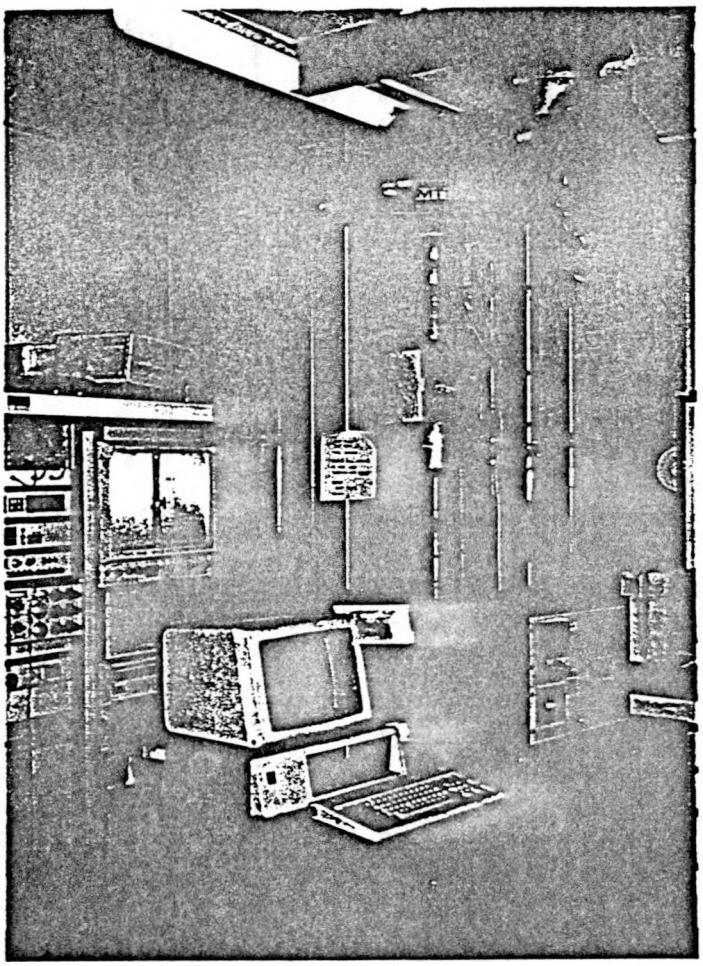

Figure 3-2: Picture of the Major Components of the Thermomechanical Testing System

chromium vs. nickel-aluminum) type K thermocouple for temperatures below 2000°F, and to a platinum-rhodium (platium-6% rhodium vs. platium-3% rhodium) type B thermocouple for temperature above 2000°F. The temperature controller is linked to the data acquisition system, to register the prescribed temperature history.

3.1.2 Retort System

The retort system was designed to apply up to 50 kips at 2800°F. It had to meet the following requirements:

1. all compression rams and load-bearing parts inside the furnace to withstand 50 kips maximum load with 2800°F maximum temperature, and

2. any part inside the furnace to resist a maximum temperature of 2800°F.

The load train inside of the furnace consists of recrystallized silicon carbide (SiC) upper rod (Crystar from Norton Co.), and high purity alumina tube (from Bolt Technical Ceramics) with an alpha SiC cap (from Sohio Eng. Co.) above it. The lower alumina tube has a 2.75 inches outside diameter (O.D.) and a 2.5 inches inside diameter (I.D.), and frames into a water cooled stainless steel grade 347 loading rod. The upper SiC rod has a 2 inches O.D. and frames into a water cooled stainless steel cap. A specimen is loaded inside the furnace between the two upper and bottom loading elements. An alumina protective cap is located around the specimen to protect the rest of the system from debris due to brittle fracture.

The whole retort system is designed to be assembled outside the loading machine then rotated into position on clamps. The picture of the furnace and retort system is shown in Fig. 3.3 and Fig. 3.4.

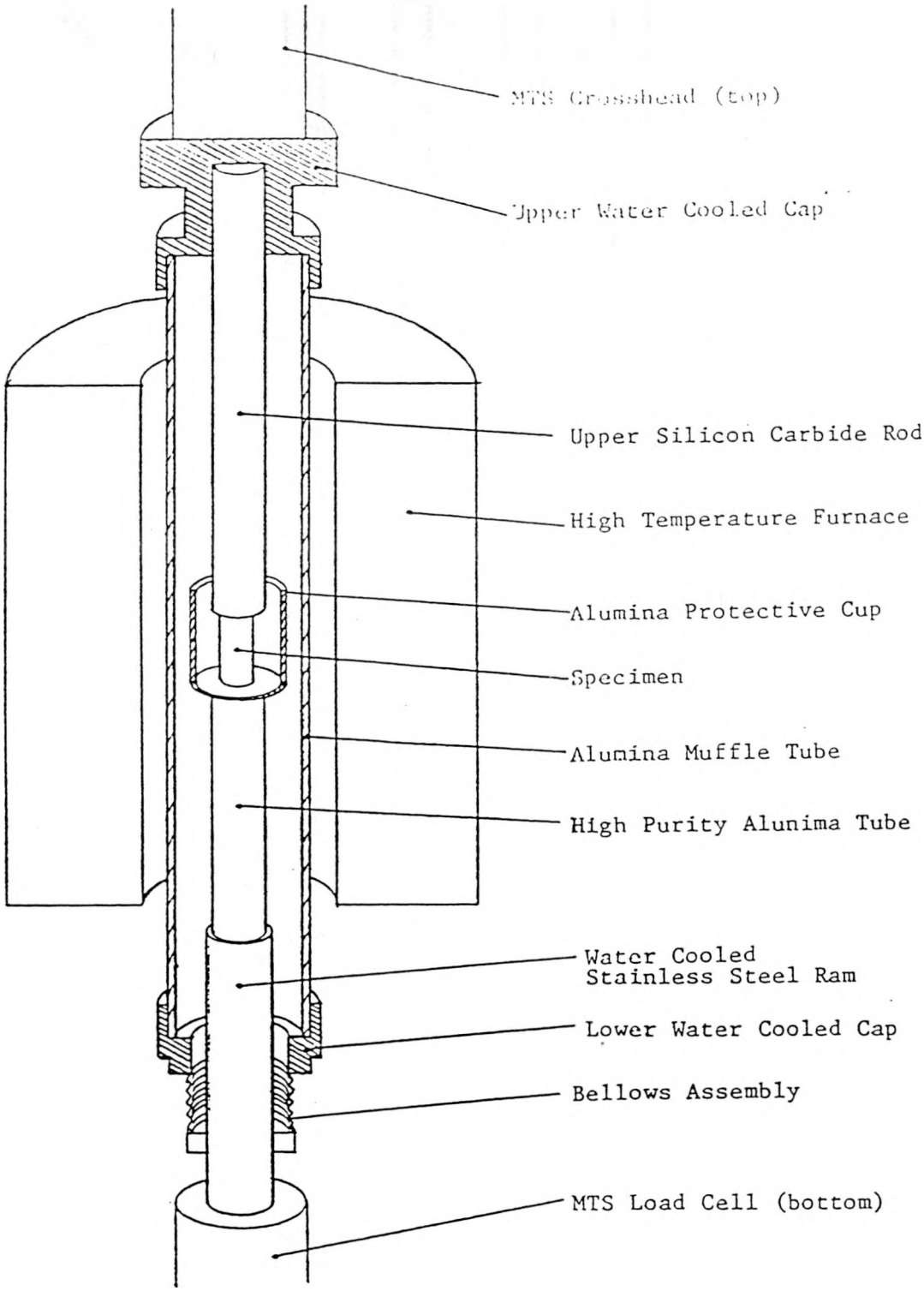

Figure 3-3: Retort Assembly for Application of Compressive Loads at High Temperatures

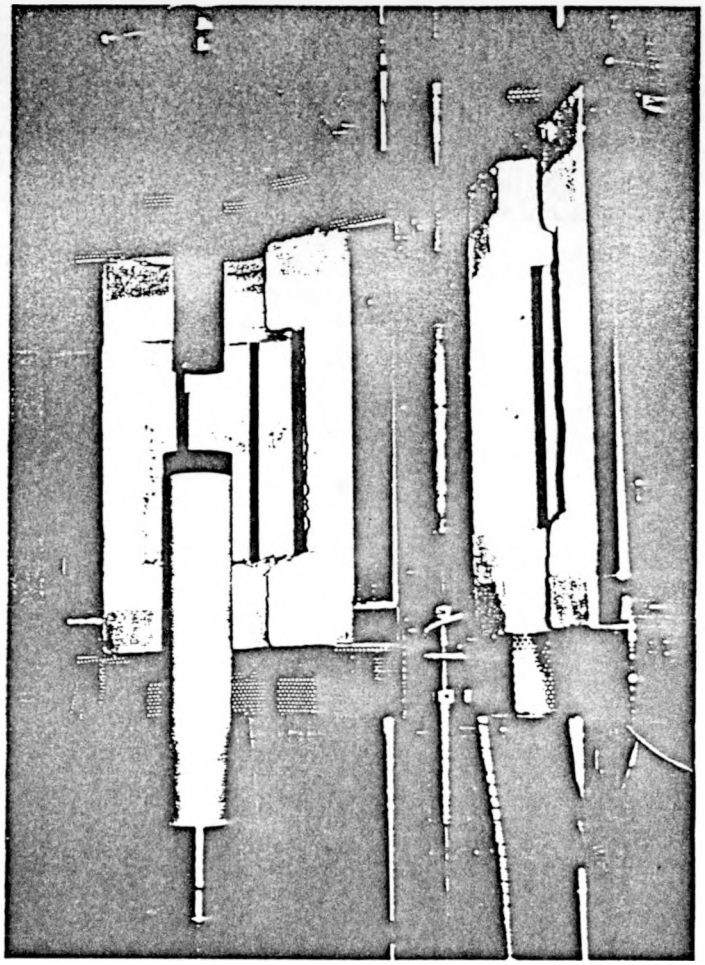

Figure 3-4: Picture of the Furnace and Retort System for High Temperatures

3.1.3 Data Acquisition and Control System

The MTS loading frame can be operated manually using the control panel, or PDP-11 computer controlled with a dual disk drive. Programs are carefully developed for monotonic, cyclic, and constant load tests at elevated temperatures. The furnace temperature is controlled by a LFE 2010 microprocessor. Type B and type K thermocouples have been used for the standard calibration. The PDP-11 computer is mainly used for control. A Fluke 2400B intelligent front end linked to an IBM XT. The disadvantages of the Fluke 2400B are (1) its slower speed, and (2) the 4 seconds minimum time-distance between each data collection, which is longer than actually expected for some tests. A user-friendly software has been used for Fluke-IBM XT data acquisition system.

3.2 TEST PROGRAM

The present research explores several types of refractory materials under different loading and temperature conditions. These data will be added to the previously obtained refractory material data-base.

3.2.1 Selection of Materials

For this research, the materials were chosen from the following categories:

1. dense brick
2. dense castable
3. insulating castable
4. insulating brick

The selection of each candidate material tested was based on its service temperature, chemical composition, and previously obtained test results. The properties of candidate

materials are summarized in Table 3.1. For dense castable, the high-alumina percentage was chosen for its good resistance to thermal shock (Bandyopadhyay et al., 1983). The high-chromia percentage is known for its good resistance to corrosion attack (Bakker et al., 1984; Bonnare et al., 1980; Kennedy, 1980; Washburn, 1982). Those materials were received from manufacturers.

Table 3.1: Properties of Selected Materials for Thermomechanical Testing

Material Classificaton	Dense Brick CPS-90A-10C	Dense Brick CPS-82C-18M	Dense Castable DC-95A-5Ca	Insulating Castable IC-55A-36S	Insulating Brick IB-39A-44S
Chemical Composition	90% Al_2O_3 10% Cr_2O_3	82% Cr_2O_3 18% MgO	95% Al_2O_3 5% CaO	55% Al_2O_3 36% Cr_2O_3	39% Al_2O_3 44% SiO_2
Manufacturing Process	Cold-Pressing Sintering	Cold-Pressing Sintering	Mix with Water	Mix with Water	Fired
Melting Point	-	-	3500°F (1927°C)	-	2750°F (1510°C)
Service Temperature	3450°F (1899°C)	3272°F (1800°C)	3400°F (1871°C)	2800°F (1538°C)	2300°F (1260°C)
Density (lb/ft^3)	206	235	166	85	31

Dense brick material CPS-90A-10C is produced by cold-pressing and sintering, and is composed of 90% Al_2O_3 and 10% Cr_2O_3. There are two minor phases present; coarse Al_2O_3 penetrated by Cr_2O_3 exhibiting a white color, and finer Cr_2O_3 grains penetrated by Al_2O_3 exhibiting a pink color. Minor impurities consist of small percentages of SiO_2, Fe_2O_3, K_2O, and Na_2O. Its average bulk density is 206 lbs/ft^3. The manufacturer's suggested maximum use temperature is 3450°F.

Another dense brick material CPS-82C-18M is produced by cold-pressing and sintering and is composed of 82% Cr_2O_3 and 18% MgO. Impurities consist of Al_2O_3, Fe_2O_3, SiO_2, CaO, and Ti_2O. Its average bulk density is 235 lbs/ft^3. The manufacturer's suggested maximum use temperature is 3272°F.

Dense castable material DC-95A-5Ca is produced by mixing with water at room temperature, and is composed of 95% Al_2O_3 and 5% CaO. Minor impurities consist of small percentage of SiO_2, Fe_2O_3, and Na_2O. The material was received from the manufacturers after casting there. Its melting temperature is 3500°F and the manufacturer suggested maximum use temperature is 3400°F. The bulk density of this material is 166 lbs/ft^3.

Insulating castable material IC-55A-36S is also produced by mixing with water at room temperature, and is composed of 55% Al_2O_3, 36% Cr_2O_3, and 5% CaO. Impurities consist of SiO_2, Fe_2O_3, MgO, and TiO_2. The material was received from the manufacturers after casting there. The manufacturer's suggested maximum use temperature is 2800°F.

Insulating firebrick material IB-39A-44S is produced by firing it. It is composed of 39% Al_2O_3, 44% SiO_2, and 16% CaO. Minor impurities consist of Fe_2O_3, Na_2O, MgO, and TiO_2. Its melting temperature is 2750°F, and the maximum use temperature suggested by the manufacturer is 2300°F. Its average bulk density is 31 lbs/ft^3.

3.2.2 Preparation of Specimens

The materials were received as bricks from manufacturers. The bricks are rectangular in shape. The dense bricks were manufactured by cold-pressing and sintering them. The insulating brick was fired at high temperature which is less than its melting temperature. The castables were mixed with water at room temperature by manufacturers. The specimens were cored out of the bricks, and the end surfaces were prepared for testing.

In choosing the diameter of the specimen, the size of the largest aggregate or the size of the largest air-void are important factors. The height of the specimen was chosen based on strength and strain considerations. For strength consideration, it has been determined empirically that H/D $\geq$ 1.7 (H is the specimen height and D is its diameter) is desired (Kotsovos, 1983). Based on strain consideration, the height of the specimen is

determined in such a way that a central zone of near-uniform uniaxial compressive stress exists. In a specimen under compressive loading, two end zones of a height $\sqrt{3}/2$ D and a central zone of H/3 exist as shown in Fig. 3.5. In the end zone, the interaction between the specimen ends and the loading device creates a complex state of stress imposed by friction restraints. By imposing a central zone height of H/3, the height of the specimen is determined to be such that $H/D \geq 2.6$. Due to these different considerations cylindrical specimens of one inch diameter and 2.5 inches to 3 inches height were adopted as standard for testing.

To obtain the cylindrical specimen from the brick, coring and surface preparation are needed. Minimizing the damage due to these operations is an important step in specimen preparation. Equipment for coring and a cylindrical specimen cored out of the brick without sawing is shown in Fig. 3.6. As far as preparing the end surfaces for testing, sawing of the end surfaces is preferred to high temperature capping and grinding, and was adopted as a standard for preparation. The sawing was done on an automatic slow-speed diamond saw, as a constant feed rate of 5/100 cm (20/1000 in.) per minute.

3.2.3 Thermomechanical Testing Programs

The thermomechanical testing program focuses on uniaxial compressive load tests with elevated temperatures.

Two categories of short-term compressive load tests are carried out on each material type:

1. Perform short-term uniaxial monotonic compressive loading tests at predetermined constant temperature levels in the range of 70°F to 2400°F.

2. Perform short-term constant compressive load tests (P between 40% and 75% of compressive strength) at predetermined constant temperature levels in the range of 70°F to 2400°F.

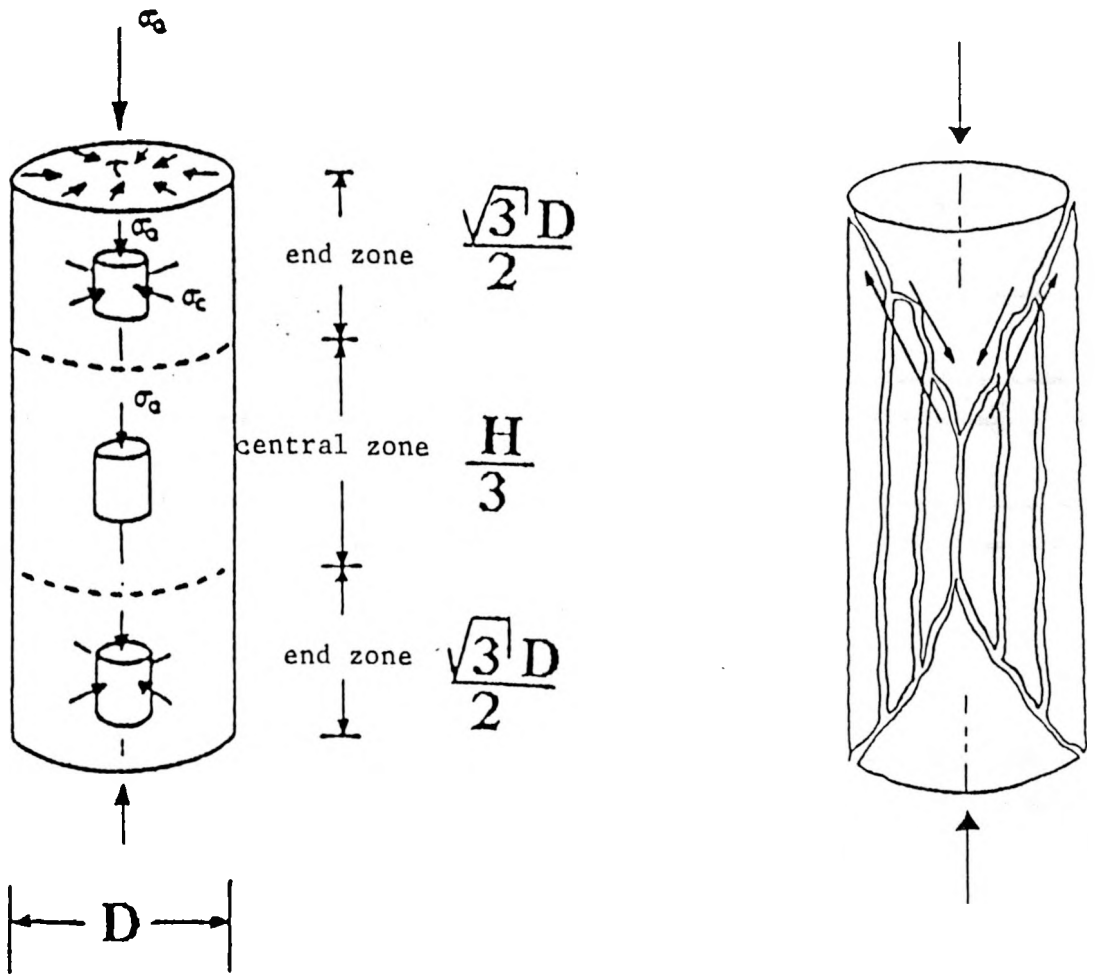

Figure 3-5: Behavior of a Cylinder under Uniaxial Compressive Loading (Kotsovos, 1983; Van Mier, 1984)

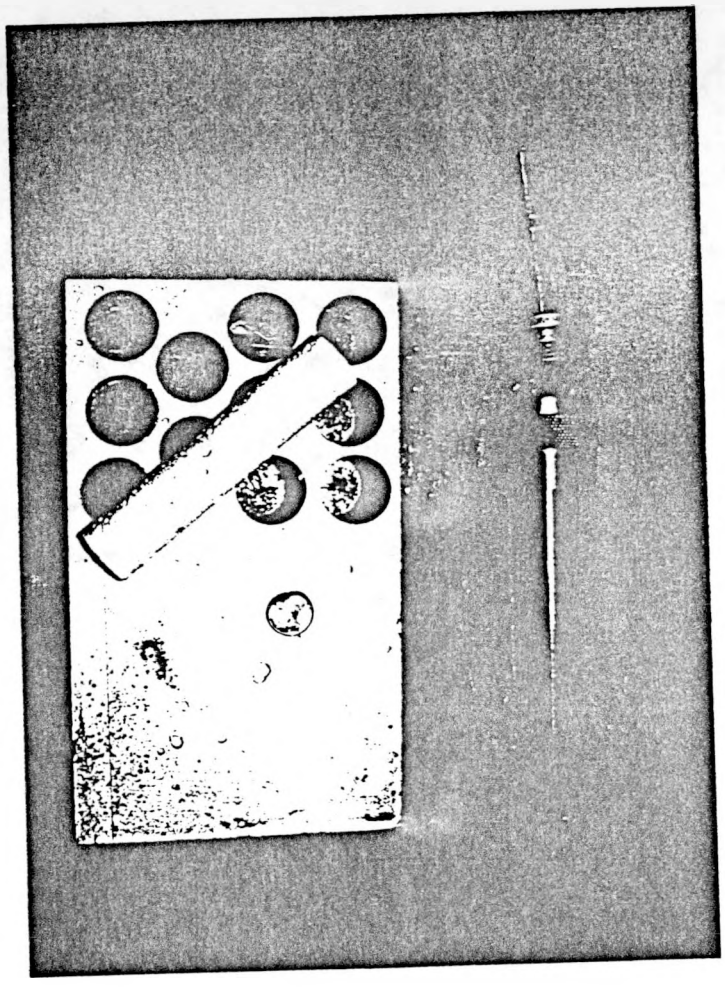

Figure 3-6: Coring Equipments and a Cylindrical Specimen Cored out of a Brick

A constant displecement rate (7.218×10^{-5} in/sec) was used for all monotonic compressive tests. To achieve a constant temperature level, after 250°F/hr temperature rate was used to increase temperature up to the desired level, the constant temperature maintained for $2\frac{1}{2}$ hours to ensure a uniform temperature around the specimen.

For the creep tests, several ranges of stresses and temperatures were used. Temperatures higher than 40% of the melting temperature were chosen.

The following explains the details of the test program.

Category 1 : Monotonically Increasing Displacement Tests

1. Material CPS-90A-10C (Dense Brick)

   Displacement rate = 7.218×10^{-5} in/sec

   Temperature levels = 75°F, 500°F, 1000°F, 1500°F, 2000°F, 2200°F, 2440°F.

2. Material CPS-82C-18M (Dense Brick)

   Displacement rate = 7.218×10^{-5} in/sec

   Temperature levels = 75°F, 500°F, 1000°F, 1500°F, 2000°F, 2275°F, 2400°F.

3. Material DC-95A-5Ca (Dense Castable)

   Displacement rate = 7.218×10^{-5} in/sec

   Temperature levels = 75°F, 500°F, 1000°F, 1500°F, 2000°F, 2400°F.

4. Material IC-55A-36S (Insulating Castable)

   Displacement rate = 7.218×10^{-5} in/sec

   Temperature levels = 75°F, 500°F, 1000°F, 1500°F, 1750°F, 2000°F.

5. Material IB-39A-44S (Insulating Firebrick)

   Displacement rate = 7.218×10^{-5} in/sec

   Temperature levels = 75°F, 500°F, 1000°F, 1500°F.

Category 2 : Constant Load, Constant Temperature Tests

1. Material CPS-90A-10C (Dense Brick)

   Constant load levels : 50% - 70% of compressive strength (f_p).

   Temperature levels = 1500°F, 2000°F, 2400°F.

2. Material DC-95A-5Ca (Dense Castable)

   Constant load levels : 55% - 71% of f_p.

   Temperature levels = 1000°F, 1500°F, 2000°F.

3. Material IC-55A-36S (Insulating Castable)

   Constant load levels : 40% - 70% of f_p.

   Temperature levels = 1000°F, 1500°F.

The total testing program represents over 50 tests. Most test cases in each category contain more than two tests carried out to confirm the results.

3.3 PROBLEMS RELATED TO THE TESTING

3.3.1 Introduction

The need for high strength materials at elevated temperatures has increased significantly in recent years. This has motivated the use of brittle materials as structural components. Brittle materials exhibit an inherent variation in their properties. There is a need for experimental work to carefully assess the effects of the specimen preparation, test methods, and the data interpretation. Care must be excercised in the interpretation of the significance of material property determinations since some material properties are not fundamental or intrinsic. Values obtained will depend on size and shape of the specimen, batching, mixing procedures, the method of sampling, and moisture conditions during

curing. It should be established that the test results represent the real material behavior, and that any variability in the results is an inherent material property. There is also a need to consider the inherent variability of the material properties obtained from laboratory specimens in the design and analysis of structures. Two types of variation are distinguished (Tamer and Buyukozturk, 1988). The first is with respect to the variation of mateiral properties at different locations and directions in the brick, and variation between bricks taken from the same production batch, and bricks taken from different production batches. This type variation is for brick property characterization. The second type of variation considered is for the specimens taken from similar location and direction from the brick, using similar sampling method with respect to a specific production batch. The type of variation in the material behavior is interpreted as inherent property variability found in the brittle materials.

The factors affecting the properties of materials in the preparation of a test specimen are summarized in Section 3.3.2. The studies of the size effect on the properties of brittle materials are controversial. ASTM (1989) and ACI code (1983) have their restriction of the diameter of the specimen related to the maximum size of the aggregate, and height ratio to the diameter. The size of the specimen was also found to be related to the end effects in compression testing. The effect of machining of the specimen is also important, and is illustrated by studies of residual stresses in ground ceramic surfaces (Johnson-Walls and Evans, 1986).

In Sections 3.3.3 and 3.3.4, the effects of test procedure, test machine, and interpretation of test results on the assessment of the mechanical properties of refractories used in the high temeprature vessels are discussed. The design and analysis of these high temperature and high pressure coal gasifiers require the development of a thermomechanical and thermophysical material data-base and modeling tools. It is essential that the properties obtained represent the real behavior of the material as closely as possible, and that the

designer be aware of the inherent variation in these properties.

3.3.2 Problems in the Preparation of Specimens

The factors affecting the properties of the materials in the preparation of a test specimen are: (1) specimen's shape and dimensions; (2) the coring speed; (3) the end-surface preparation. In the case of slag-present, the slag-impregnation procedure is also an important factor.

The main considerations in choosing the specimen shape are:

1. Obtaining temperature uniformity around the specimen for high temperature test using a circular heat zone.

2. Obtaining load uniformity over the cross-section, and

3. Minimizing end effects.

ASTM(1989) recommends a rectangular STET for standard test methods for cold crushing strength and MOR for refractory materials. The recommended size is a 9 by $4\frac{1}{2}$ by $2\frac{1}{2}$ (or 3) inches for cold crushing strength for all kinds of refractory bricks. Another test standard for insulating firebrick in ASTM is to use a $4\frac{1}{2}$ by $4\frac{1}{2}$ by $2\frac{1}{2}$ (or 3) inches rectangular specimen loaded perpendicular to the $4\frac{1}{2}$ by $4\frac{1}{2}$ inches surface. It may be because the high porosity of insulating firebrick requires a test that differs from the procedure used for dense refractory brick. For the current tests at elevated temepratures, however, a cylindrial specimen was preferred to a rectangular one due to the conditions specified above.

The diameter of the specimen is recommended with the consideration of the size of the largest aggregate or the largest air-void present in the specimen. American Society for Testing and Materials (ASTM, 1989) specifies the diameter as 3 to 4 times the size of

the largest aggregate in concrete. ACI code (1983) recommends the diameter as 5 times the size of the largest aggregate in concrete. Among the dense bricks, CPS-90A-10C has fused grains of alumina that are 0.85 cm (1/3 in.) long. For the CPS-82C-18M the largest aggregates are picochromite grains with 0.64 cm (1/4 in.) length. A one inch diameter was chosen to comply with the minimum required size imposed by the ASTM. For castable materials DC-95A-5Ca and IC-55A-36S and the insulating firebrick IB-39A-44S, air-voids were usually larger than the size specified by ASTM. Therefore, the largest size of air-void exposed on surfaces were checked in preparing specimens.

For the height of the specimen, the ratio of the height to diameter (H/D) is important. The influence of constraints between loading platens and the specimen is well understood. An increase of the specimen height H, leading to H/D-values of 2.5 to 3, results in a bounding value for the uniaxial compressive strength. For higher values of H/D no further decrease of strength was observed. Decreasing the ratio H/D however would lead to a sharp increase of measured strength (Van Mier, 1984). The height of the specimen is determined in such a way that a central zone of near-uniform uniaxial compressive stress exists as shown in Fig. 3.5. ASTM recommends to use the size of the height as twice as that of the diameter of a concrete specimen (ASTM, 1989).

In order to extract a cylindrical specimen from the brick, coring and surface preparation are needed. To minimize the damage due to these operations a constant and appropriate coring speed is required to obtain a sufficient strength. Strength variations according to the different coring speeds were investigated and are presented in Fig. 3.7 and Fig. 3.8 (Tamer and Buyukozturk, 1988).

With respect to the preparation of the end surfaces for testing, sawing of the end surfaces is preferred to high-temperature capping and grinding. Since the specimen deformation is obtained by subtracting the load train deformation from the total deformation, high-temperature capping is not desirable. The high-temperature capping would deform under load at high temperature, thus, introducing errors in the system calibra-

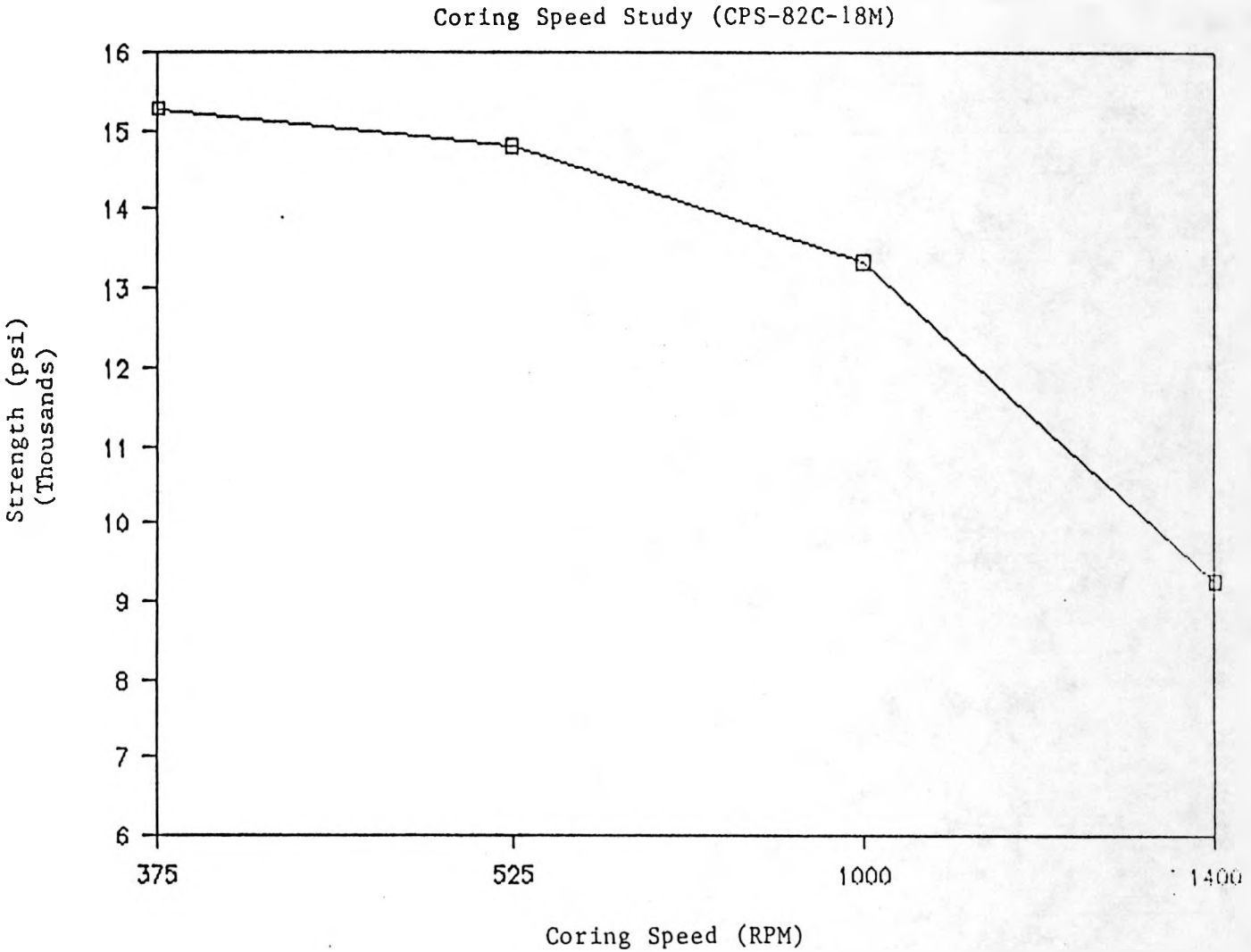

Figure 3-7: Strength Values at Different Coring Speeds

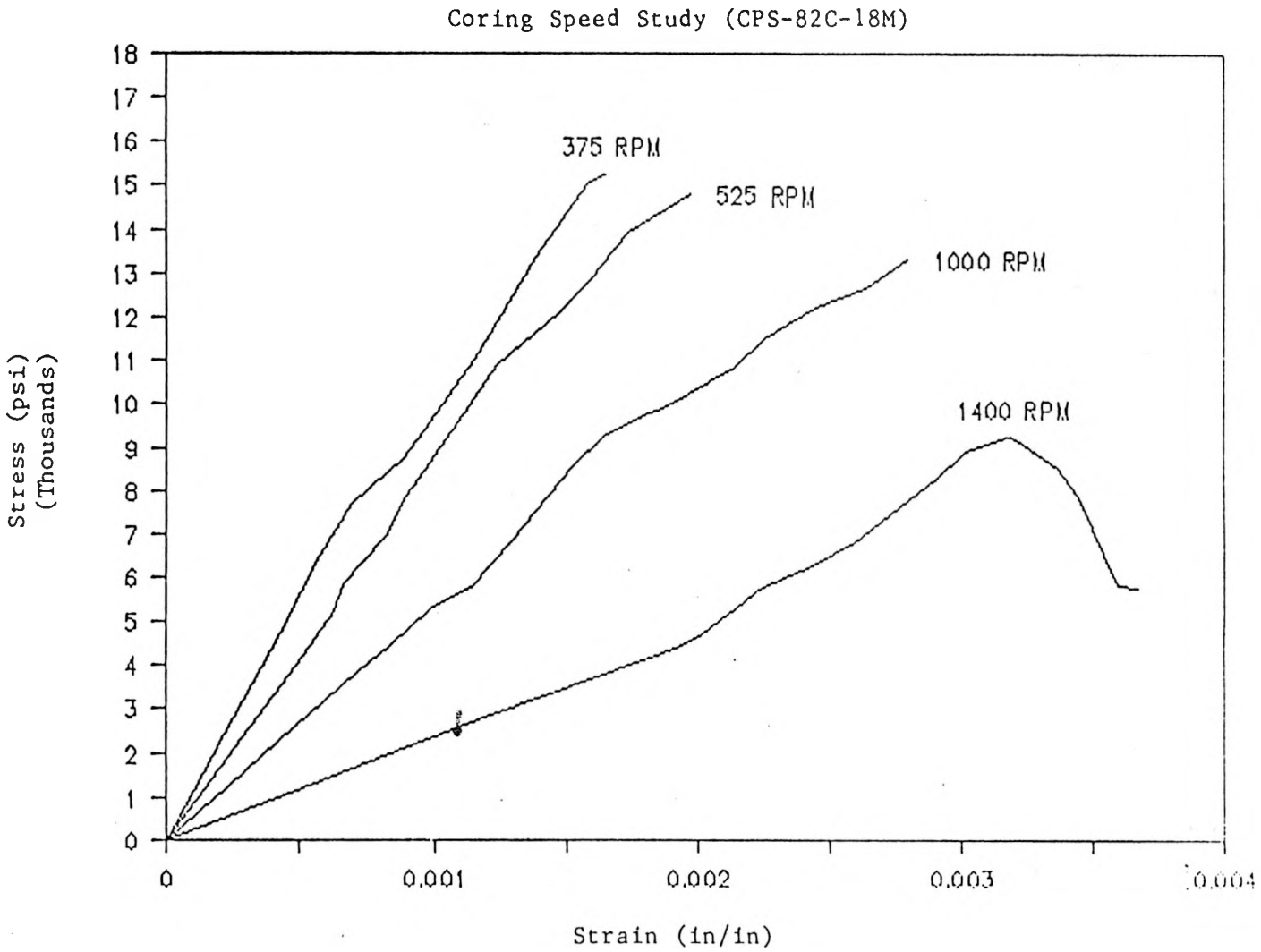

Figure 3-8: Stress-strain Curves at Different Coring Speeds

tion. Grinding of the specimen end surfaces is not used since it may cause grains at the surface to separate, and produce chipping at the specimen edges. Therefore, sawing of the specimen ends to produce parallel and smooth surfaces for testing was adopted as a standard for testing.

3.3.3 Problems in Test Machine

The strength and deformational response will depend to a large extend on the lay-out of the experimental machine, and the boundary condition of the loading application system (Van Mier, 1984).

Regarding the application system, two major boundary conditions can be distinguished. Either we can choose for a uniform stress distribution along the specimen boundary, or we can choose for a uniform boundary displacement (Fig. 3.9).

Under the condition of uniform boundary stress, the normal stress-distribution in the specimen will be very well defined. However, the displacements will be less smoothly distributed, and will take a form dependent on the grain distribution within the specimen. A uniform boundary stress can be obtained by means of a loading application system with zero-shear-stiffness. The displacements can be obtained by averaging them. In this system no shear forces are developed at the specimen-loading system interface, while shear deformation of the specimen is allowed.

The uniform boundary displacement can be applied to the specimen when an infinitely stiff system like dry platen is used. In this case a non-uniform stress-distribution will emerge and only an average strength can be determined under the assumption that both loading platens are fixed. A typical failure mode for the infinitely stiff platen with a specimen of H/D ratio between 2.5 and 3 is shown in Fig. 3.5. Due to the triaxial compressive stress-state in the end zone, microcracks may initiate and propagate along the boundaries of these relatively stiff zones. A split action is usually induced in the central part of the cylinder, resulting in a decreasing strength when compared to less

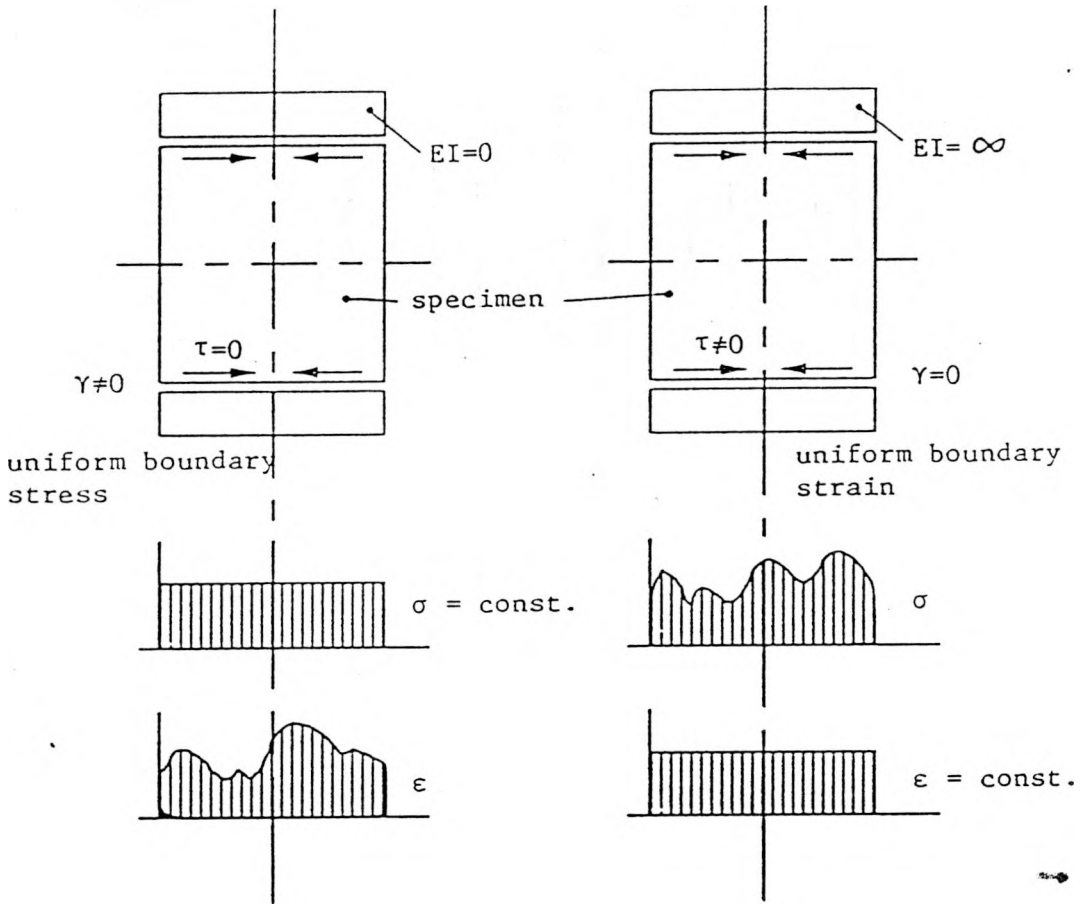

Figure 3-9: Boundary Conditions in the Testing of Material Stress-strain Response (Van Mier, 1984)

slender specimens. It may be assumed that the results obtained from such specimens, loaded between rigid platens, do not represent the "true" material behavior (Van Mier, 1984). For insulating firebrick material IB-39A-44S, however, the failure mode was totally different. Because of its high porosity due to the firing manufacturing method, the inside structure of IB-39A-44S is like a form material. Therefore, IB-39A-44S specimens were failed by crushing leading to the perfect elastic-plastic behavior in stress-strain relationship.

To arrive at a uniform stress state within the specimen and to reduce the constraints between loading application device and specimen, many loading application systems with more or less boundary conditions have been developed (Newman, 1979). Those are (a) rigid steel plate without friction reducing measures; (b) rigid loading plate with friction reducing measures by means of intermediate layers; (c) loading through non-rigid platens; and (d) fluid cushions.

The most desirable requirements for choosing a loading application system are; (1) unconstrained boundary conditions are necessary in order to obtain strength and deformation results with limited scatter; and (2) friction reducing measures are needed to acquire reliable strength results and also for measuring correct stress-strain relationships. The most effective device satisfying the requirements may be brushing bearing plates (Buyukozturk et al., 1972; Van Mier, 1984; Chen et al., 1985). For the present research, however, a rigid Silicon-cabide cylindrical rod and a high purity alumina cylinder were chosen because of the high temperature limitation as shown in Fig. 3.2.

3.3.4 Problem in Data Interpretation

Eibl states: *"The fact that a priori known experimental results, especially load-deformation relations can be described after the experiment has taken place, should not be overestimated. Everybody doing such calculations knows how many parameter changes are possible and sometimes done to gain such data - fit."* (Eibl, 1981).

This statement explains well the importance of the data interpretation. The final test results can be different according to the method used for interpreting the data obtained from the experiment.

Forces were measured by means of calibrated load cells installed in an MTS testing machine. The available scales of load cells are 10, 20, 50, and 100 kips. Among these scales, 10 and 20 kips were used for the proposed test. For each load scale, ± 10 Volts represent the maximum and minimum load of that scale (i.e. in 20 kips scale, 2-volts is equivalent to 4 kips). Therefore, final forces, which were measured as electric voltages at first, were converted to the real forces by simple calculation. The load-cells have been checked carefully by a technician from MTS company.

Deformations were measured as the movement of the lower loading platen of the MTS machine, while the upper platen was fixed (Fig. 3.1). The scales of displacement are 10, 20, 50, and 100 mm. Among these only 10 mm scale was used for the tests. For deformation, ± 10 volts also represent the maximum or minimum displacement of the current scale, and the electric voltage results were converted to the real diplacements. Because of the difficulties from high temperature, more accurate deformation measurements (such as LVDT) and a direct strain measurement could not be used. Therefore, the stroke-control (constant displacement of loading application system) was chosen as the controlling option. This stroke-control acts actually somewhere between the load-control and the strain-control. With the consideration of the deformation of the loading system at elevated temperatures, real deformations were calculated by subtracting the deformation of the system itself at each high temperature level from the deformations measured ($\delta = \delta_{measured} - \delta_{system}$). Prior to the main tests, the system's deformation at each high temperature level was measured without a specimen, and was converted to cubic-polynomial equations as a function of load.

Stress and strain were calculated by dividing the obtained forces and displacements by the area and height of the specimen, respectively. When a stress-strain curve was derived,

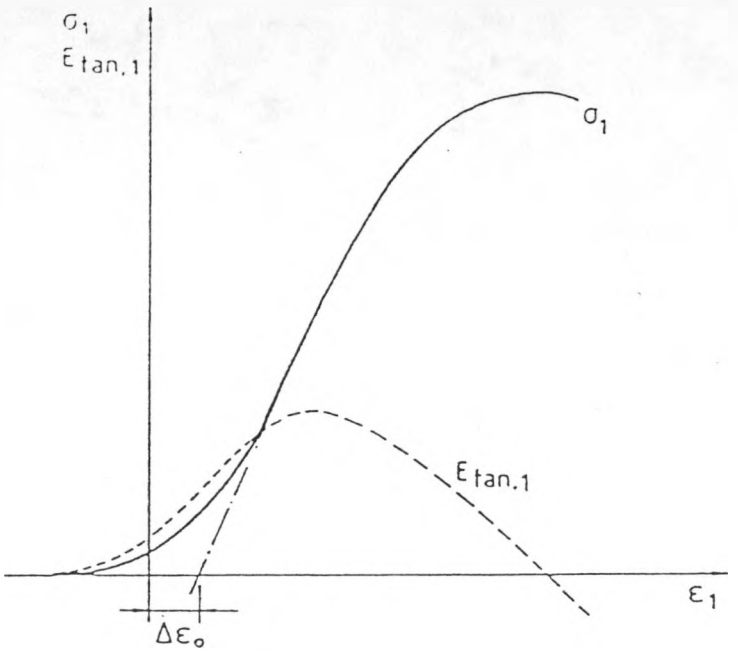

Figure 3-10: Zero-correction for Stress-strain Curves (Van Mier, 1984)

a small 'initial run' was always observed as shown in Fig. 3.10. An overestimation of initial deformation is the result of non-smoothness of specimen and the loading plate surface that are in contact, and the friction between them (Van Mier, 1984). A zero correction (transition along the ϵ-axis) was carried out to the stress-strain curve by calculating the maximum slope in the ascending branch. The zero strain was calculated from the maximum slope and the stress-level of which it was measured as shown in Fig. 3.10.

Chapter 4

HIGH-ALUMINA AND HIGH-CHROMIA DENSE BRICK MATERIALS

4.1 SYNOPSIS

This chapter reviews the behaviors of cold-pressed sintered high-alumina CPS-90A-10C and high-chromia CPS-82C-18M dense brick refractories at elevated temperatures, and discusses the results of compressive tests done at MIT (Tamer and Buyukozturk, 1988). The elevated temperature behavior under short-term compressive loads is discussed in Section 4.2 and 4.3. In Section 4.2, the thermomechanical behavior of dense brick refractories under monotonic uniaxial compressive loading at constant temperatures is presented. The behavior under constant compressive loads at constant temperature is presented in Section 4.3. These thermomechanical properties and additional information including thermophysical properties are summarized in Appendix A.1.

4.2 THERMOMECHANICAL BEHAVIOR UNDER MONOTONIC UNIAXIAL COMPRESSIVE LOADS AT CONSTANT TEMPERATURES

Effects of temperature on the behavior of materials CPS-90A-10C and CPS-82C-18M under monotonically increasing uniaxial compressive loading with constant displacement rate (7.218×10^{-5} in/sec) were studied. Cylindrical specimens with 1 inch diameter and 2.5-3.0 inch height were used as the standard specimen. The specimens were prepared by coring them out of the cold-pressed sintered refractory bricks, and prepared for testing by automatic slow-speed sawing on both end surfaces. Stress-strain curves for different temperature levels are shown in Fig. 4.1 and 4.2, for materials CPS-90A-10C and CPS-82C-18M, respectively.

For both of these materials, two distinct deformation and fracture behavioral regions are identified with respect to temperature. There appears to be a transition temperature that separates these behavioral regions, and this transition temperature is found to correspond to about one-half the melting point of the material. The two distinct behavioral trends are :

1. For temperature levels below roughly 1/2 T_M (where T_M is the melting temperature of the material), the deformation behavior is linear elastic with a brittle fracture. A sudden fracture of the specimen was observed at a load level corresponding to the peak stress on the stress-strain curve, and thus, no post-peak behavior was obtained.

2. At temperature levels between 0.5 T_M and 0.7 T_M (tests were limited to a maximum temperature level of 0.7 T_M for these cases), the deformation behavior of the material is initially linear, but exhibits significant non-linearities at stress levels close to the peak strength. In the post-peak region, the observed non-linear

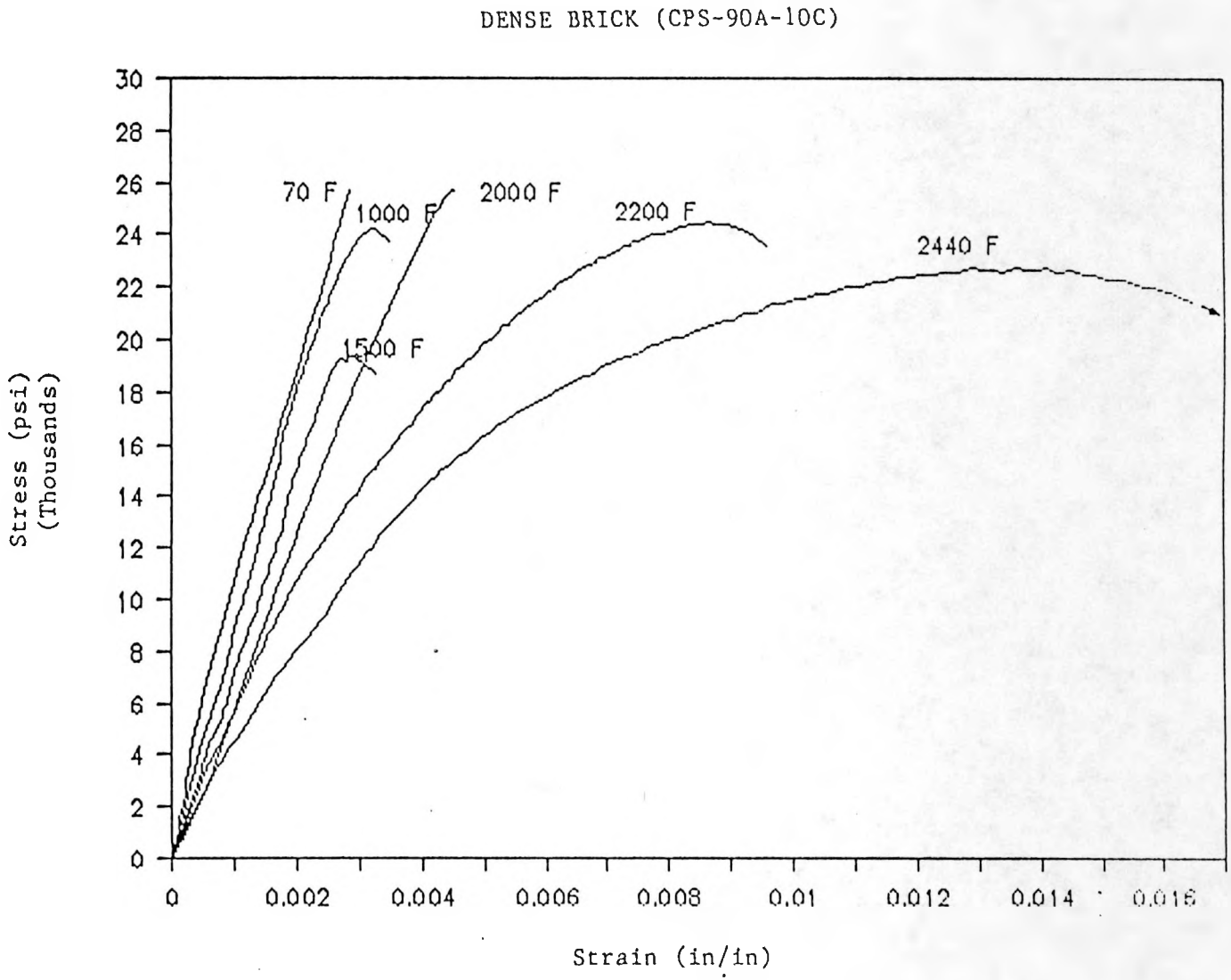

Figure 4-1: Stress-strain curves for CPS-90A-10C at different temperature levels and a constant displacement rate of 7.218×10^{-5} in/sec

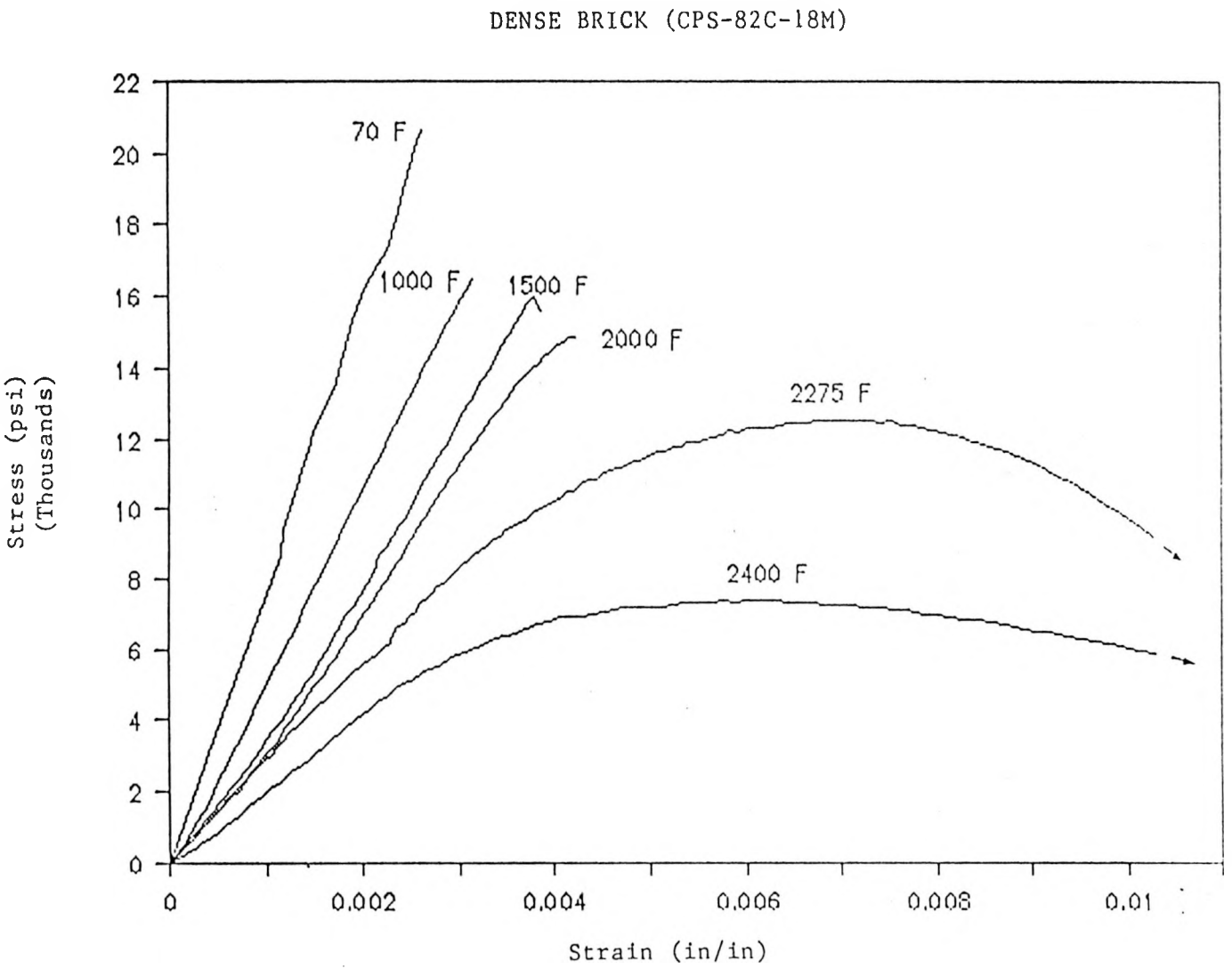

Figure 4-2: Stress-strain curves for CPS-82C-18M at differernt temperature levels and a constant displacement rate of 7.218×10^{-5} in/sec

deformations are even more pronounced.

The strain rate effect at different temperature levels was also studied for both materials. It was determined that the material behavior at temperatures below $T_M/2$ is essentially strain-rate independent in the range from 10^{-4} to 10^{-6} sec^{-1}. However, the strain rate at temperatures above $T_M/2$ was investigated to determine its effect the material behavior; such as the strength, the associated peak strain, the initial modulus, and the post-peak behavior in stress-strain curve, etc..

To define the thermomechanical properties of refractories quantitatively, some specific material characteristics, such as strength, the initial slope of the stress-strain curve, the associated peak strain, and the equivalent toughness defined as the area under the stress-strain curve were studied.

The strength of the dense brick material CPS-82C-18M seems to follow two different mechanisms as shown in Fig. 4.3: a slight decrease in strength with temperature was observed for temperatures below 0.5 T_M, followed by an increased rate of decrease in strength for temepratures above 0.5 T_M.

For the dense brick material CPS-90A-10C, an increase in strength is observed between 1500°F(816°C) and 2000°F(1093°C) as shown in Fig. 4.4, and the material strength at 2000°F is higher than the room temperature strength. The strength increase at 2000°F represents a 25% increase with respect to the strength at 1500°F. This has been confirmed by 4 tests per case. This increase in strength for intermediate temperatures has been observed for alumina-silica bricks (Miller and Davis, 1966), alumina-cement refractory concrete (Heindl and Post, 1954), low carbon steels (MacGregor and Fisher, 1946), and other mixed refractory oxides (Folk and Bohling, 1968; McCullough and Rigby, 1971). This phenomenon is usually observed in systems containing more than one mineralogical phase. The peak at intermediate temperatures is even more pronounced for systems containing both crystalline and glassy phases.

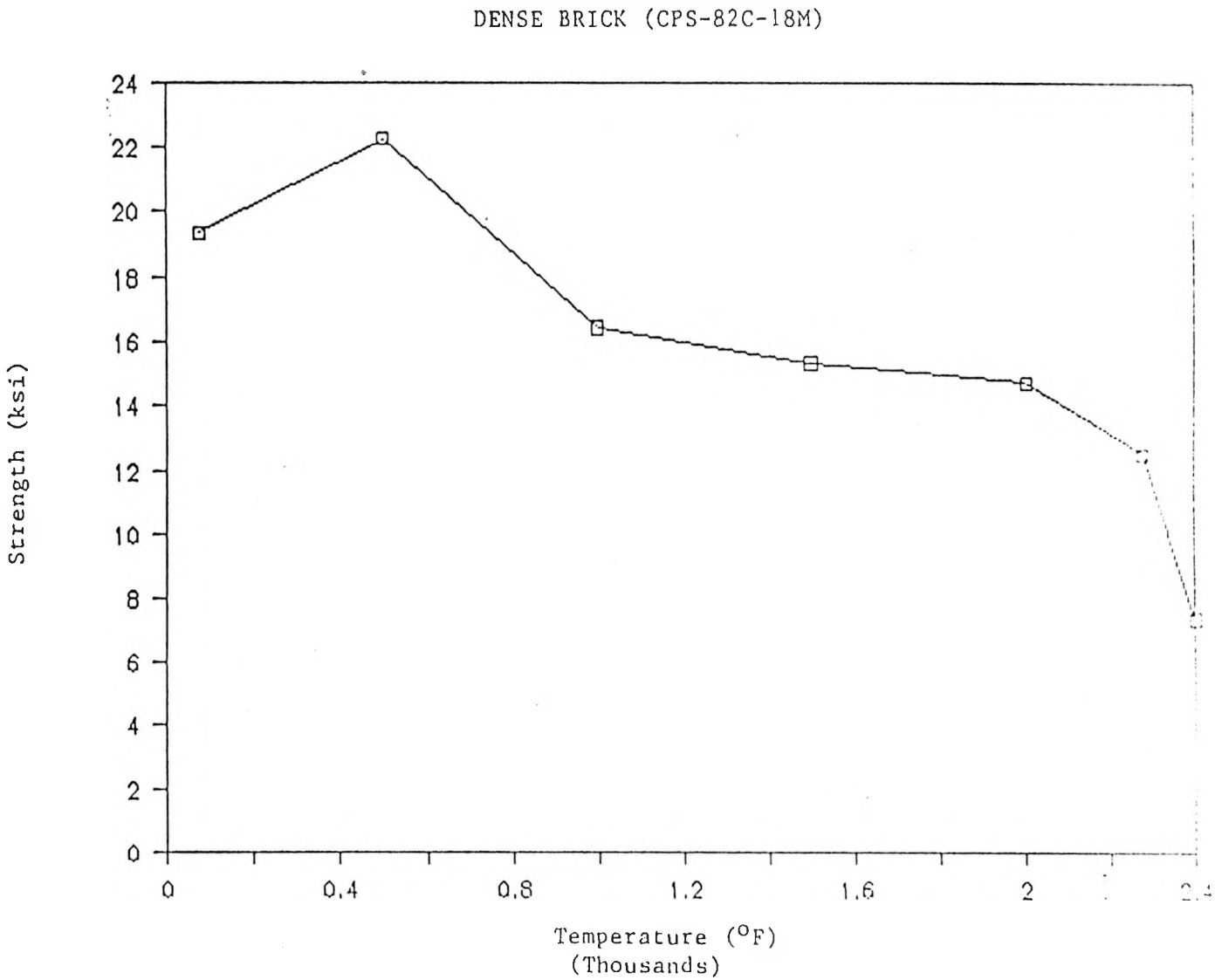

Figure 4-3: Strength Variation with Temperature for CPS-82C-18M

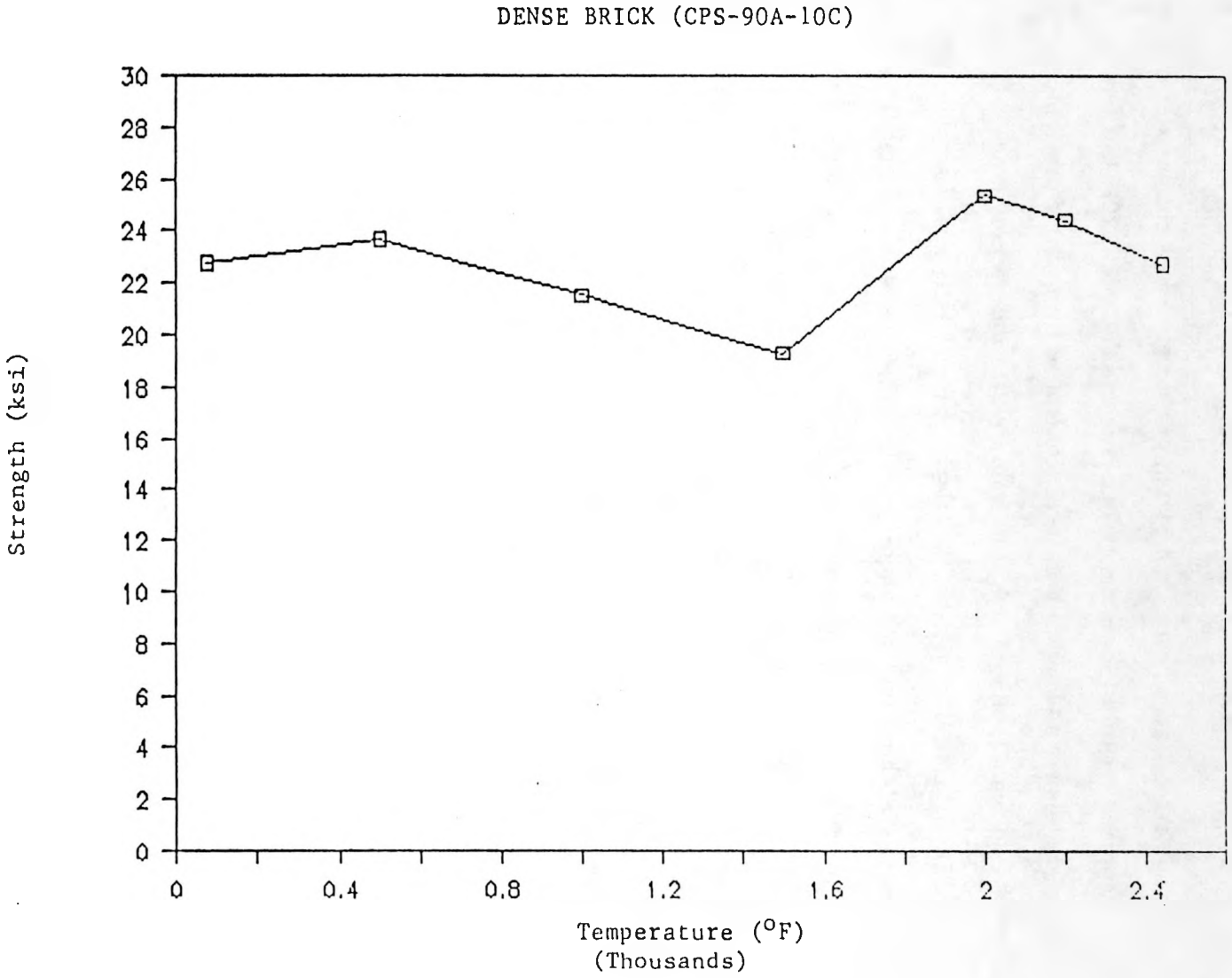

Figure 4-4: Strength Variation with Temperature for CPS-90A-10C

The transition temperature, which separates linear deformation behavior with brittle fracture from a ductile behavior has also been observed for alumina ceramic (Kingery et al., 1976) for which at 2300°F(1260°C) the failure is by fracture, and at 2318°F(1270°C) an upper yield stress and a lower yield plateau are observed. A similar strength variation has been reported for ceramics in general (Evans and Langdon, 1976), where the fracture stress decreases slowly at low temperatures, controlled by a simple crack propagation. At intermediate to high temperatures, the fracture stress decreases much faster, governed by a so-called deformation assisted brittle fracture (Evans and Langdon, 1976). And finally, there is a third region, where ductile fracture occurs at higher temperatures. The present tests appear to represent the first two behaviorial regions for refractory ceramics. The temperature level of 0.5 T_M (which represents the transition temperature in the performed tests) is usually taken as the lower limit for the initiation of diffusional processes.

The initial slope of the stress strain curve decreases sharply with increased temperatures. This is shown in Fig. 4.5 and Fig. 4.6 for material CPS-82C-18M and CPS-90A-10C, respectively. It is difficult to measure true modulus at high temperatures, because of creep contributions as the temperature is raised. In this case the measured modulus is effectively a relaxed modulus. The obtained data is similar to those by other researchers for brittle solids, such as the obtained variation with temperature for Portland Cement concrete (Anderberg and Thelanderson, 1976; Cruz, 1966), and granite rocks (Heuze, 1983). It is found that the ratio of the material's strength to the cubic root of the initial modulus is about constant for temperatures below 0.5 T_M (Tamer and Buyukozturk, 1988).

The variation with temperature of the peak strain values associated with the peak stress, for the material CPS-90A-10C, is studied in Fig. 4.7. The rate of increase in the peak strain is lower for temperatures below 0.5 T_M than those above 0.5 T_M. A similar

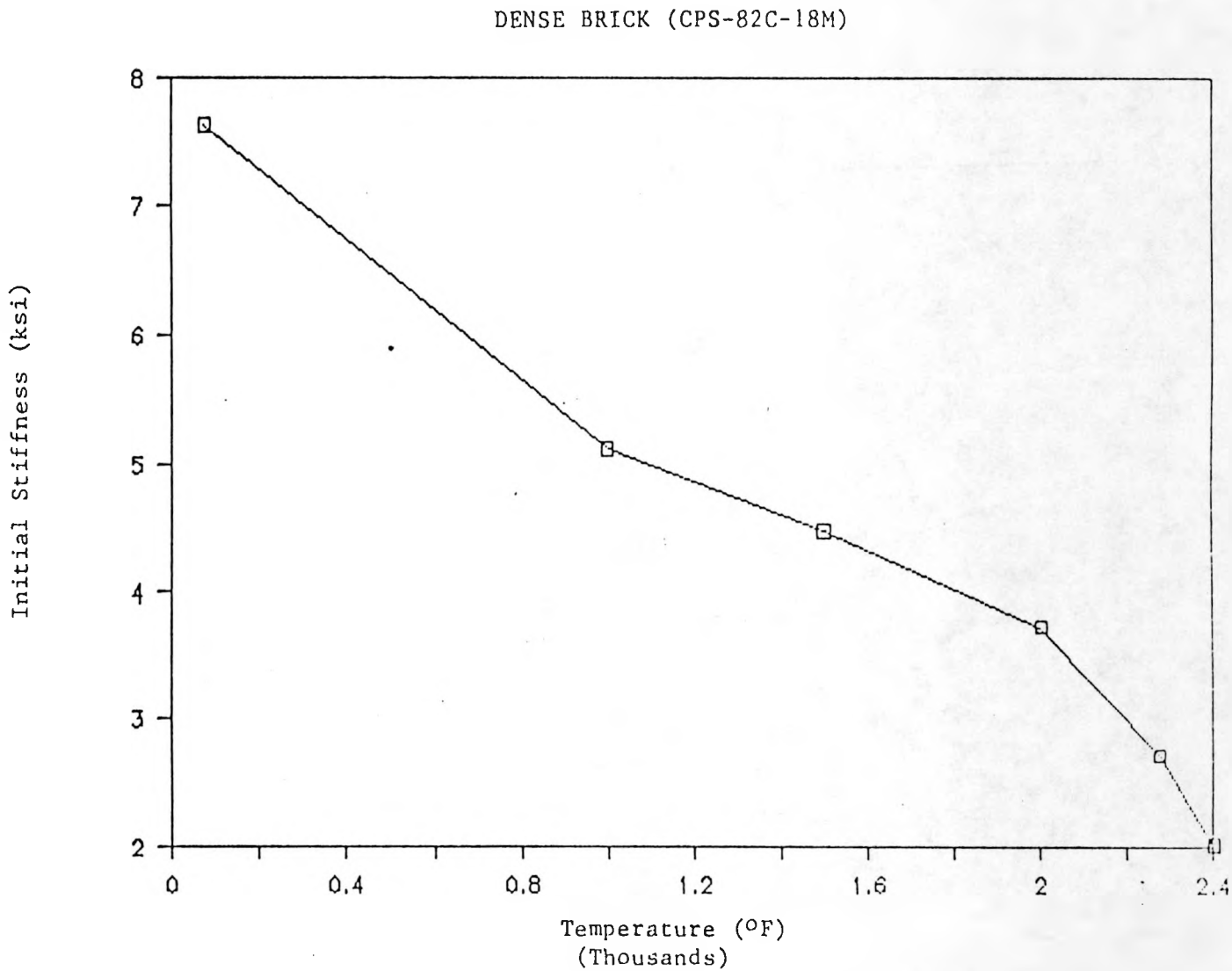

Figure 4-5: Initial Stiffness Variation with Temperature for CPS-82C-18M

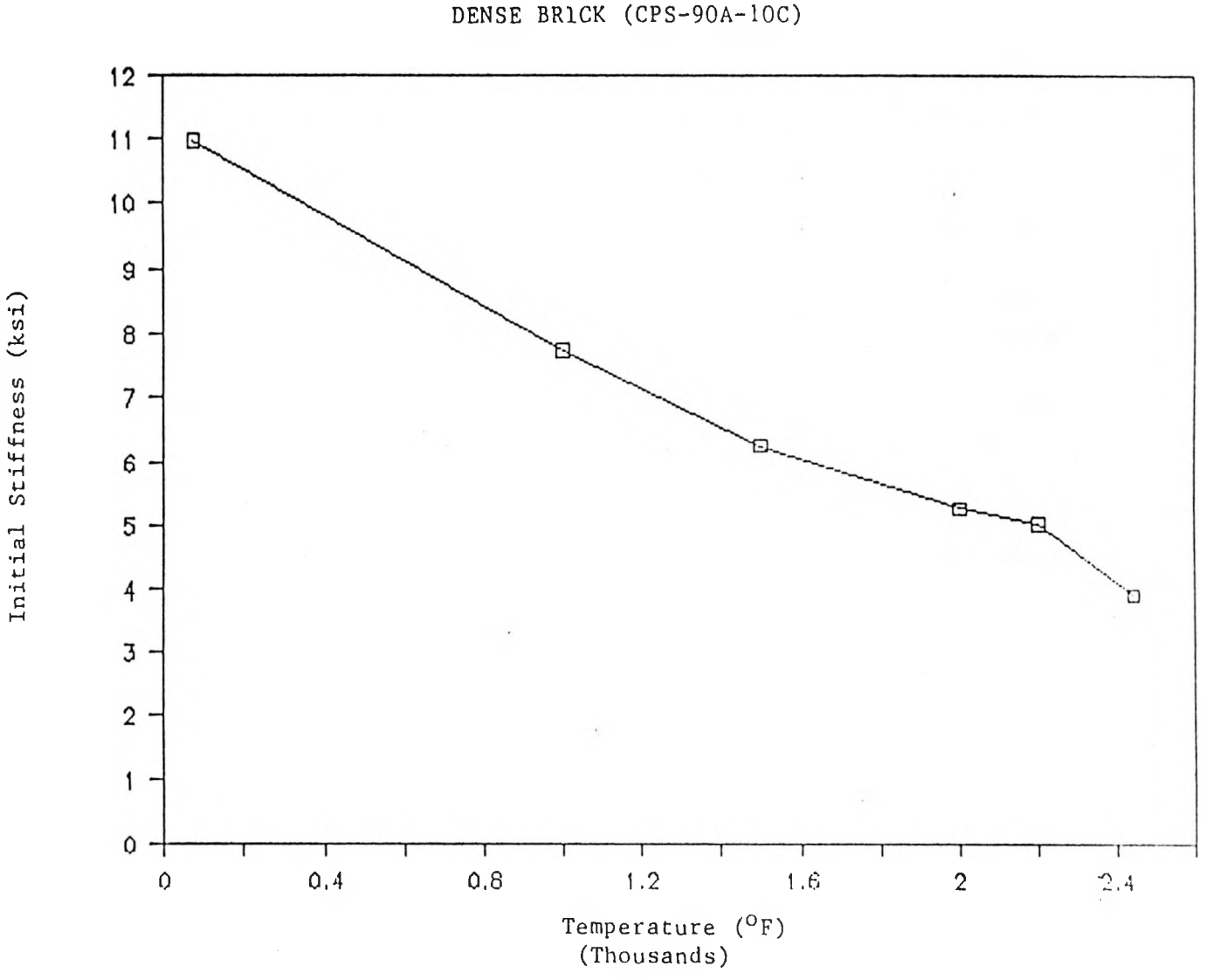

Figure 4-6: Initial Stiffness Variation with Temperature for CPS-90A-10C

behavior is observed for material CPS-82C-18M in Fig. 4.8.

Below 0.5 T_M the specimen fails in a brittle manner. In materials such as metallic glasses (Megusar et al., 1979) this manner could be observed for temperatures below 0.6 T_g (T_g defined as the glass transition temperature). Below 0.5 T_M the associated peak strain and the final fracture strain are equal. For temperature above 0.5 T_M, the final fracture strain is significantly larger than the associated peak strain due to significant non-linear deformations in the post peak region.

The equivalent toughness (defined as the area under the stress strain curve) variation with temperature is shown in Fig. 4.9 for material CPS-82C-18M. The equivalent toughness is approximately constant for temperatures below 0.5 T_M, and increases sharply for temperatures above 0.5 T_M. The reason for this increase may be that although the material strength decreases with higher temperatures, the associated peak strain and the final fracture stain are increasing faster. In the brittle fracture region it is reasonable to assume that the strength is proportional to the equivalent toughness. The slow decrease in strength for temperatures below 0.5 T_M, although the equivalent toughness is about constant, can be attributed to the decrease in the initial stiffness of the stress-strain curve. Similar considerations have been studied for material CPS-90A-10C as shown in Fig. 4.10.

It appears that the variation in the perviously discussed properties is larger at room temperature than at high temperatures. This is observed consistently for both materials CPS-90A-10C and CPS-82C-18M, and is explained by the less brittle behavior of the refractory oxides at higher temperatures.

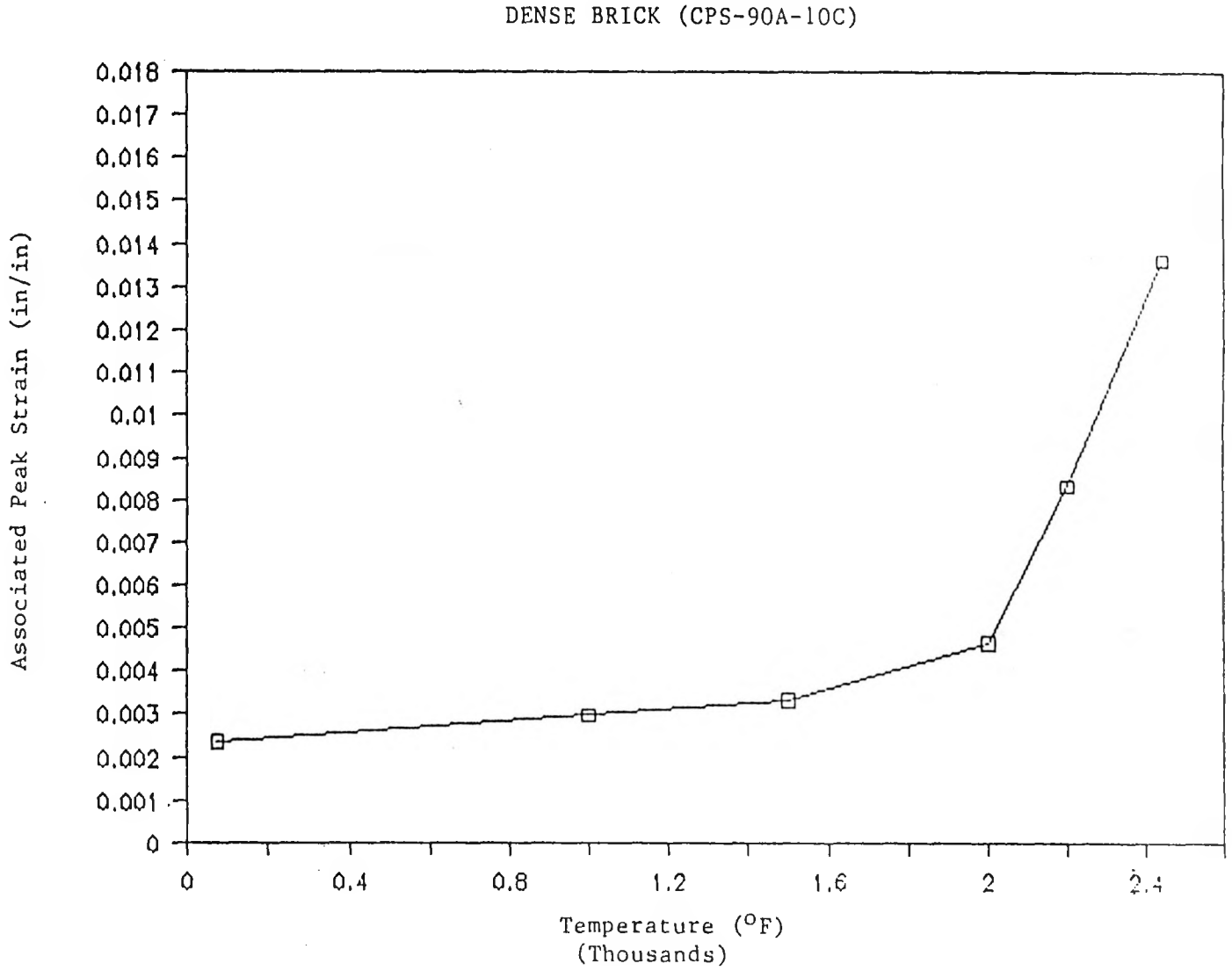

Figure 4-7: Variation of the Associated Peak Strain with Temperature for CPS-90A-10C

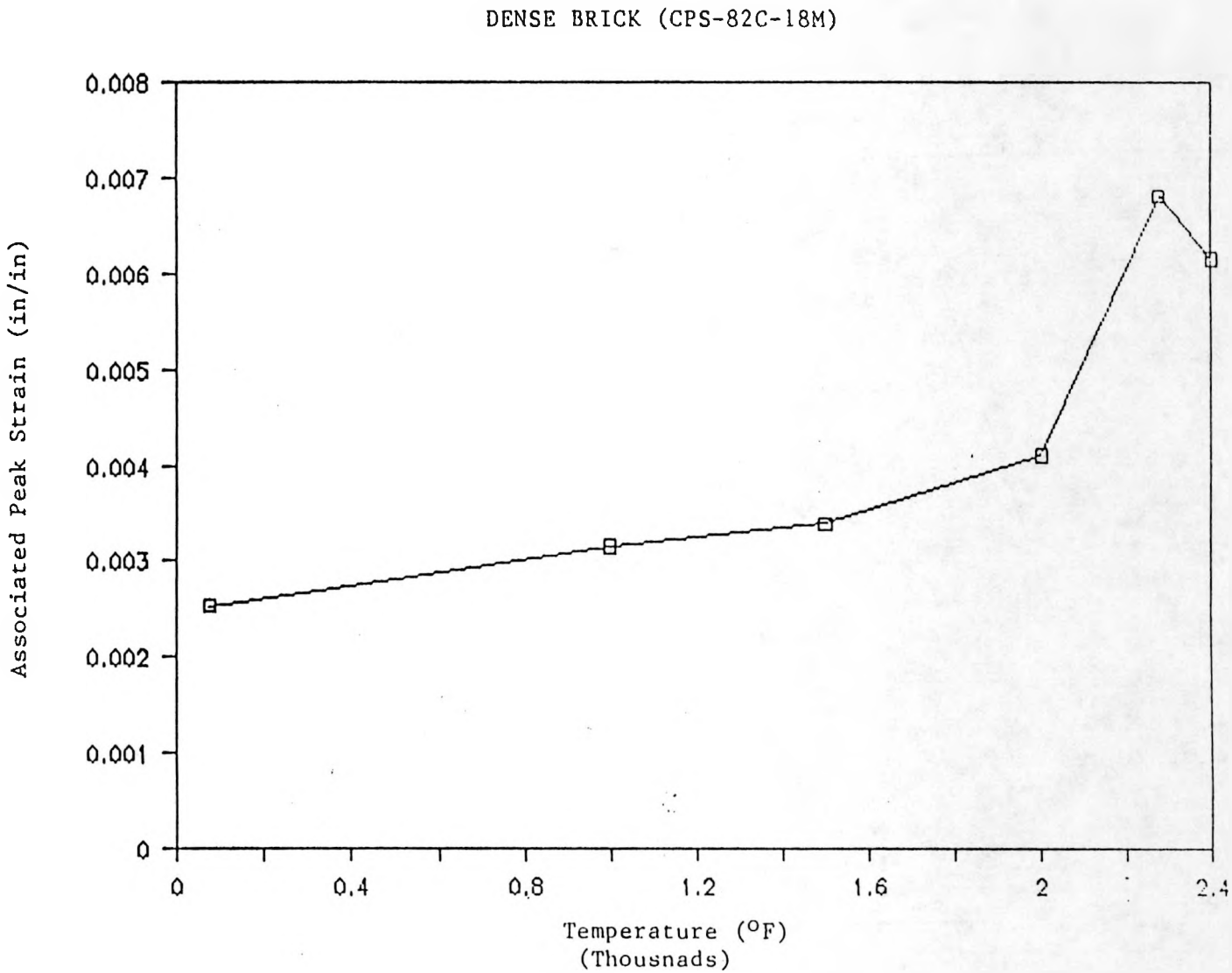

Figure 4-8: Variation of the Associated Peak Strain with Temperature for CPS-82C-18M

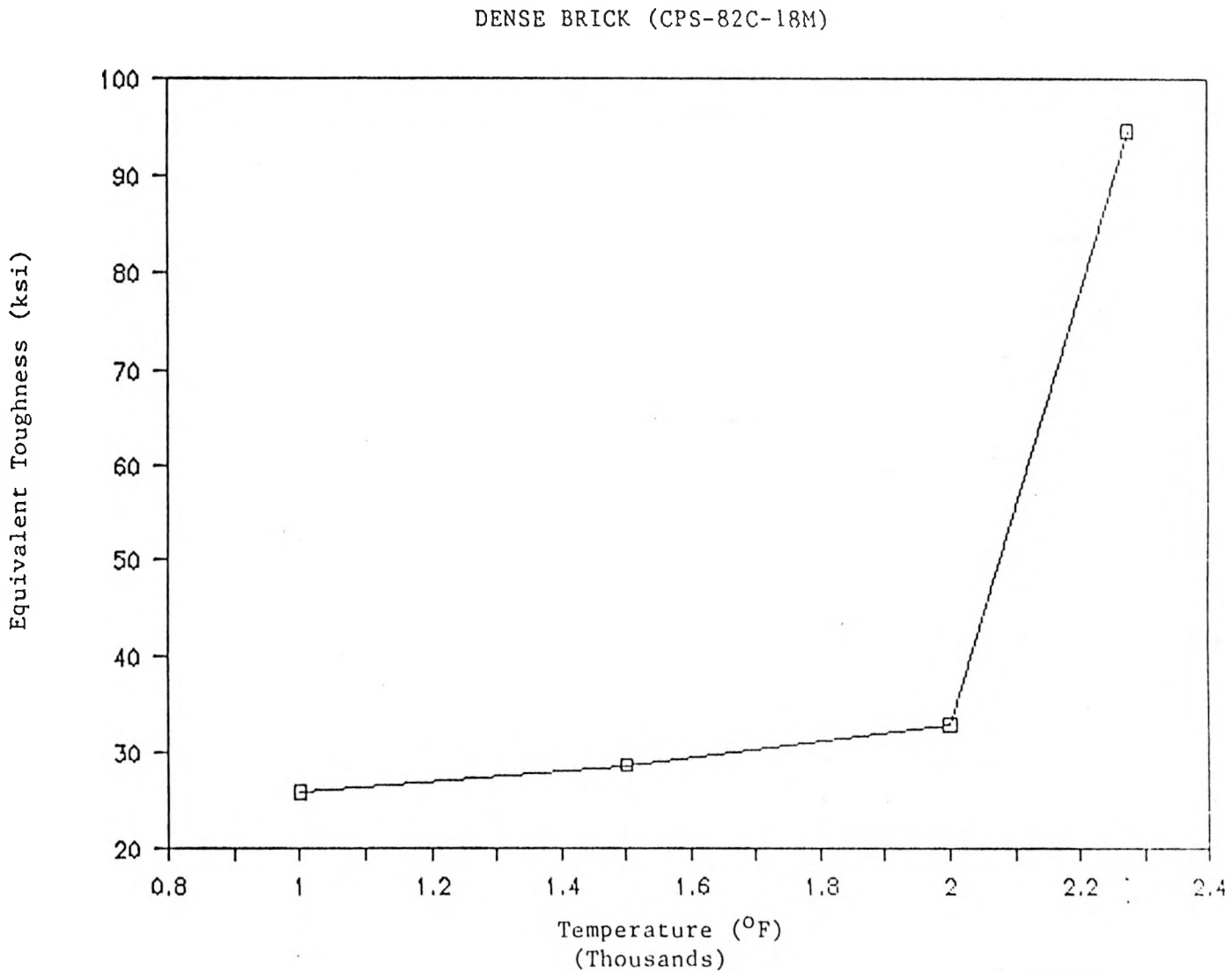

Figure 4-9: Variation of Toughness Measure with Temperature for CPS-82C-18M

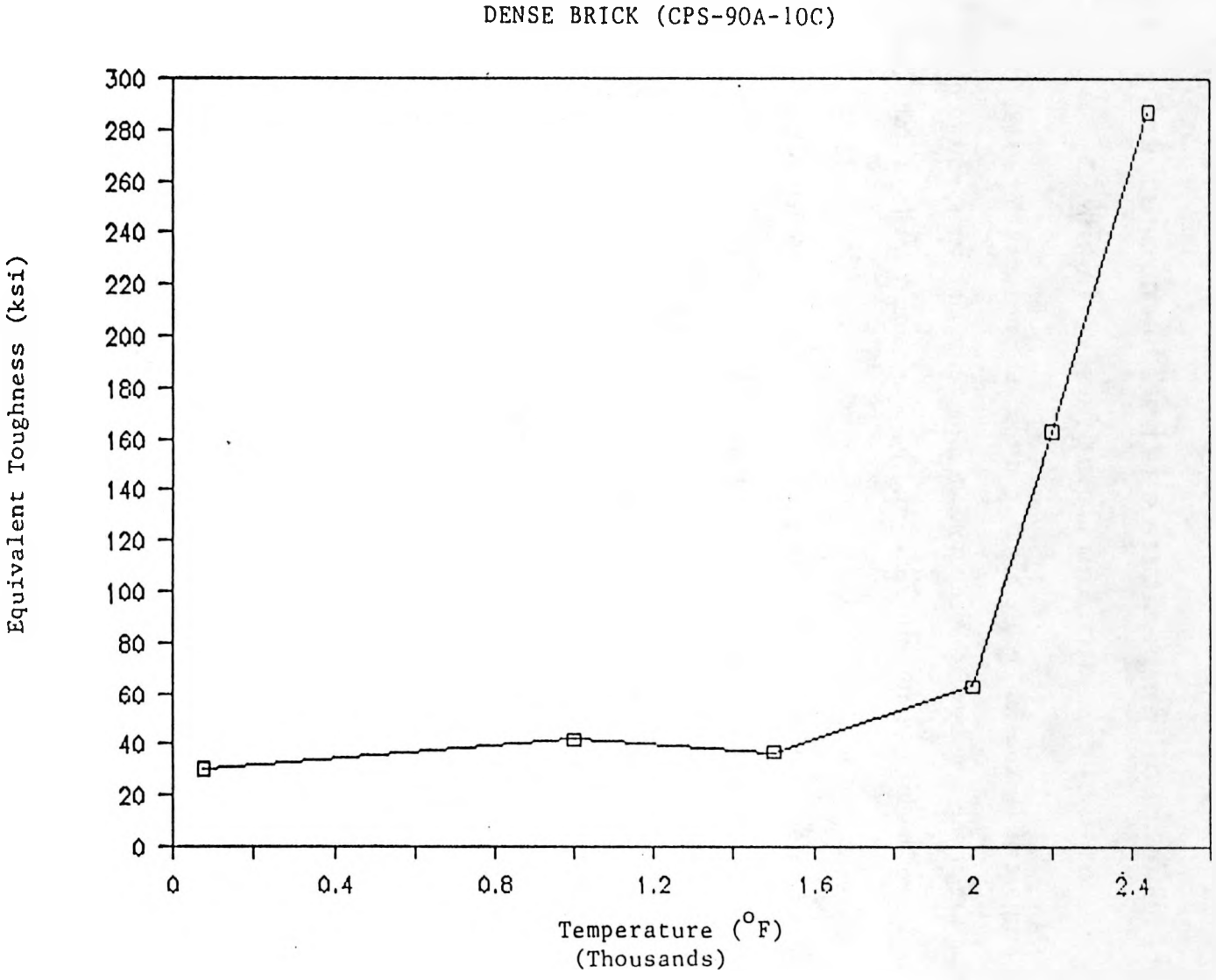

Figure 4-10: Variation of Toughness Measure with Temperature for CPS-90A-10C

4.3 BEHAVIOR UNDER CONSTANT COMPRESSIVE LOADS AT CONSTANT TEMPERATURES

4.3.1 Effects of temperature on the Thermomechanical Behavior Under Constant Compressive Loads

The purpose of the constant compressive load tests at constant temperature was to study the nature of the non-linear deformations in monotonic load tests, and to quantitatively characterize the high temperature material behavior under high constant loads (up to 85% of the monotonic strength). Longer term creep tests carried out by other researchers characterize the behavior of similar materials for constant load levels generally below 15% of the monotonic strength (McGee and Konrady, 83-87).

Figure 4.11 shows the variation of the creep strain for CPS-90A-10C at temperature levels of 1500°F, 2000°F, and 2400°F, under 66%, 55%, and 57% of the uniaxial monotonic compressive strength, respectively. For the tests at 2000°F and 1500°F, the contribution of the short-term creep deformation to the total deformation appears to be negligible. However, at 2400°F the contribution of the creep deformation to the total deformation of monotonic tests seems to be significant. The creep strain rate($\dot{\epsilon}_{creep}$) initially decreases at a fast rate with time, but its variation is slower afterwards. This is shown in Fig. 4.12 where the results are plotted as $\log(\dot{\epsilon}_{creep} \times 10^8)$ vs. time for different temperature levels. The results of the short term creep tests on material CPS-82C-18M are similar to the ones on CPS-90A-10C as shown in Fig. 4.13. The variation of creep strain rate for CPS-82C-18M is shown in Fig. 4.14. It is noted that CPS-82C-18M exhibits higher deformation rates than CPS-90A-10C under short-term creep.

The effect of load histories on the results of short term creep tests is presented in Fig. 4.15. Two specimens of CPS-90A-10C were tested at 2400°F (1316°C). The first one was subjected to a constant load level of 57% of the monotonic strength for 4000

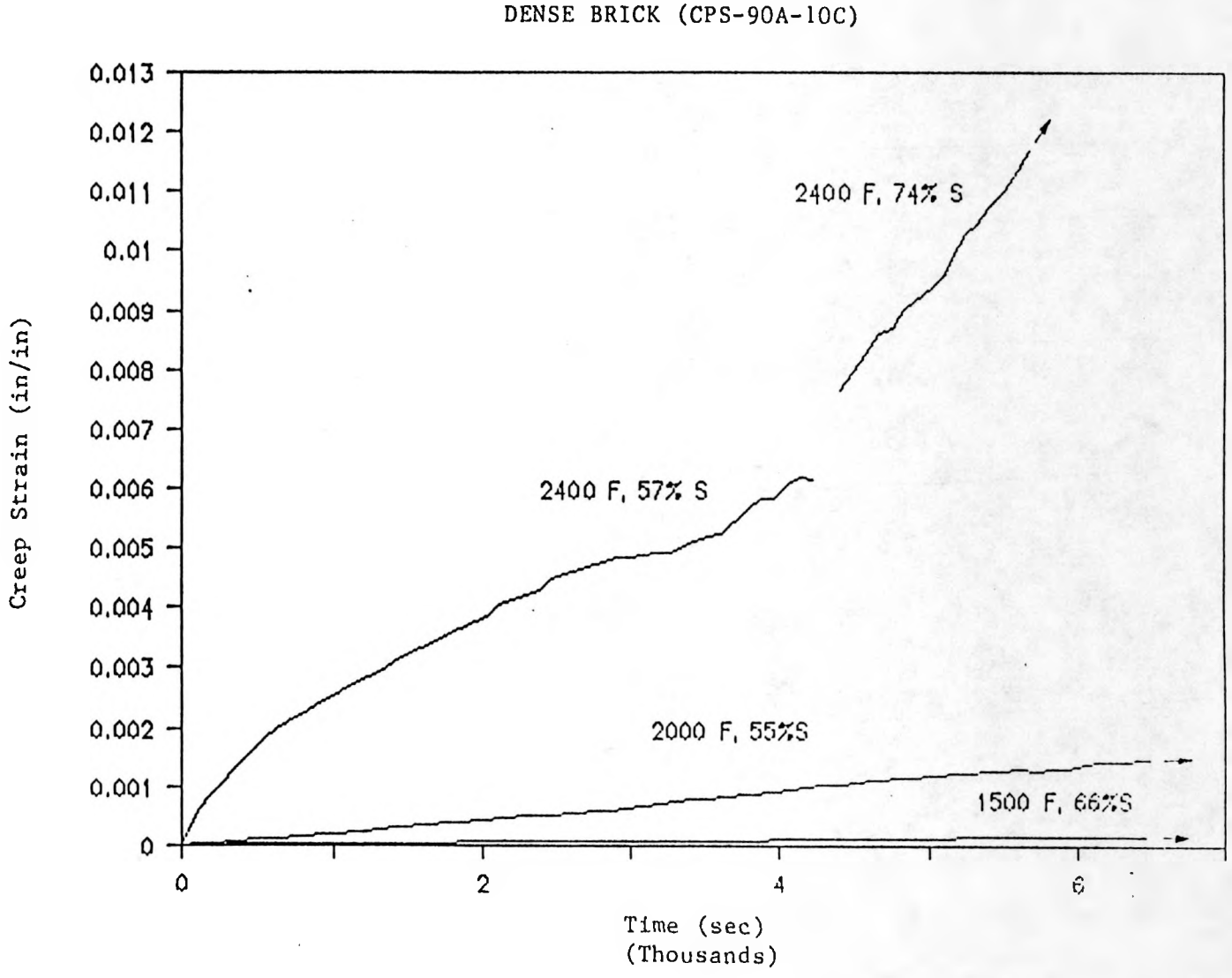

Figure 4-11: Creep Strains for CPS-90A-10C at Different Temperature and Load Levels

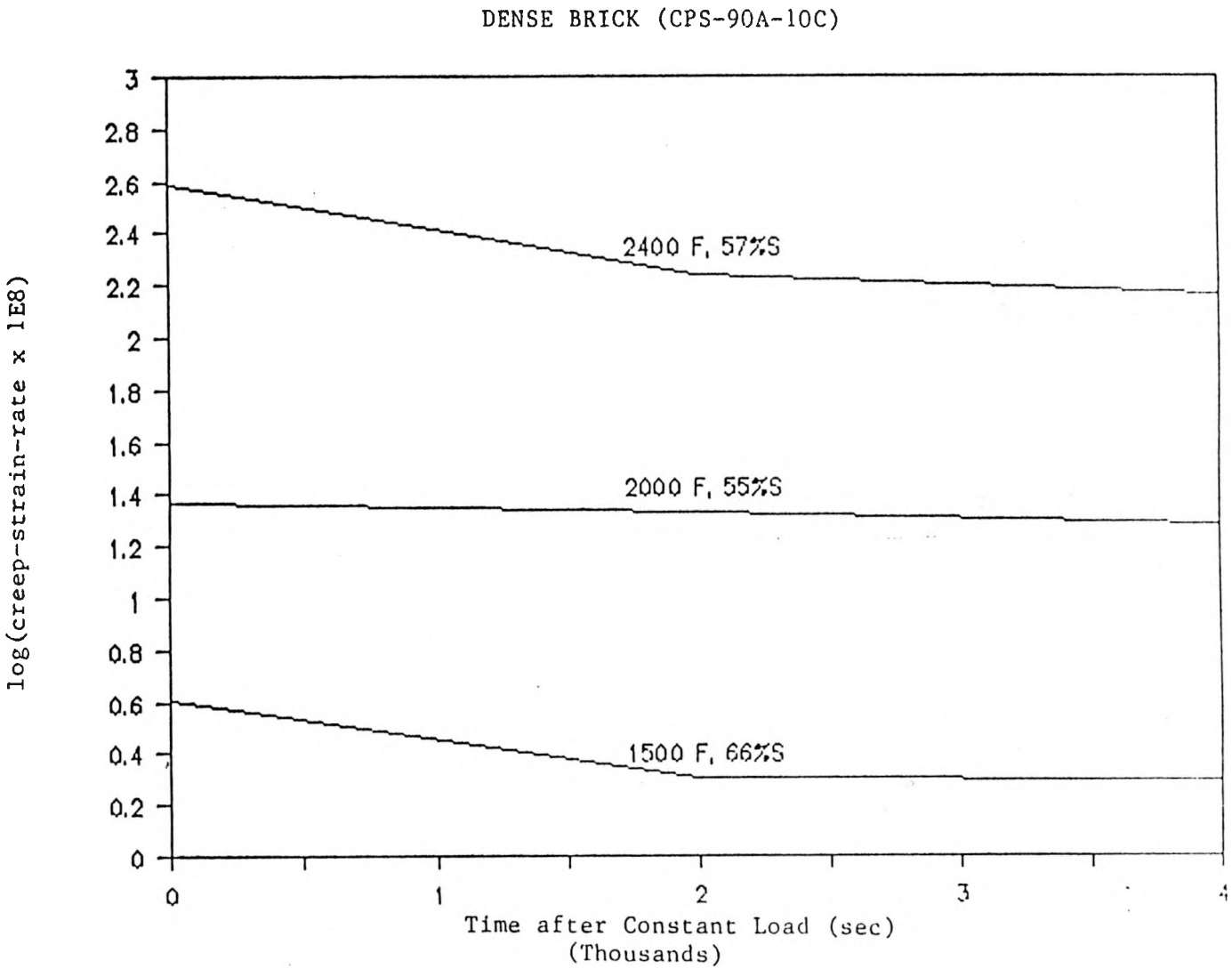

Figure 4-12: Variation of the Log of the Creep Strain-rate at Different Temperature and Load Levels for CPS-90A-10C

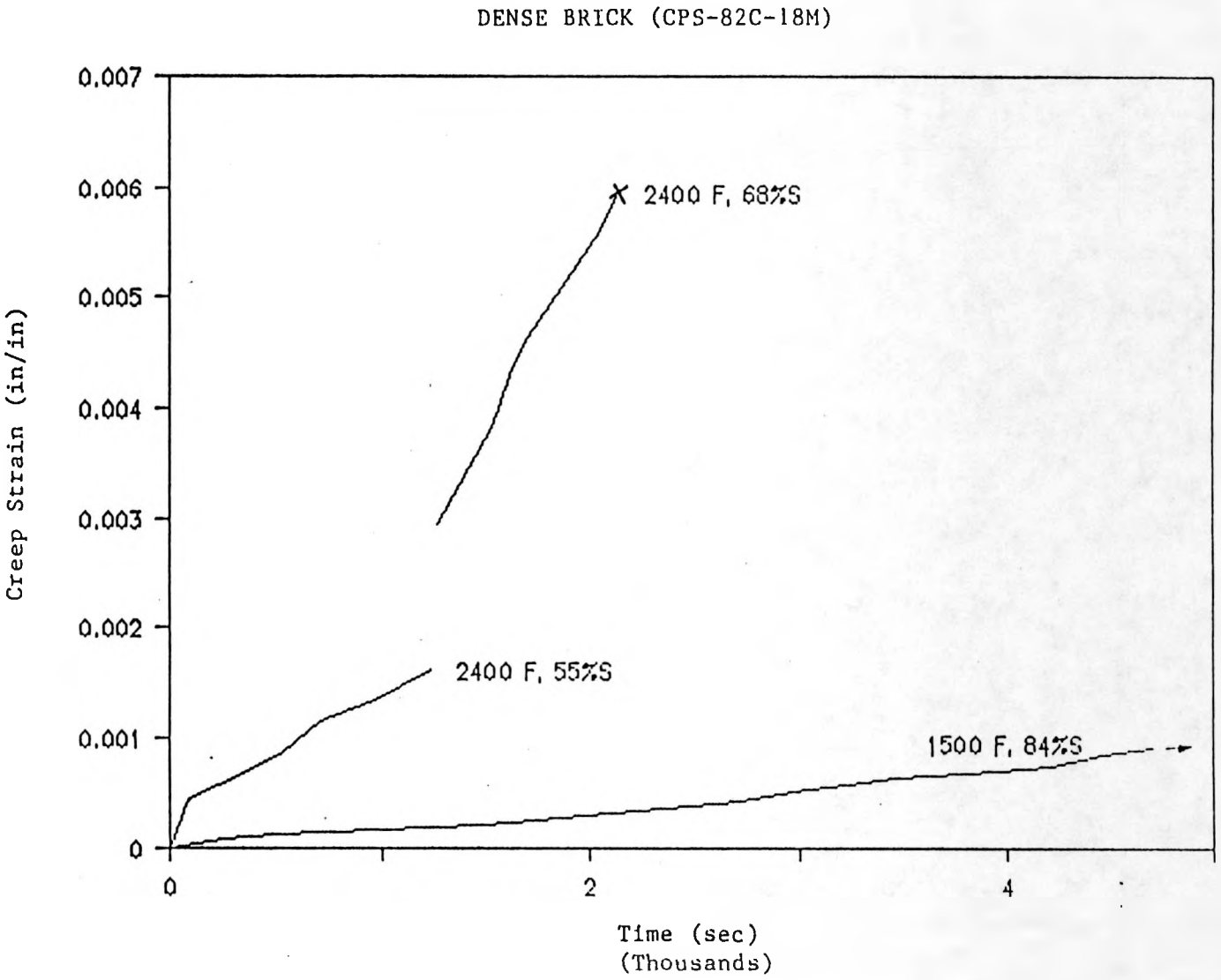

Figure 4-13: Creep Strains for CPS-82C-18M at Different Temperature and Load Levels

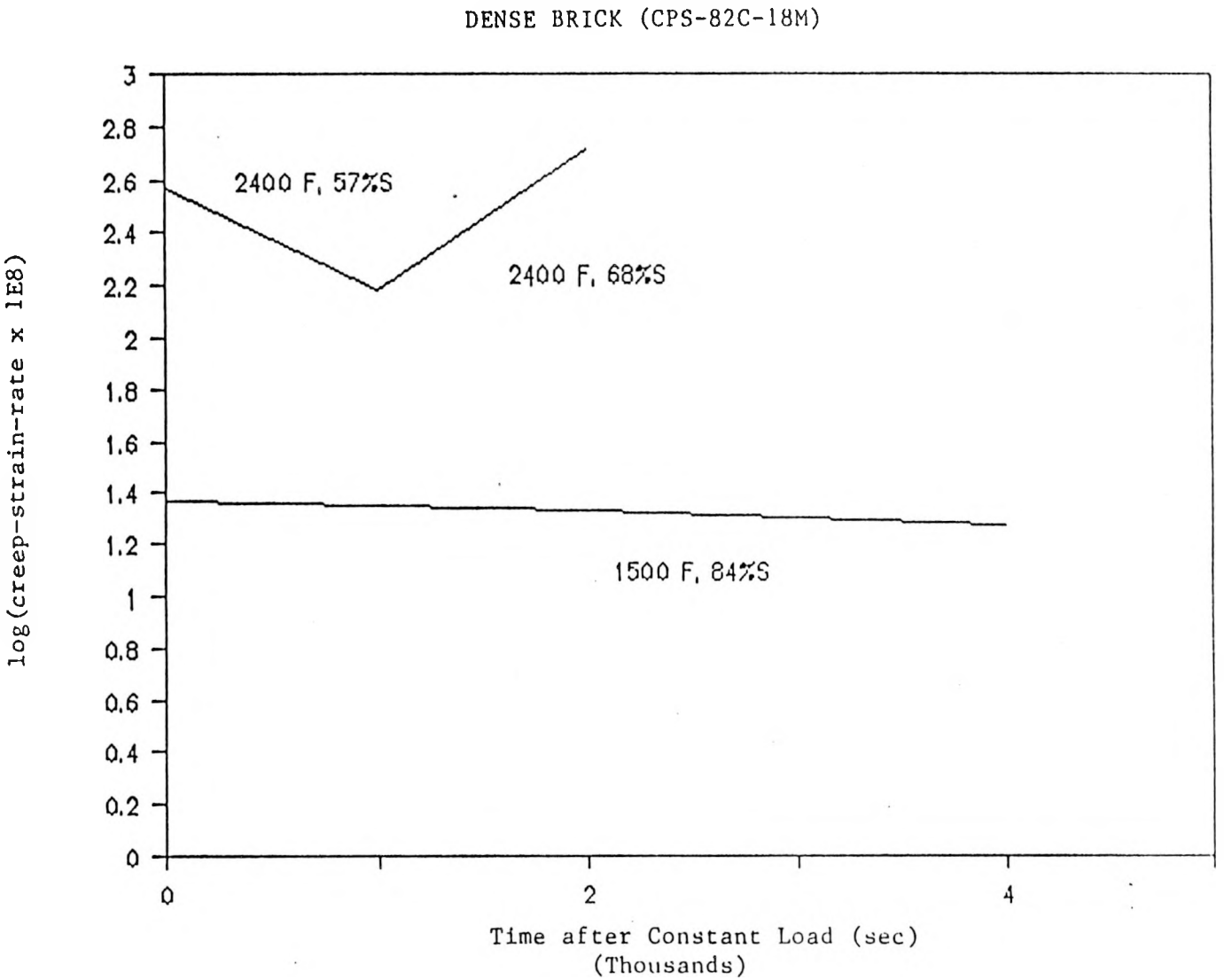

Figure 4-14: Variation of the Log of the Creep Strain-rate at Different Temperature and Load Levels for CPS-82C-18M

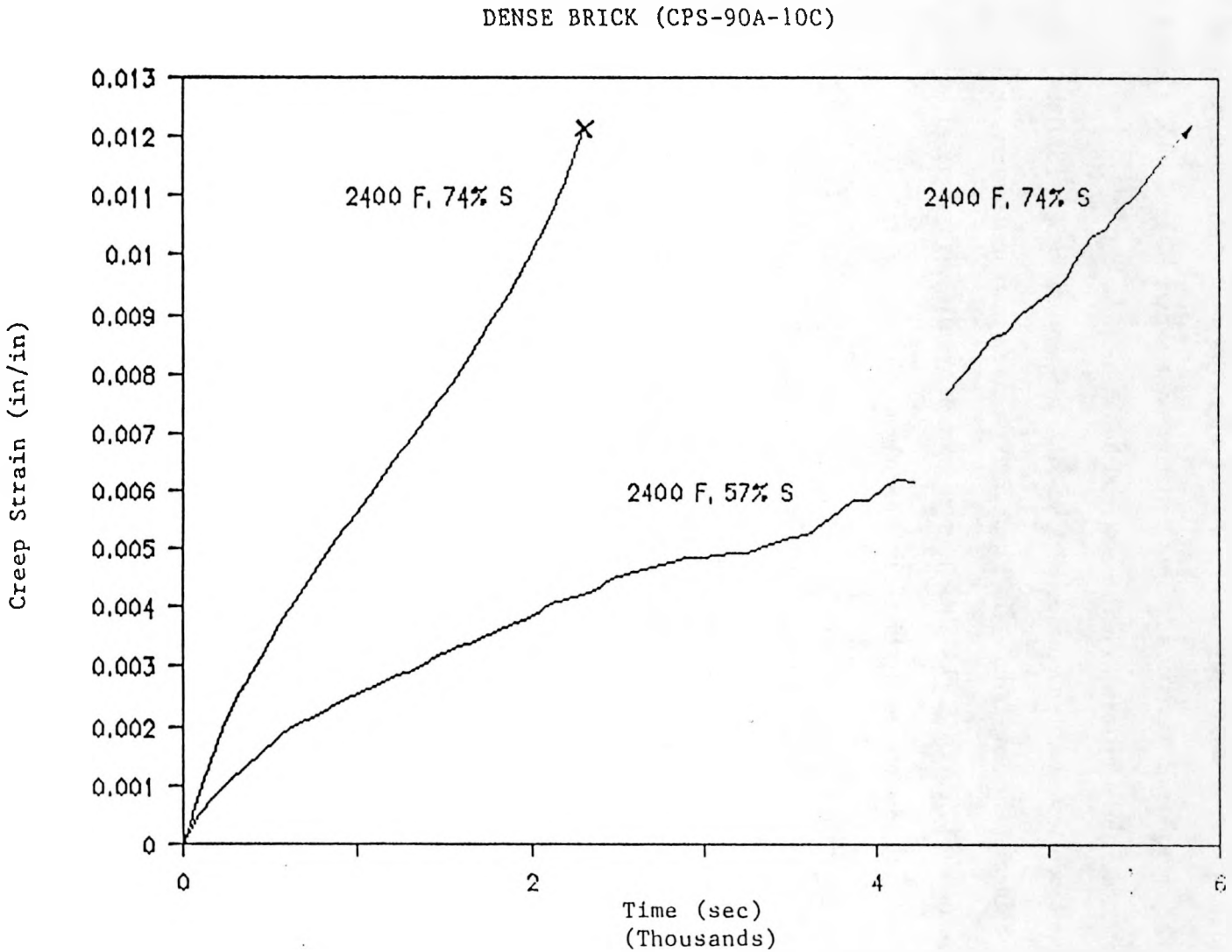

Figure 4-15: Creep Strains for CPS-90A-10C at the Same Temperature and Final Load Level, but Different Load Histories

sec, before the load level was raised to 74%, and kept at 74% for 2000 sec. The second specimen was loaded directly to 74% of the monotonic strength, and failed after 3000 sec. The creep strain variation for both specimens is shown in Fig. 4.15. This shows the importance of load histories on the material behavior.

The creep test results of materials CPS-90A-10C and CPS-82C-18M are summarized in the tables of the Appendix A.1. These include creep tests under varying temperatures for the dense brick CPS-90A-10C, and creep test results with thermal cycling at zero loads followed monotonically increasing crosshead displacements.

4.3.2 Deformation Mechanism

A useful way to represent the deformation of the material with respect to temperature is by the use of deformation mechanism maps (Frost and Ashby, 1982). These maps display the relationship between the three macroscopic variables such as stress, temperature, and strain-rate. Details of the deformation mechanism map are well explained in Section 8.2.2. For the present case, the best way to represent the data is with T/T_M as its x-axis and τ / $\hat{\tau}$ (normalized stress) as its y-axis, where τ is the shear strength and $\hat{\tau}$ is the ideal shear strength of the material. The strain rate effect is incorporated into the map as well. In this paper, deformation maps are used in two ways. First, comparison of the test data with available deformation mechanism maps is carried out. Next, deformation maps combining the results of the short-term tests, with published long-term creep tests (McGee and Konrady, 1983-1987; Wiederhorn and Krause, 1986) are constructed.

The data obtained from the short term creep and monotonic tests have been combined with data obtained by McGee and Konardy (1983-87) to produce deformation maps for the materials under consideration. The results are shown in Fig. 4.16 and Fig. 4.17 for CPS-90A-10C and CPS-82C-18M respectively. For both materials the results of the short-term creep tests (total time about two to three hours, and constant load values ranging from 50% to 85% of the monotonic strength) conducted under the current project corre-

late nicely with the results of the long-term creep tests from McGee and Konrady (total test time exceeding 100 hours, and constant load values less than 10% of the material monotonic strength). The deformation maps facilitate the comparison of deformation rates between materials. The deformation rates of CPS-82C-18M are about an order of magnitude greater than the ones for CPS-90A-10C (as an example, from Fig. 4.16 and Fig. 4.17, at 2000°F and 1000 psi the maps predict deformation rates of about 5 x 10^{-7} sec^{-1} for CPS-90A-10C and about 5 x 10^{-6} sec^{-1} for CPS-82C-18M). These deformation maps are also ueful in showing the whole spectrum of loading conditions generally encountered in high temperature containment vessels.

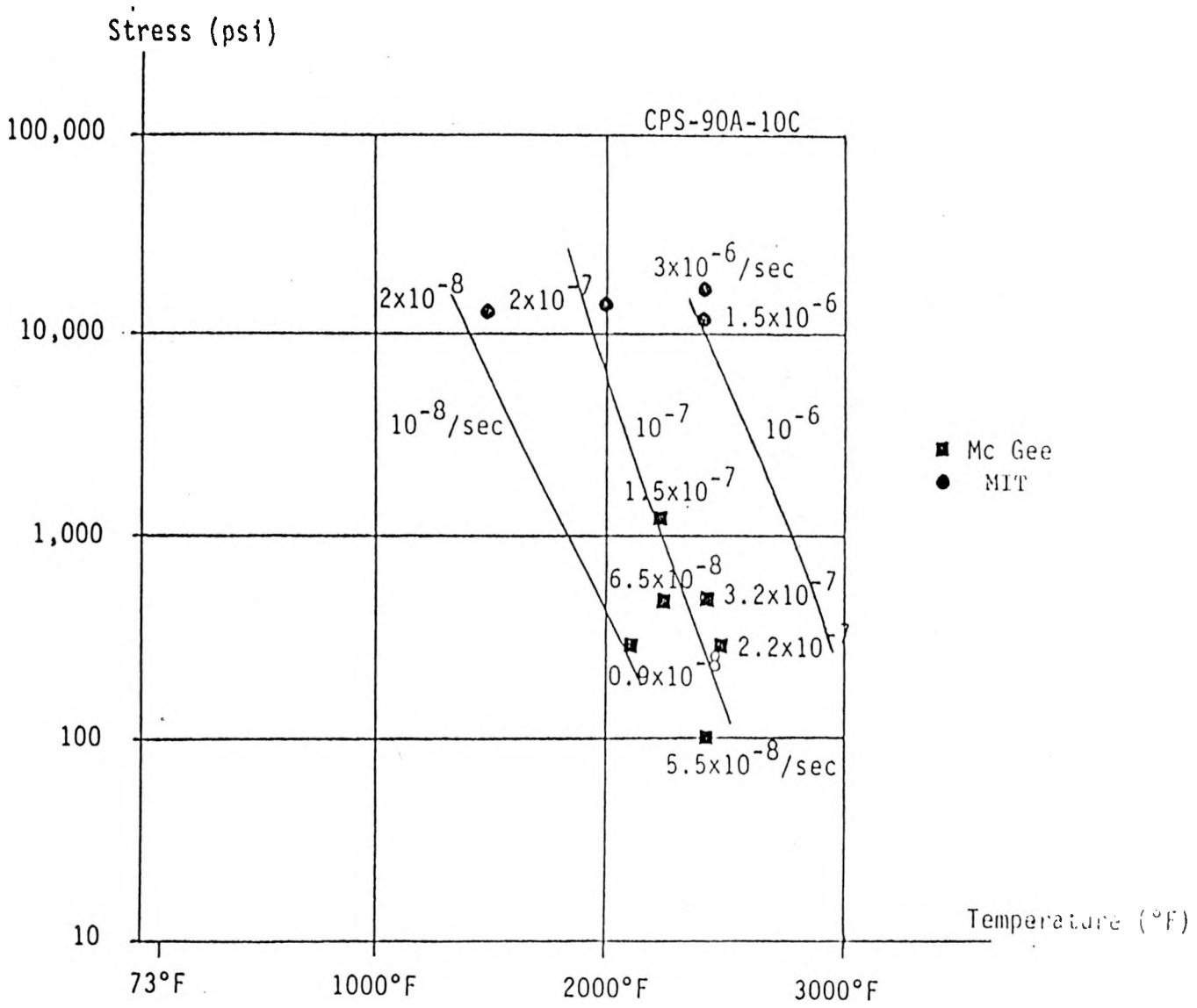

Figure 4-16: Deformation Mechanism Map for CPS-90A-10C (Tamer and Buyukozturk, 1988)

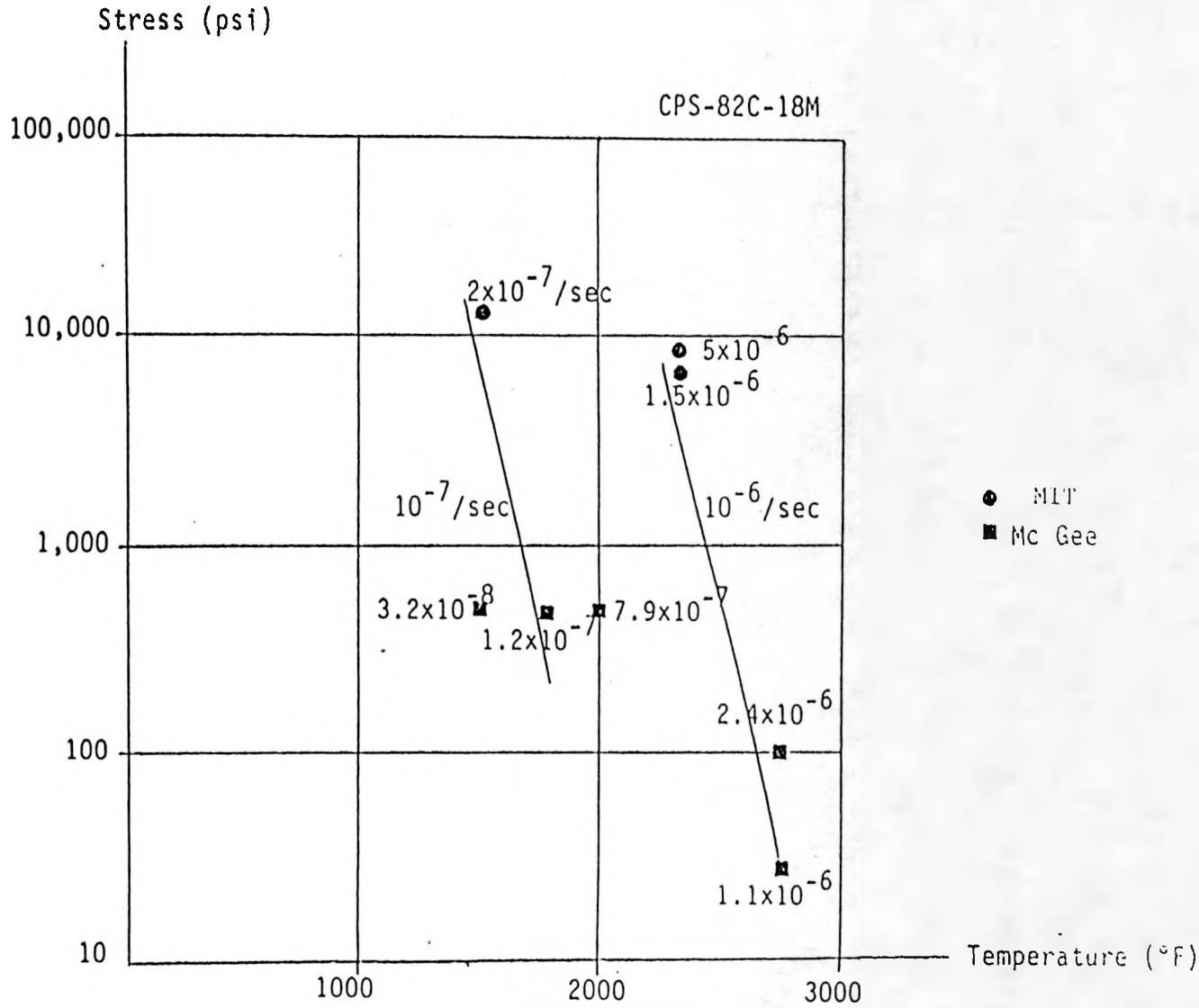

Figure 4-17: Deformation Mechanism Map for CPS-82C-18M (Tamer and Buyukozturk, 1988)

Chapter 5

HIGH-ALUMINA DENSE CASTABLE MATERIAL

5.1 SYNOPSIS

In this chapter the behaviors of a high alumina dense castable material DC-95A-5Ca are examined under short-term uniaxial monotonically increasing and constant loads at elevated temperatures. The thermomechanical properties under monotonic uniaxial compressive loading at constant temperatures are presented in Section 5.2. In Section 5.3 the behavior under constant compressive loads at predetermined constant temperature is investigated. These thermomechanical properties are summarized in Appendix A.2.

5.2 THERMOMECHANICAL BEHAVIOR UNDER MONOTONIC UNIAXIAL COMPRESSIVE LOADS AT CONSTANT TEMPERATURES

The effects of elevated temperature on the behavior of a dense castable material DC-95A-5Ca under loading with constant displacement rate (7.218×10^{-5} in/sec) were studied. Cylindrical specimens with 1 inch diameter and 2.5-3.0 inches height were used for the

tests. Automatic slow-speed sawing was used for preparing both surfaces of a specimen for the tests. The specimens were prepared by coring them out of the dense castable bricks cast by the manufacturer as shown in Fig. 3.6. Stress-strain curves for different temperature levels, and a constant displacement rate are shown in Fig. 5.1. Similarly to the dense brick materials, the dense castable material DC-95A-5Ca exhibits two distinct deformation and fracture behavioral regions with respect to temperature. The transition temperature that separates these behaviors is about one- half of the melting point (1750°F; 954°C). The two different behaviors are:

1. For temperature levels below 0.5 T_M (where T_M is the melting temperature of the material), the failure pattern is brittle with a sudden fracture. In the temperature levels:

   (a) Below 0.3 T_M, the deformation behavior is linear elastic. A sudden fracture of the specimen was observed at a load level corresponding to the peak stress on the stress-strain curve, and thus, no post-peak behavior was obtained.

   (b) For temperature levels between 0.3-0.5 T_M, a small amount of stress softening in the stress-strain curve occurs before a sudden brittle fracture. Therefore, the final stress level is about 90% of the peak stress (i.e. strength) and the final fracture strain is a little bit larger, usually less than 10%, than the peak strain associated with the peak stress.

2. For temperature levels between 0.5-0.7 T_M (tests were limited to a maximum temperature level of 0.7 T_M for DC-95A-5Ca), the deformation behavior is initially linear, but exhibits significant non-linearity at stress levels close to the peak strength and in the post-peak region.

The variation of the strength of the dense castable material DC-95A-5Ca can be explained by the internal bond change. Since castable materials do not experience elevated

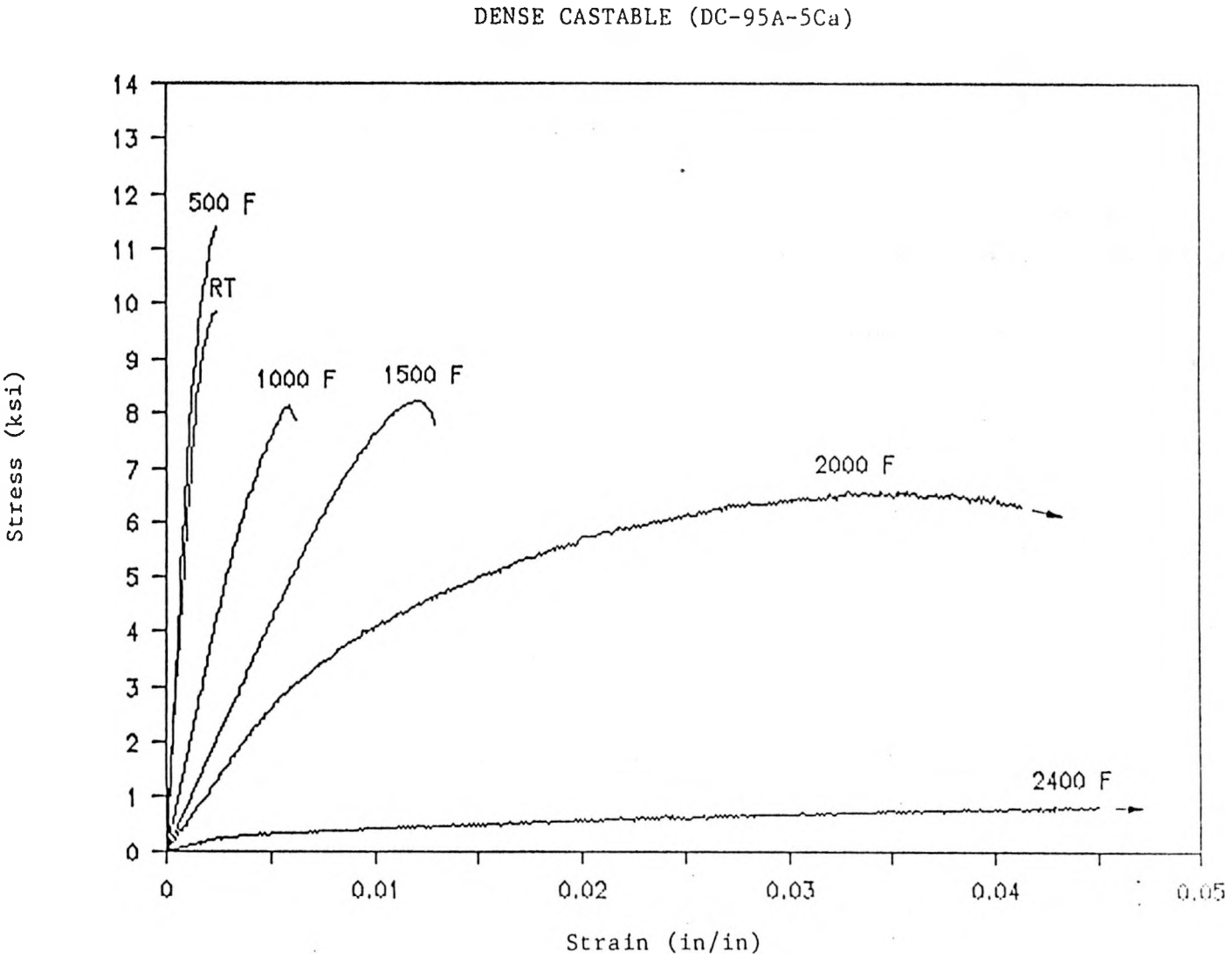

Figure 5-1: Stress-strain Curves for DC-95A-5Ca at Different Temperature Levels and a Constant Displacement Rate of 7.218×10^{-5} in/sec.

temperatures before being fired, the internal molecular bonding is changing during the first heating. This bonding change may be figured out from the change of colors of the specimen. Depending on the maximum temperature level which the castable material could experience, the color of the castable materials changes. The milk color of the dense castable material at room temperature changes to white grey color at 1000°F, and pure white color after 2000°F. Details of the bonding change are explained in Section 2.2.1. As shown in Fig. 5.2 the dense castable material DC-95A-5Ca shows a slight increase in strength for temperature levels between room temperature and 500°F. The strength increase at 500°F represents a 16% increase with respect to the strength at room temperature. After 500°F, a slight decrease in strength with temperature is observed below 0.5 T_M, followed by an increased rate of decrease in strength for temperatures above 0.5 T_M. This trend is almost the same as the dense brick materials as observed in Chapter 4. The strength level at 1000°F is already lower than that at room temperature. The sudden drop of strength after 2000°F results in a low strength at 2400°F, which is only 16% of the strength at 2000°F. This low strength at 2400°F may restrict the use of this dense castable material DC-95A-5Ca to a limited temperature range (lower than 2000°F hot temperature).

The variation of the peak strain values associated with the peak stress at elevated temperatures for the material DC-95A-5Ca is observed in Fig. 5.3. The rate of increase in the associated peak strain is lower for temperatures below 0.5 T_M than those above 0.5 T_M. Because the specimen fails in a brittle manner below 0.5 T_M, the associated peak strain and the final fracture strain have almost the same values. Especially, for the temperature levels lower than 0.3 T_M, those values are equal. For temperatures above 0.5 T_M, the final fracture strain is significantly larger than the associated peak strain due to significant non-linear deformations in the post-peak region.

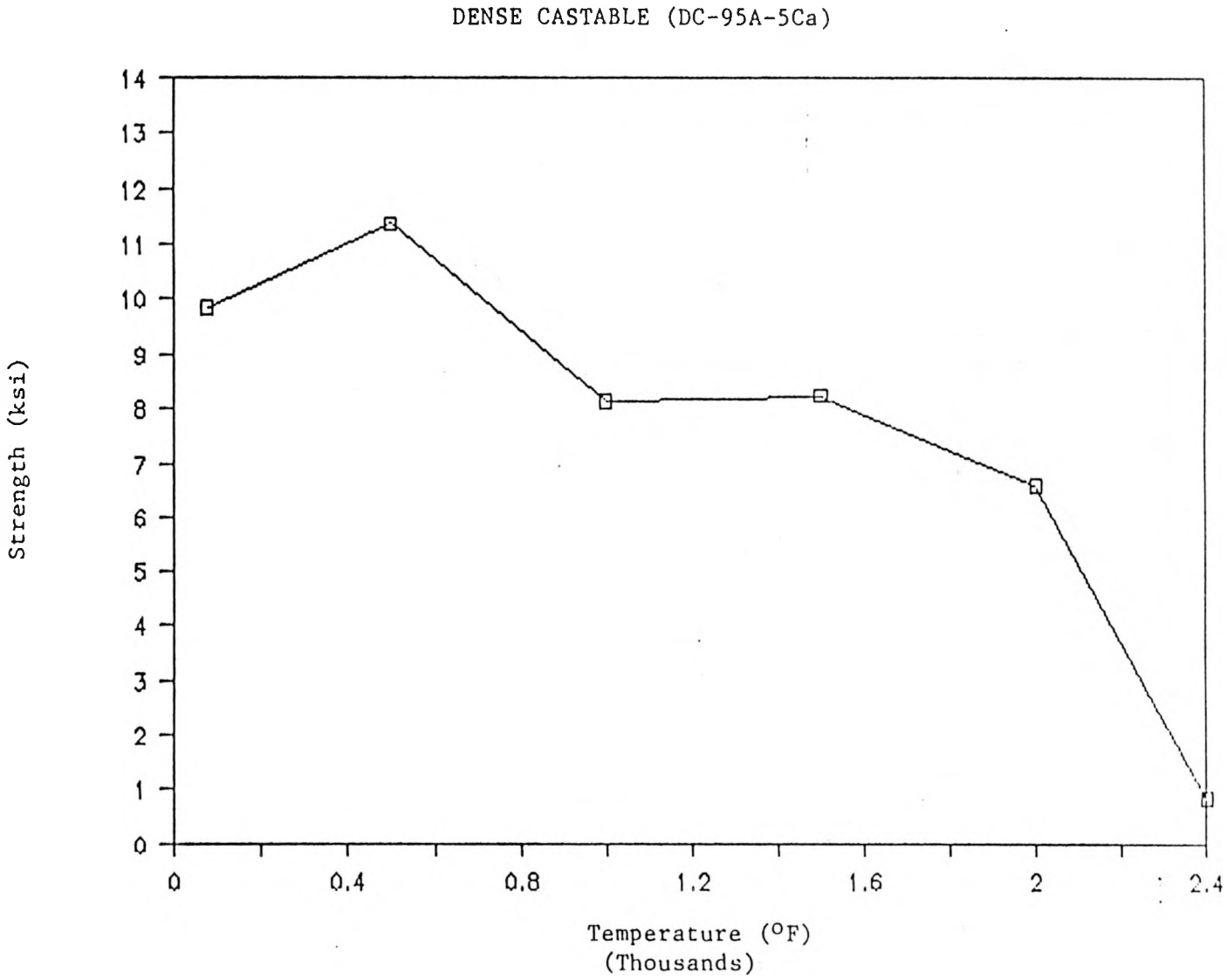

Figure 5-2: Strength Variation with Temperature for DC-95A-5Ca

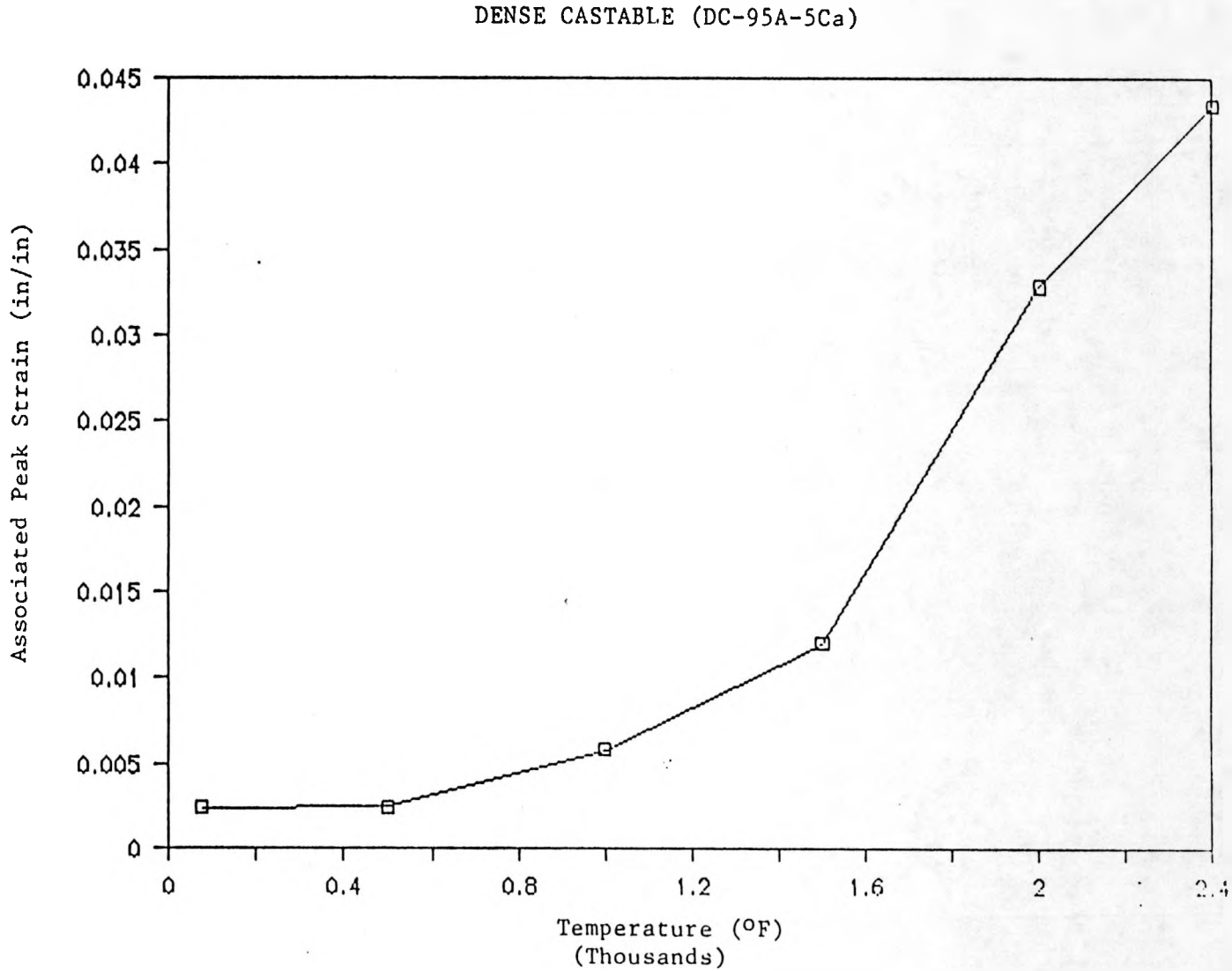

Figure 5-3: Variation of the Associated Peak Strain with Temperature for DC-95A-5Ca

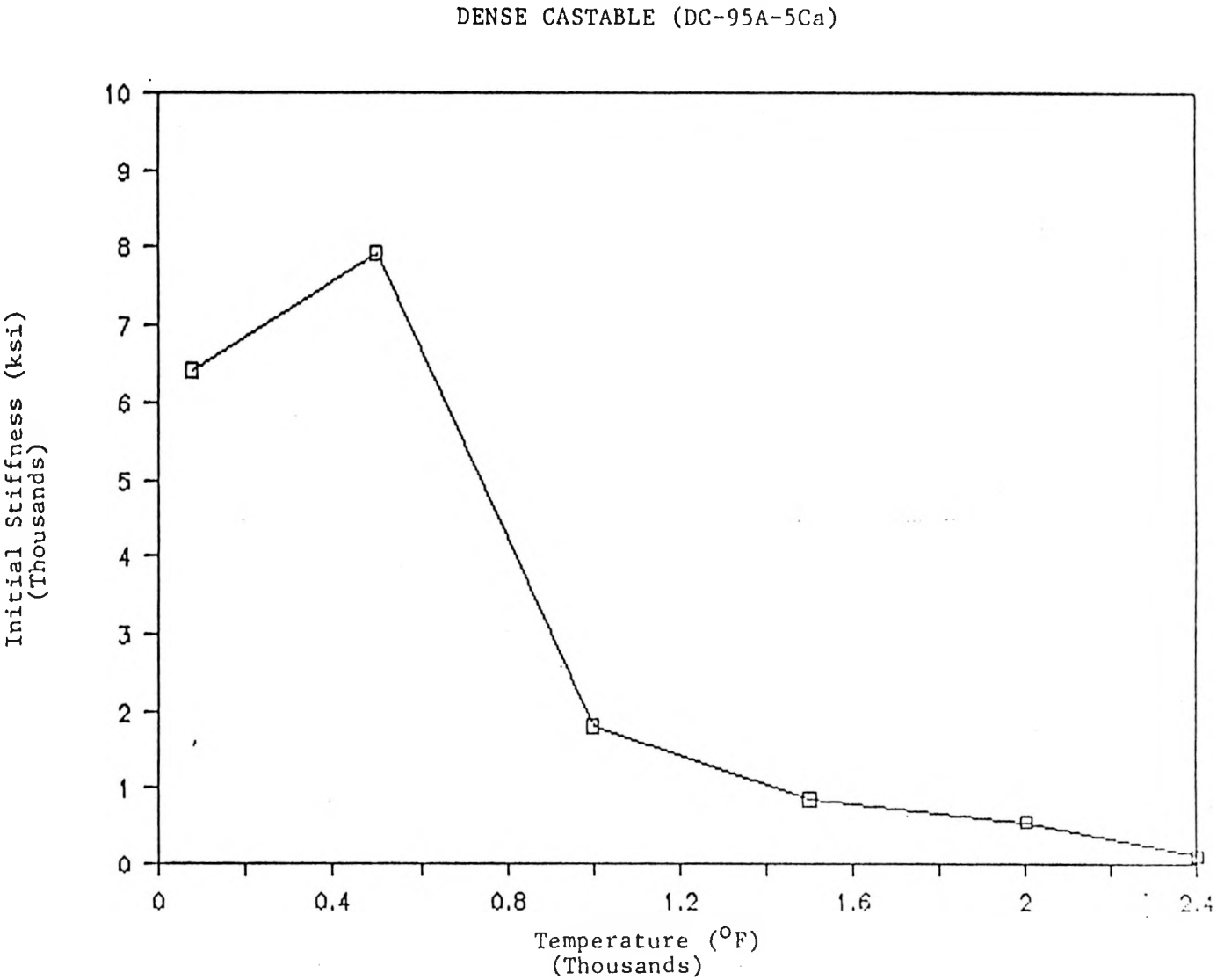

Figure 5-4: Variation of Initial Stiffness with Temperature for DC-95A-5Ca

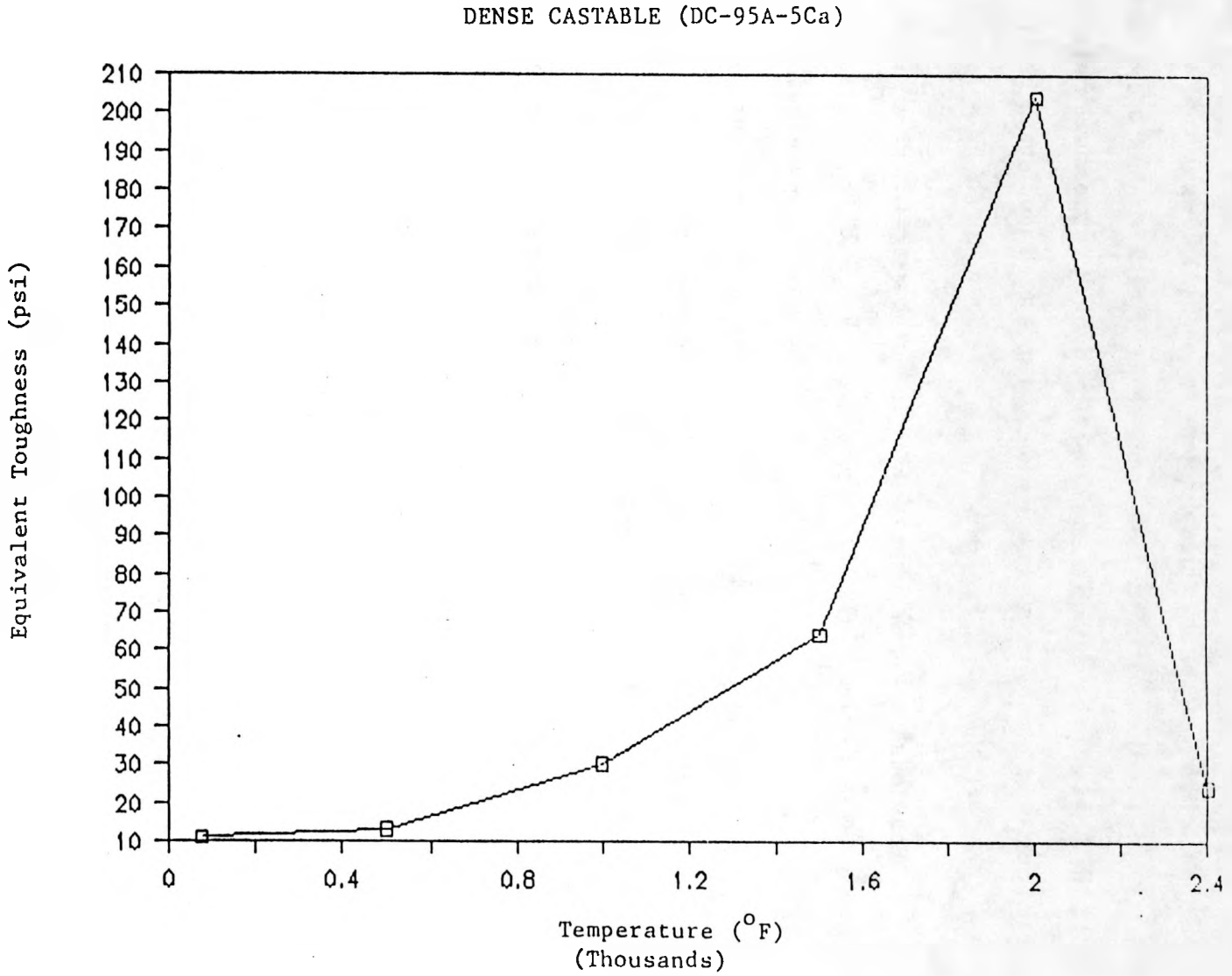

Figure 5-5: Vaiation of Toughness with Temperature for DC-95A-5Ca

The initial slopes of the stress-strain curves decreas sharply with elevated temperatures after a slight increase between room temperature and 500°F, as shown in Fig. 5.4. Fig. 5.4 supports the trend of the three different regions; (1) linear elastic and brittle below 0.3 T_M, (2) brittle but a little non-linear behavior between 0.3-0.5 T_M, and (3) almost ductile behavior above 0.5 T_M. Because it is difficult to measure true modulus at high temperatures due to creep contribution, the measured modulus is effectively a relaxed modulus.

The equivalent toughness (defined as the area under the stress-strain curve) variation with temperature for material DC-95A-5Ca is shown in Fig. 5.5. The equivalent toughness is approximately constant for temperatures below 0.5 T_M, and increases sharply at 2000°F. But above that temperature level, the equivalent toughness drops suddenly, which may be associated with the two low strength at the temperature level above 2000°F. The equivalent toughness at 2400°F represents 12% of the toughness at 2000°F.

5.3 BEHAVIOR UNDER CONSTANT COMPRESSIVE LOADS AT CONSTANT TEMPERATURES

The variation of the creep strain for the dense castable material DC-95A-5Ca was examined at temperature levels of 1500°F and 2000°F under high constant compressive loads (up to 70% of the monotonic strength). Fig. 5.6 shows the variation of the creep strain depending on the temperature levels under a constant compressive stress. The selected temperature levels are 1500°F (816°C) and 2000°F (1093°C) under 4.47 ksi, which is 54% and 68% of the monotonic compressive strength at 1500°F and 2000°F, respectively. The increase in creep strain at increased temperatrue is clearly shown in Fig. 5.6. Variation of creep strain rate at different temperatures under a constant stress level is shown in Fig. 5.7, where the results are plotted as the scale of $\log(\dot{\epsilon}_{creep} \times 10^8)$ vs. time for different temperatures.

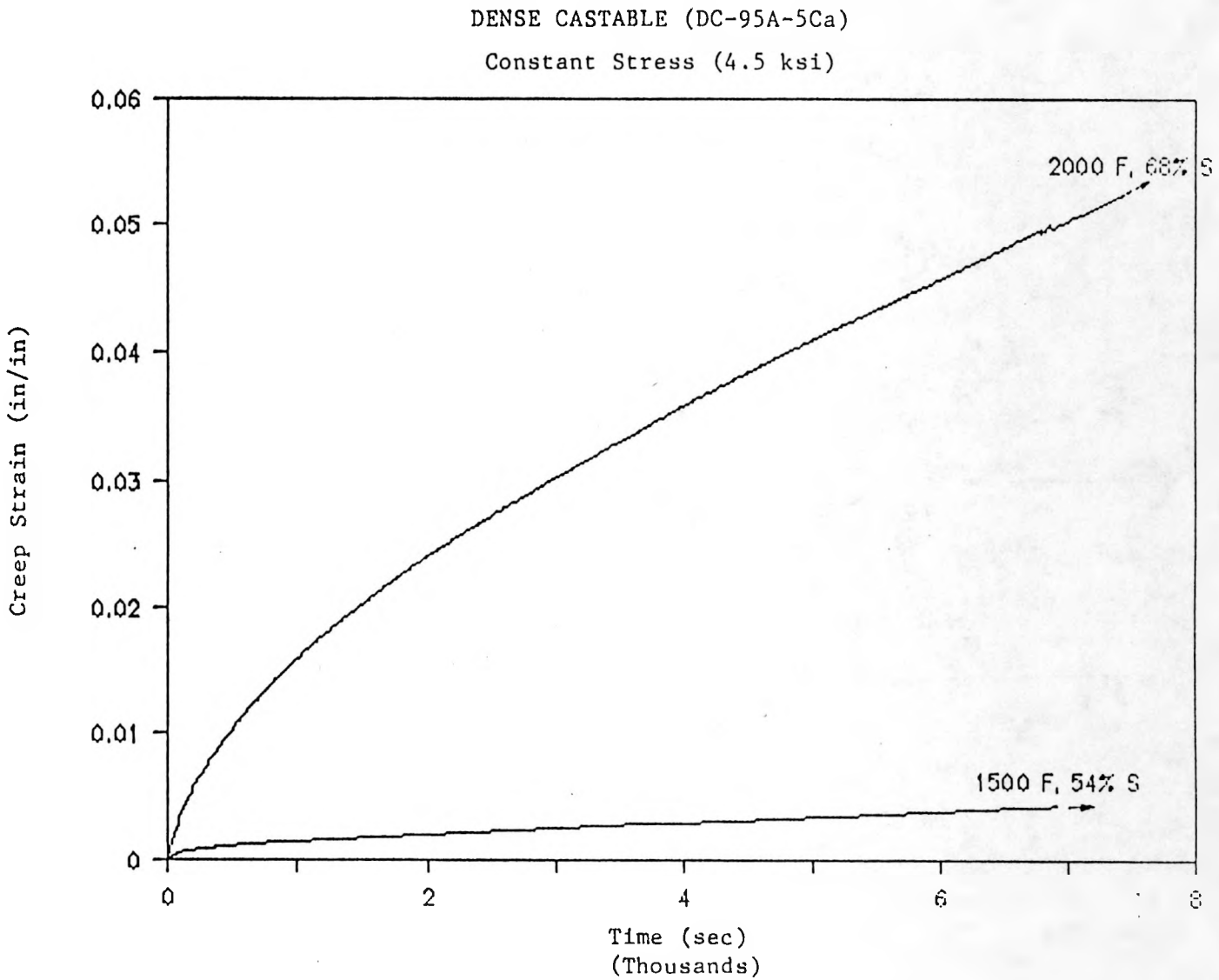

Figure 5-6: Creep Strains for DC-95A-5Ca at Different Temperatures under the Constant Stress Levels

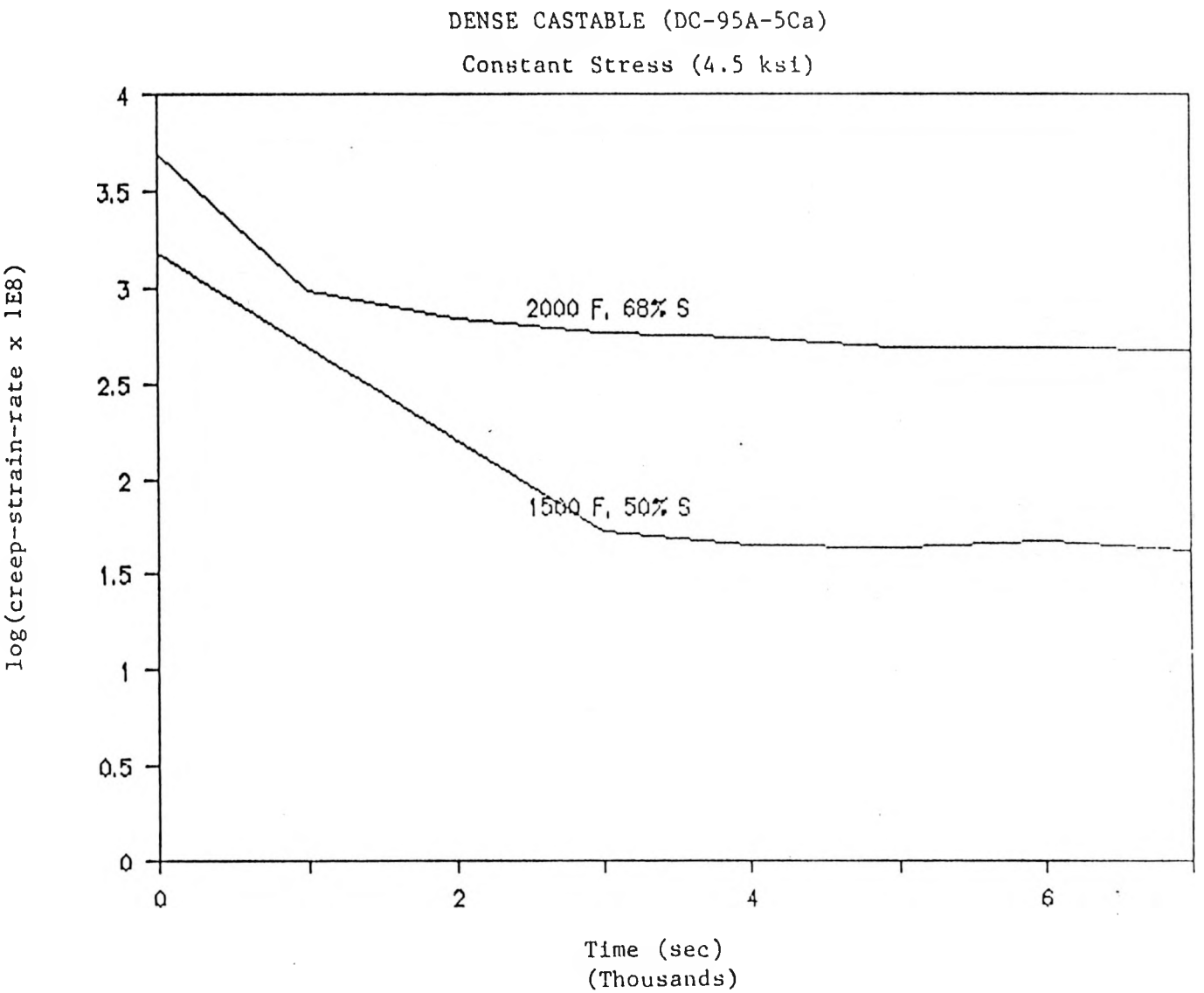

Figure 5-7: Variation of the Log of the Creep Strain-rate at Different Temperatures under the Constant Stress Levels

The variation of creep strain depending on the stress levels at a constant temperature level is shown in Fig. 5.8. The constant temperature was 1500°F with different stress levels of 41%, 54%, and 71% of the compressive strength at 1500°F. The effect of unloading on creep strain is examined in Fig. 5.8 at the time of 7500 seconds. after a constant stress is attained. This illustrates the irrecoverable creep during the unloading of the material, which is one of the typical properties of brittle materials. The dropped creep strain amount is approximately the same as the amount of the primary creep strain. Variation of creep strain rate under different stresses at constant temperature level is shown in Fig. 5.9. The plot shows that all stress levels have almost the same value of final creep strain rate (so called the steady-state creep strain rate). The differences in the creep strains of the three different levels of stresses are the amount and the duration of the primary creep strain.

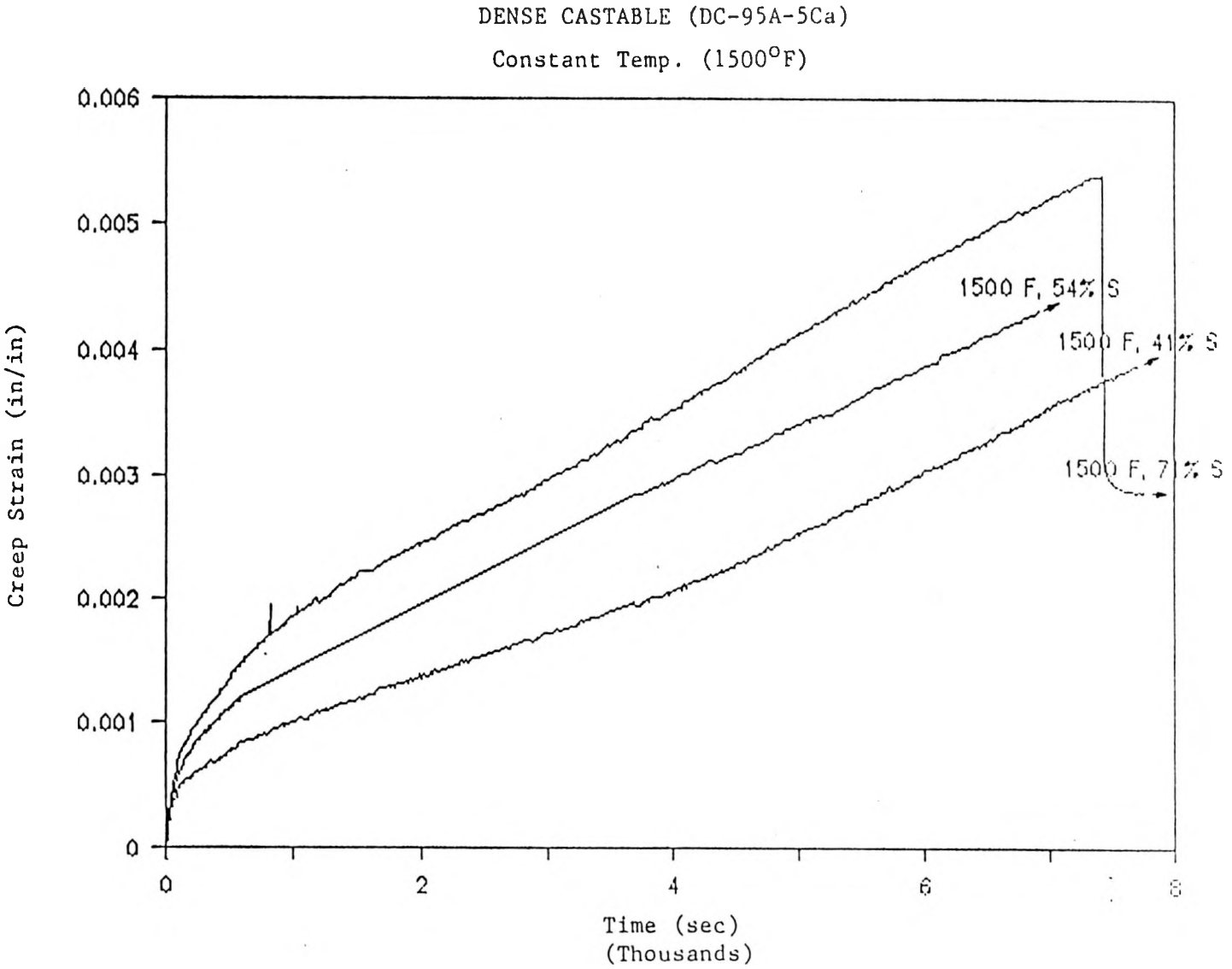

Figure 5-8: Creep Strains for DC-95A-5Ca under Different Stresses at Constant Temperature Level

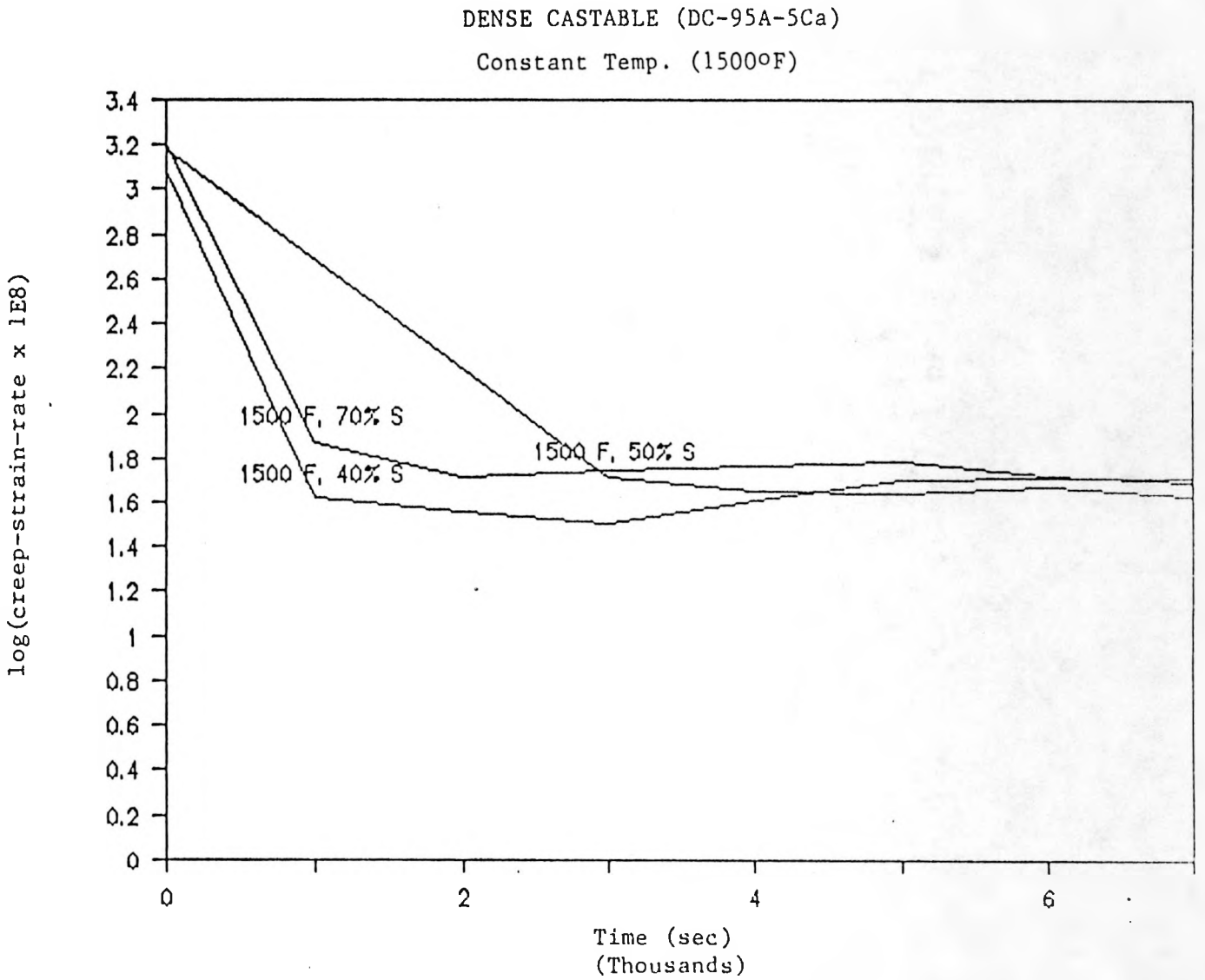

Figure 5-9: Variation of the Log of the Creep Strain-rate under Different Stresses at Constant Temperature Level

Chapter 6

INSULATING CASTABLE MATERIAL

6.1 SYNOPSIS

In this chapter the deformation and fracture behavior of an insulating castable material IC-55A-36S is examined under short-term uniaxial monotonically increasing and constant loads. In Section 6.2 the thermomechanical behavior under monotonic compressive loads at predetermined temperatures is discussed. In Section 6.3 the behavior under constant compressive loads at predetermined constant temperature is discussed. These thermomechanical properties are summarized in Appendix A.3.

6.2 BEHAVIOR UNDER MONOTONIC COMPRESSIVE LOADS AT CONSTANT TEMPERATURES

The effects of elevated temperature on the behavior of an insulating castable material IC-55A-36S under loading with constant displacement rate of 7.218×10^{-5} in/sec were studied. Cylindrical specimens with 1 in. diameter and 2.5-3.0 inches height were used for the tests. The specimens were prepared by boring them out of the insulating castable bricks casted by the manufacturer, and by sawing both ends. Stress-strain curves for different temperature levels, and a constant displacement rate are shown in Fig. 6.1. The

insulating castable material also shows two different deformation and fracture behavioral regions with respect to temperature. The transition temperature is around one-half of the melting temperautre. The distinct behaviors are:

1. For temperature levels below 0.5 T_M (where T_M is the melting temperature of the material), the failure pattern is brittle with a sudden fracture. In this temperature levels:

   (a) Below 0.3 T_M, the deformation behavior is linear elastic. A sudden fracture of the specimen was observed at a load level corresponding to the peak stress on the stress-strain curve, and thus, no post-peak behavior was obtained.

   (b) For temperature levels between 0.3-0.5 T_M, a small amount of stress softening in the stress-strain curve occurs before a sudden brittle fracture. Therefore, the final stress level is about 90% of the peak stress (i.e. strength) and the final fracture strain is a little bit larger, usually less than 10%, than the peak strain associated with the peak stress.

2. For temperature levels above 0.5 T_M, the deformation behavior is initially linear, but exhibits significant non-linearity at stress levels close to the peak strength and in the post-peak region.

The variation of the strength of the dense castable material IC-55A-36S is shown in Fig. 6.2. Since the castable material IC-55A-36S did not experience elevated temperatures before being fired, the internal molecular bonding is changing during the first heating. This bonding change may be established out from the change of colors of the specimen. Depending on the maximum temperature level which the castable material could experience, the color of the castable materials changes. The grey color of the insulating castable material at room temperature changes to light pink color above 1000°F

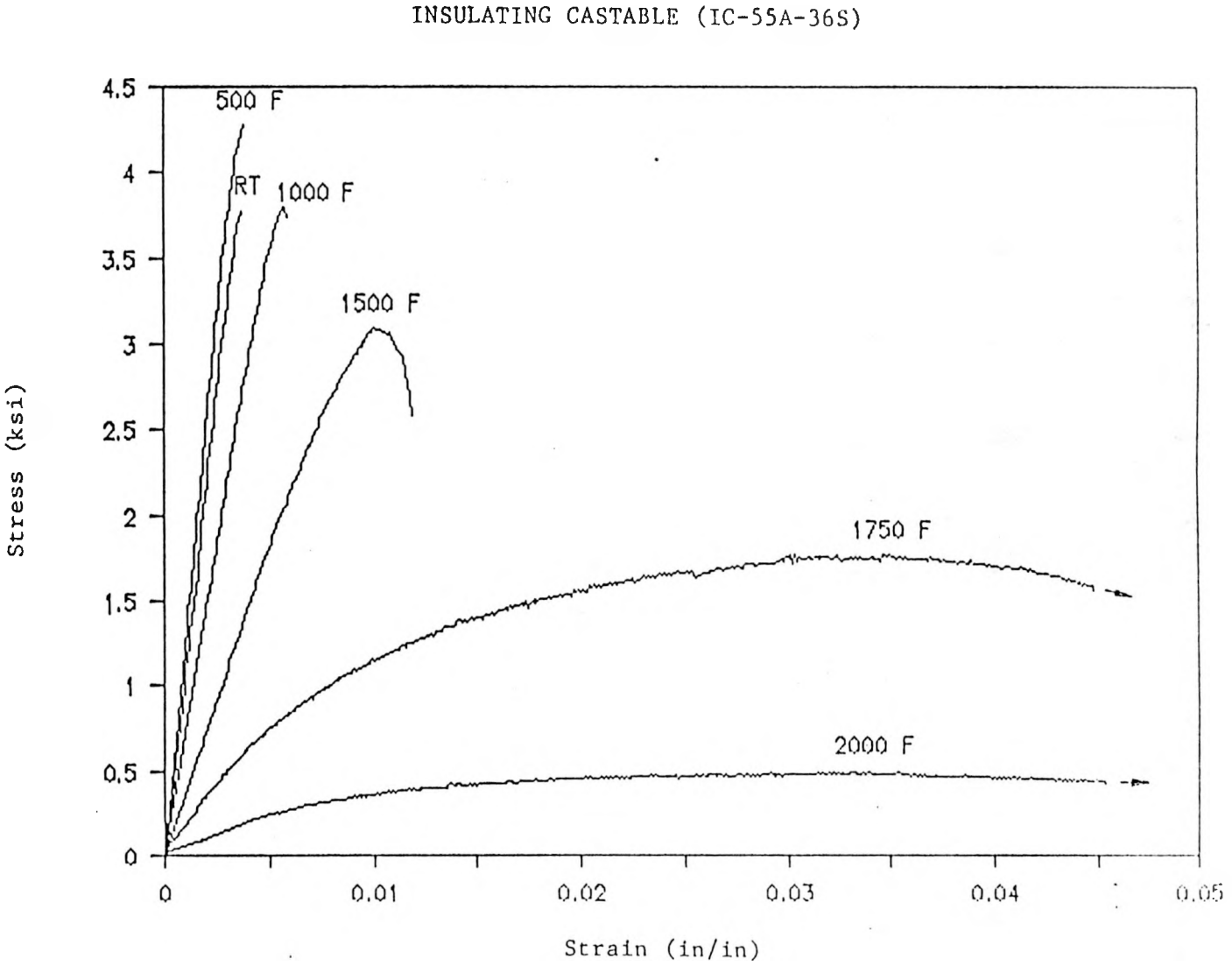

Figure 6-1: Stress-strain Curves for IC-55A-36S at Different Temperature Levels and a Constant Displacement Rate of 7.218×10^{-5} in/sec.

with grey spots. This spots change to brown ones at 1750°F, and light green and red spots at 2000°F.

As shown in Fig. 5.2 the dense castable material IC-55A-36S shows a slight increase in strength for temperature levels between room temperature and 500°F. The strength increase at 500°F represents 13% increase with respect to the strength at room temperature. After 500°F, a slight decrease in strength with temperature is observed below 0.5 T_M, followed by an increased rate of decrease in strength for temperatures above 0.5 T_M. This trend is almost the same as the dense castable materials as discussed in Chapter 5. The strength level at 1000°F is nearly the same as that at room temperature. The sudden drop of strength after 1750°F results in a low strength at 2000°F, which is only 28% of the strength at 1750°F. This low strength at 2000°F may restrict the use of this insulating castable material IC-55A-36S to the limited temperature range (lower than 1750°F).

The variation of the peak strain values associated with the peak stress at elevated temperatures for the material IC-55A-36S is observed in Fig. 6.3. The rate of increase in the associated peak strain is low for temperatures below 0.5 T_M. It increases sharply above 0.5 T_M. Because the specimen fails in a brittle manner below 0.5 T_M, the associated peak strain and the final fracture strain have almost the same values. Especially for the temperature levels lower than 0.3 T_M, those values are equal. For temperatures above 0.5 T_M, the final fracture strain is significantly larger than the associated peak strain due to significant non-linear deformations in the post-peak region.

The initial slope of the stress-strain curves decreases sharply with elevated temperatures after a slight increase between room temperature and 500°F, as shown in Fig. 6.4. For the temperature levels above 0.5 T_M, the initial stiffness decreases very slowly, but those are already too small compared with that at room temperature. Those initial stiffnesses are less than 40% of the initial stiffness at room temperature. Because it is

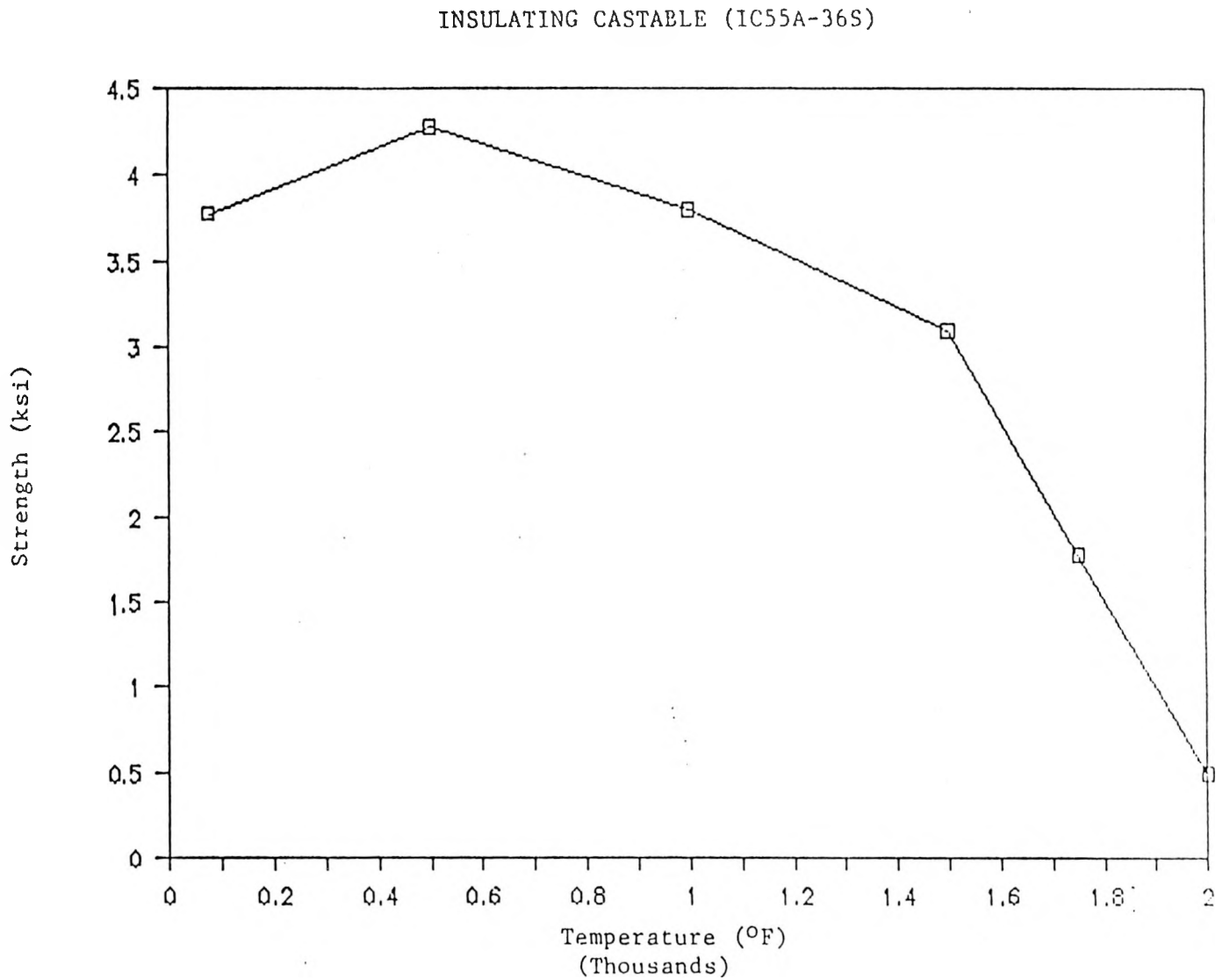

Figure 6-2: Strength Variation with Temperature for IC-55A-36S

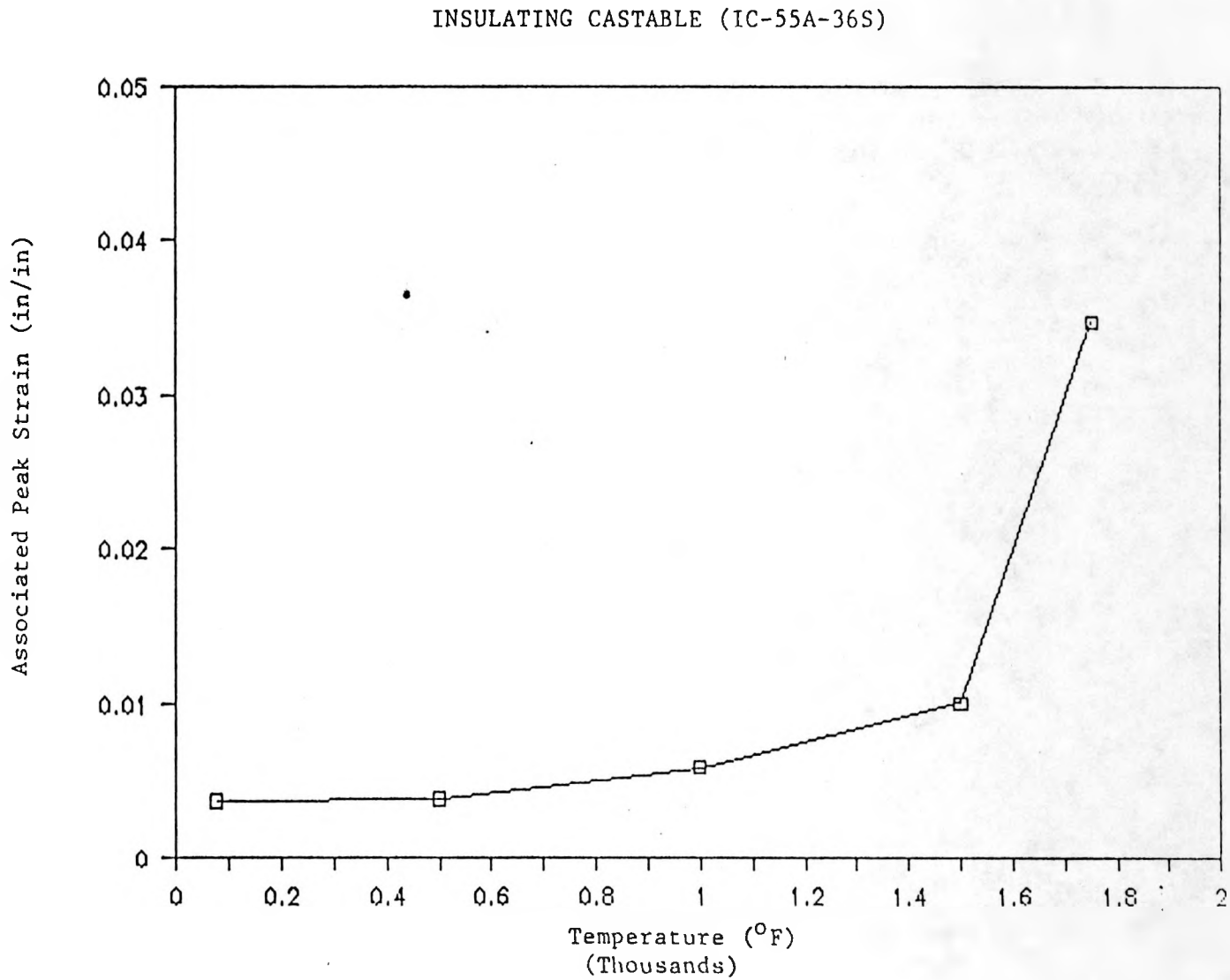

Figure 6-3: Variation of the Associated Peak Strain with Temperature for IC-55A-36S

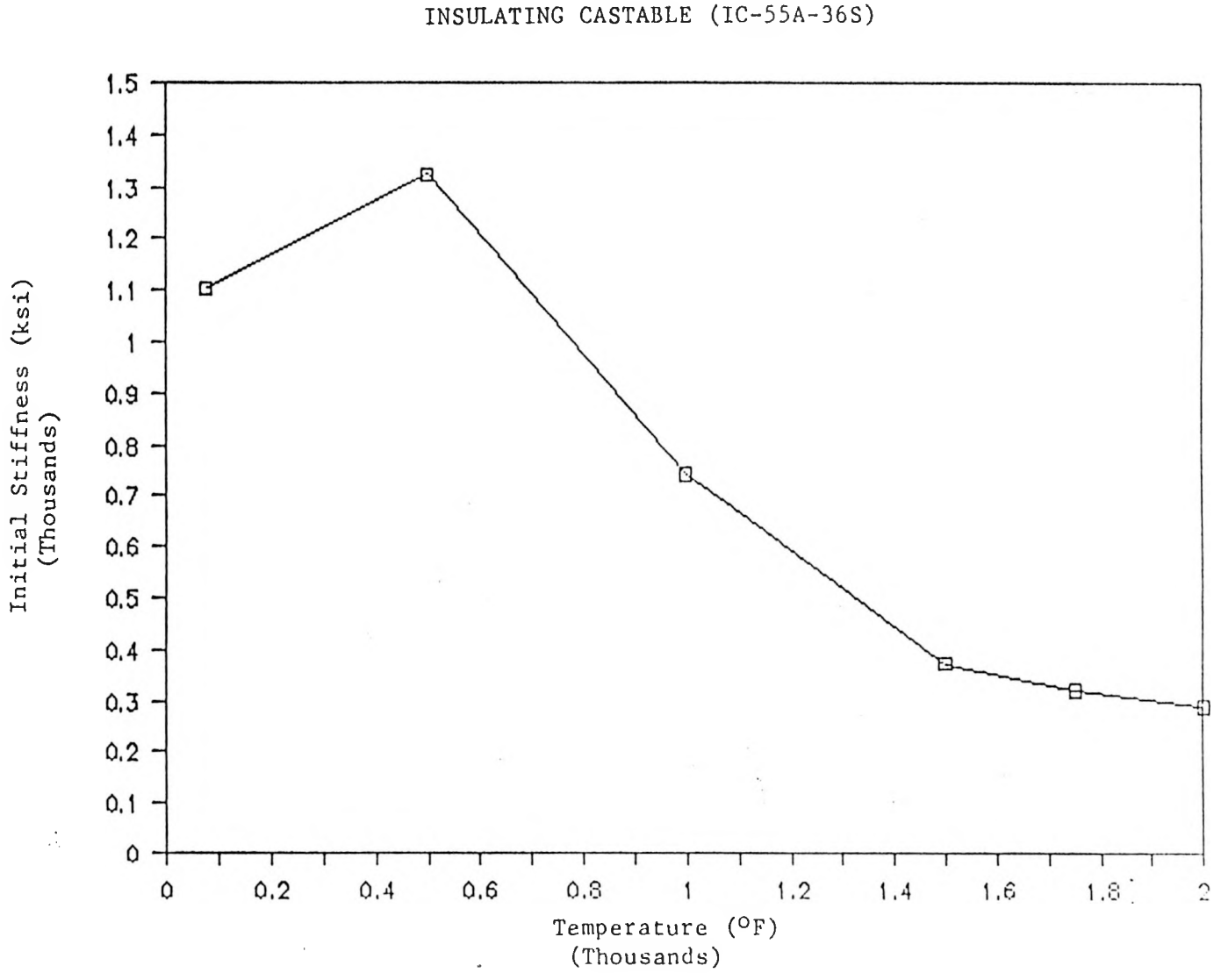

Figure 6-4: Variation of Initial Stiffness with Temperature for IC-55A-36S

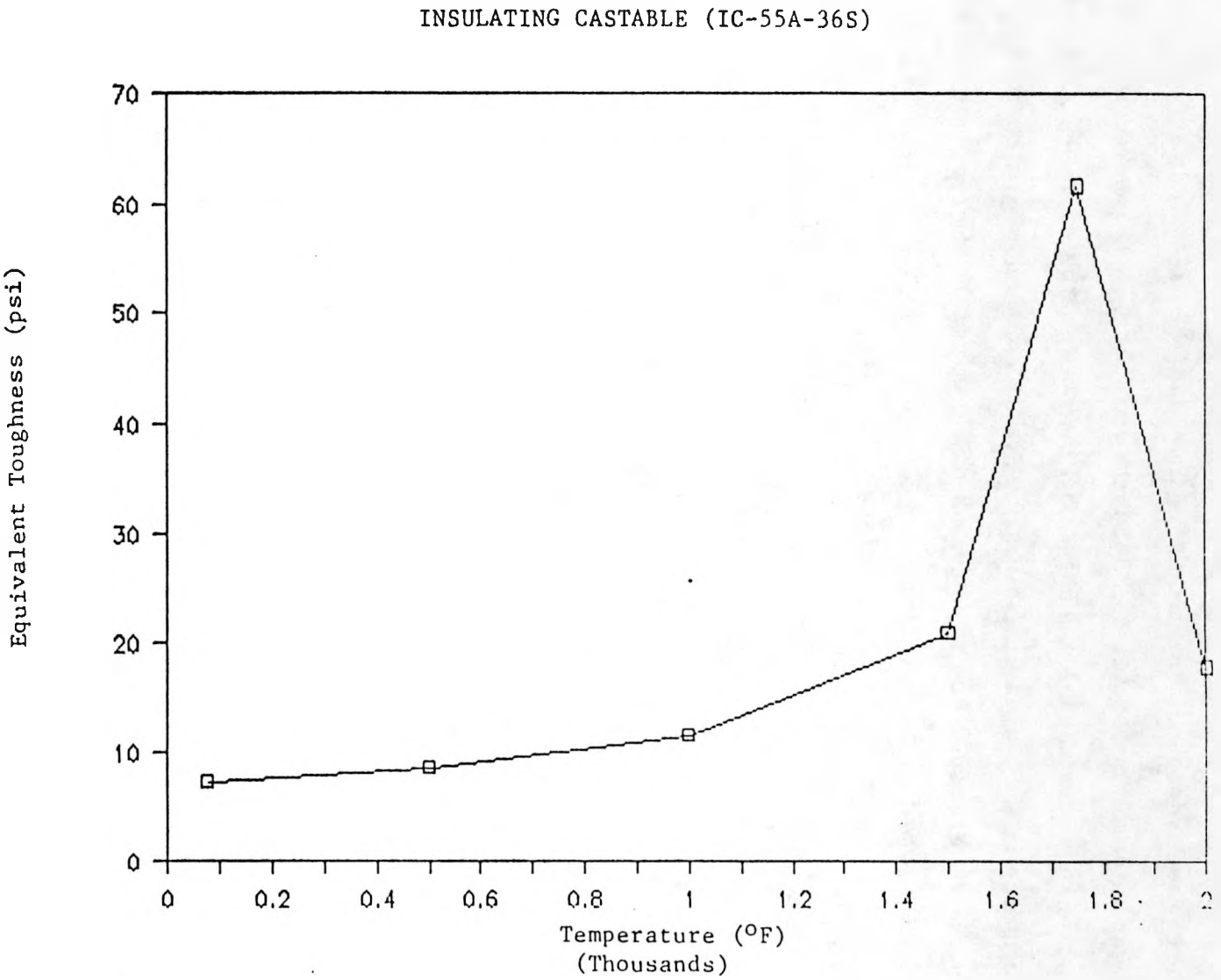

Figure 6-5: Vaiation of Toughness with Temperature for IC-55A-36S

difficult to measure true modulus at high temperatures due to creep contribution, the measured modulus is effectively a relaxed modulus.

The equivalent toughness (defined as the area under the stress-strain curve) variation with temperature for material IC-55A-36S is shown in Fig. 6.5. The equivalent toughness is approximately constant below 0.5 T_M, and increases sharply at 1750°F; followed by a sudden drop in the toughness. This may be related to the low strength for the temperature level above 2000°F. The equivalent toughness at 2000°F represents 20% of the toughness at 1750°F.

6.3 BEHAVIOR UNDER CONSTANT COMPRESSIVE LOADS AT CONSTANT TEMPERTURES

The variation of the creep strain for the insulating castable material IC-55A-36S was examined at temperature levels of 1500°F and 2000°F under high constant cmpressive loads (up to 70% of the monotonic strength). Fig. 6.6 investigates the variation of the creep strain depending on the temperature levels under a constant compressive stress. The selected temperature levels are 1000°F (538°C) and 1500°F (816°C) under 2.0 ksi, which is 53% and 67% of the monotonic compressive strength at 1000°F and 1500°F, respectively. The increase in creep strain at increased temperatrue is clearly shown in Fig. 6.6. The specimen of the insulating castable material IC-55A-36S under 67% of the compressive strength at 1500°F was fractured at the time of 3500 seconds after a constant stress level has been achieved. Variation of creep strain rate at different temperatures under a constant stress level is shown in Fig. 6.7, where the results are plotted as $\log(\dot{\epsilon}_{creep} \times 10^8)$ vs. time for different temperatures. The dropping of the creep strain-rate for the temperature level of 1000°F is more pronounced than that for the temperature level of 1500°F at the initial period of loading duration.

The variation of creep strain depending on the stress levels at a constant temperature

level is shown in Fig. 6.8. The used constant temperature was 1500°F with different stress levels of 46%, 57%, and 67% of the compressive strength at 1500°F. Variation of creep strain rate under different stresses at constant temperature level is shown in Fig. 6.9. The plot shows that all stress levels have almost the same value of the initial creep strain rate and the final creep strain rate (the steady-state creep strain rate). The differences in the creep strains of the three different levels of stresses are the amount and the duration of the primary creep strain.

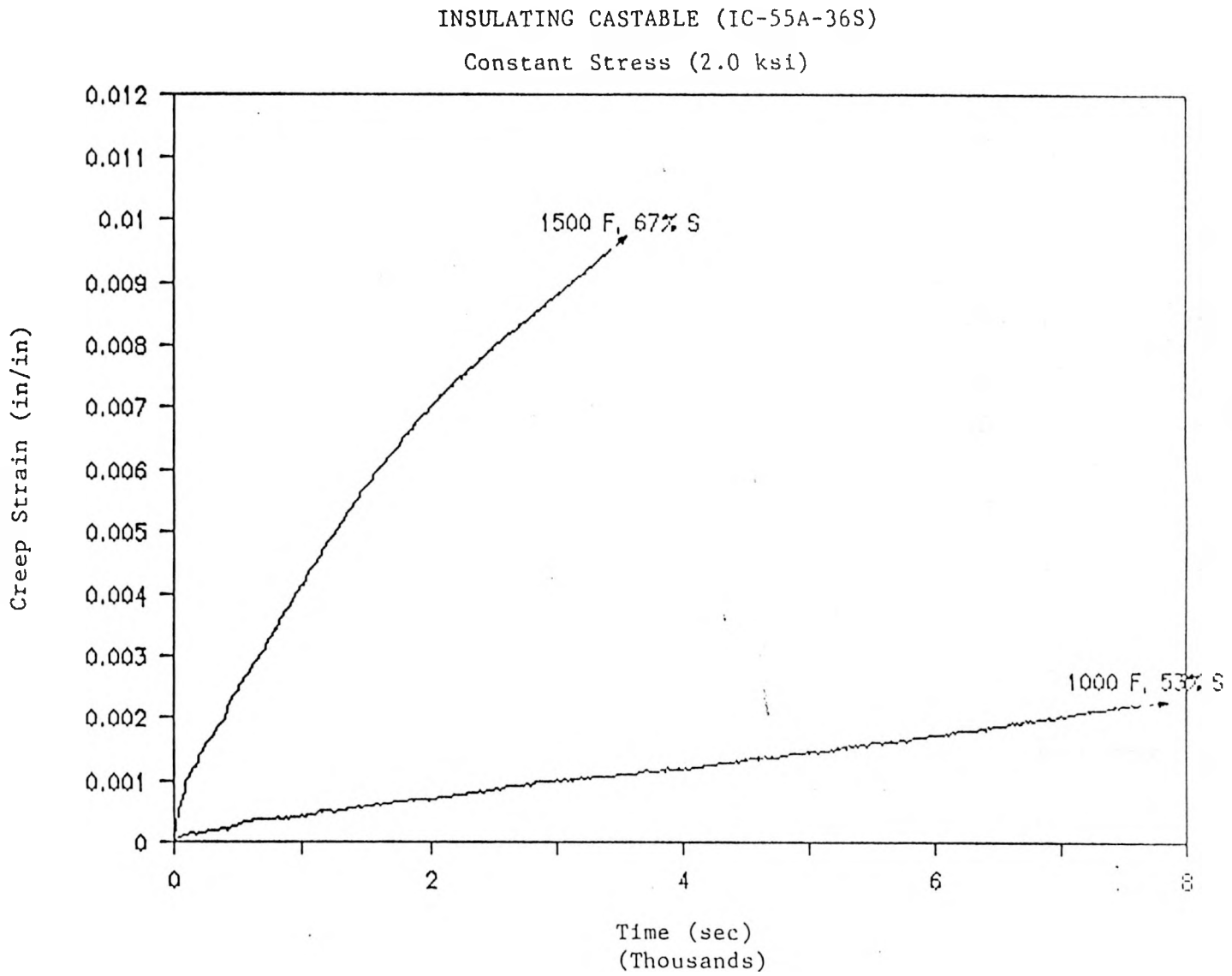

Figure 6-6: Creep Strains for IC-55A-36S at Different Temperatures under the Constant Stress Levels

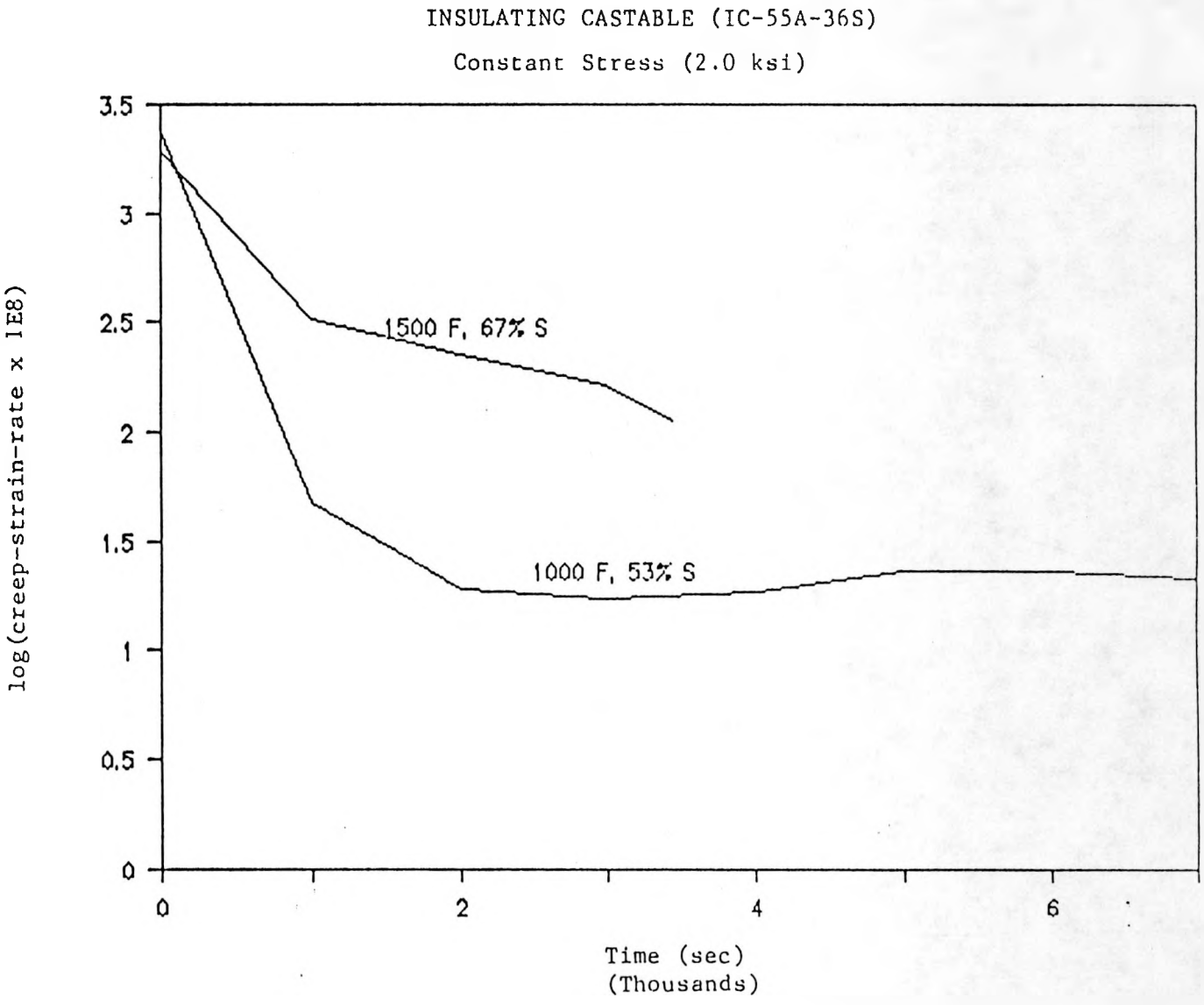

Figure 6-7: Variation of the Log of the Creep Strain-rate at Different Temperatures under the Constant Stress Levels

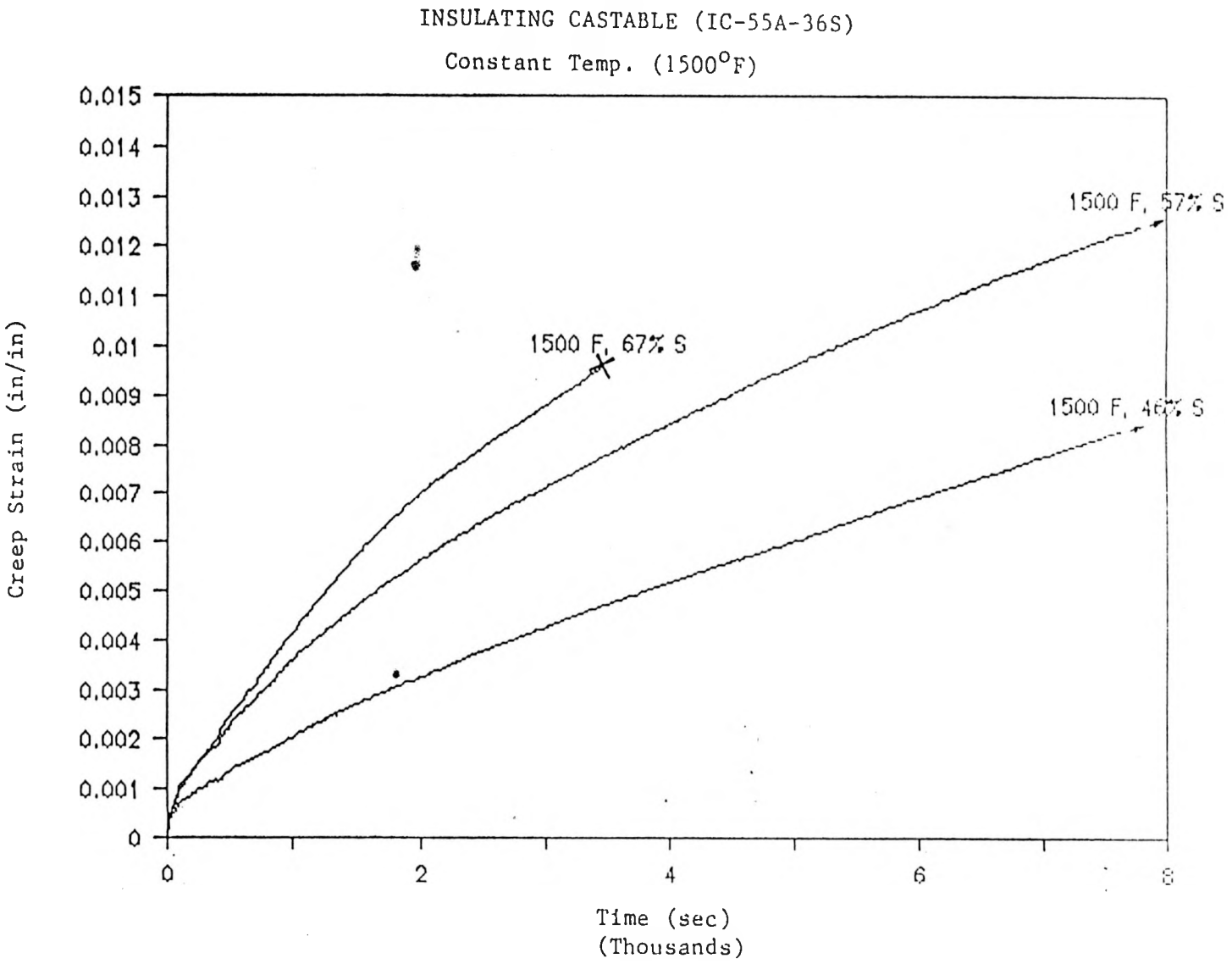

Figure 6-8: Creep Strains for IC-55A-36S under Different Stresses at Constant Temperature Level

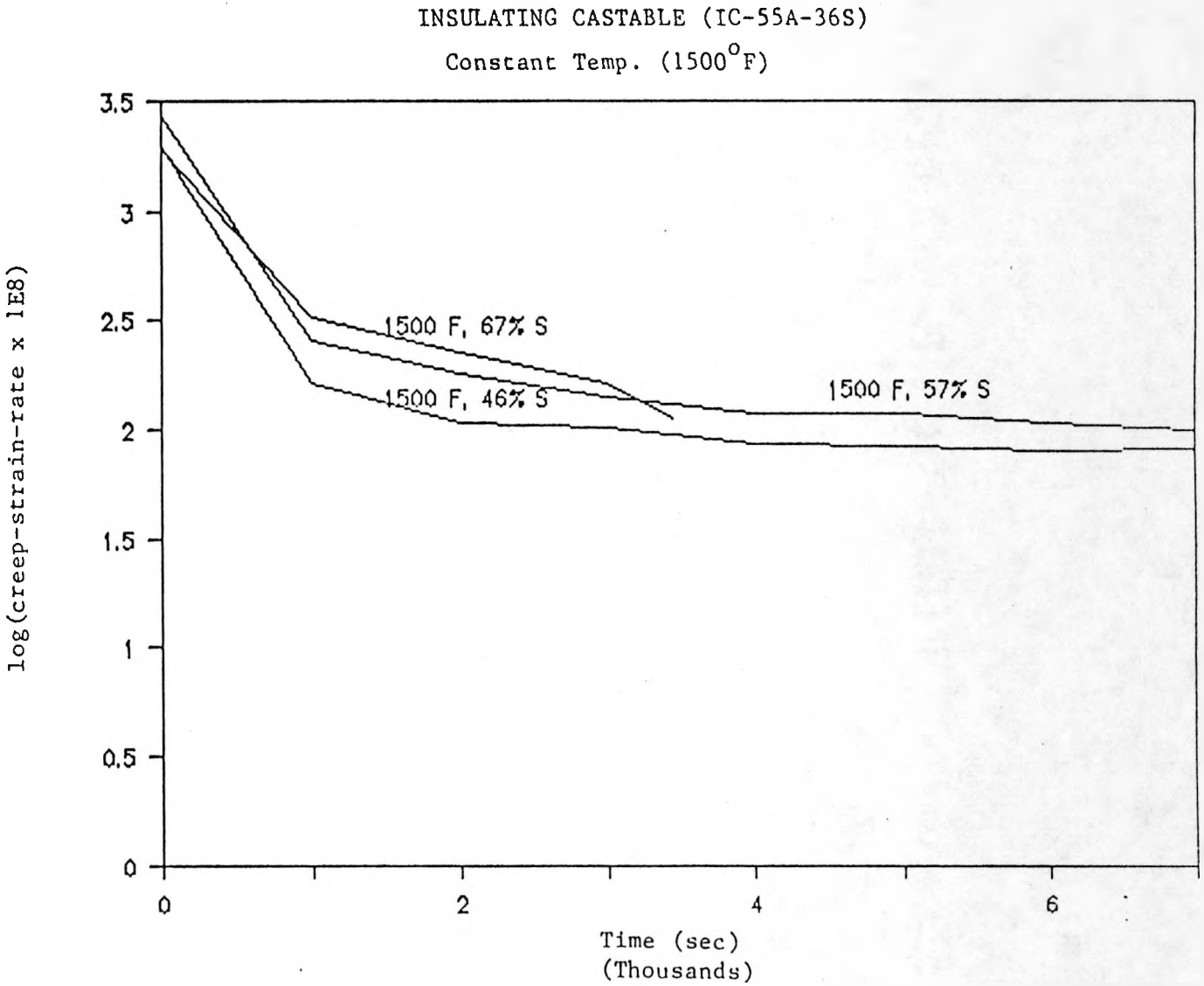

Figure 6-9: Variation of the Log of the Creep Strain-rate under Different Stresses at Constant Temperature Level

Chapter 7

INSULATING FIRE-BRICK MATERIAL

7.1 SYNOPSIS

This chapter presents the behavior of an insulating brick material IB-39A-44S. The elevated temperature behaviors under monotonic short term compressive loads are discussed in Section 7.2. Because of the low strength, the behavior under constant compressive loads at predetermined constant temperature could not be investigated. These themomechanical properties are summarized in the Appendix A.4.

7.2 BEHAVIOR UNDER MONOTONIC COMPRESSIVE LOADS AT CONSTANT TEMPERATURES

The effect of elevated temperature on the behavior of an insulating firebrick material IB-39A-44S under loading with constant displacement rate (7.218×10^{-5} in/sec) was studied. Cylindrical specimens with 1 inch diamter and 2.5-3.0 inches height were used for the proposed tests. Automatic sawing was used for preparing side surfaces of a specimen for testing. Parallel sides were preserved for preventing a local failure during testing. Stress-strain curves for different temperature levels, and a constant displacement rate are shown in Fig. 7.1. Different from other castable materials, the insulating firebrick material IB-

39A-44S shows almost a perfect elastic-plastic behavior regardless of the temperature levels. Therefore, the deformation behavior is initially linear up to the peak stress level, and changes to the permanently nonlinear shape without stress softening and/or stress hardening. The simplified stress-strain curves are shown in Fig. 7.2 by averaging the stress values which are in the range after the stress reaches a sharp changing point of the tangential stiffness (i.e a constant stress level). Therefore, no transition temperatures that separate the behaviors may be found in the insulating firebrick IB-39A-44S. This supports the concepts of the effects of the bonding changes on the strength of refractory materials explained in Section 2.2.1. Because the insulating firebrick IB-39A-44S was already fired at high temperature (above 2300°F(1260°C)), the bonding characteristics inside of the material would be retained until the temperature level exceeds the firing temperature. The material IB-39A-44S maintained the same light yellow color regardless of the temperature changes in the proposed tests, although small parts of burned points on the surfaces could be found after finishing the test. The dark burned points may be due to localized hot temperature before an uniform temperature level is achieved inside the furnace.

The variation of the strength of the insulating firebrick material IB-39A-44S is presented in Fig. 7.3. A slight decrease in strength is observed for temperature levels between room temperature and 500°F. The strength at 500°F represents a 13% decrease with respect to the strength at room temperature. Above 500°F, strength increases slightly with temperature up to 1000°F, followed by another smooth decrease in strength above 1000°F. However, the variation of the strength is so small (less than 10%) that it may be neglected in design considerations.

Since the peak strength values of the insulating firebrick material IB-39A-44S are too low, the use of this material for structural components is doubtful. As discussed in Section 3.3.2, a different test method for this insulating firebrick can be selected to verify

these test results.

The variation of the initial stiffness of the stress-strain curves is shown in Fig. 7.4. Even if the figure shows a slight change in the initial stiffness, the variation may be assumed negligible.

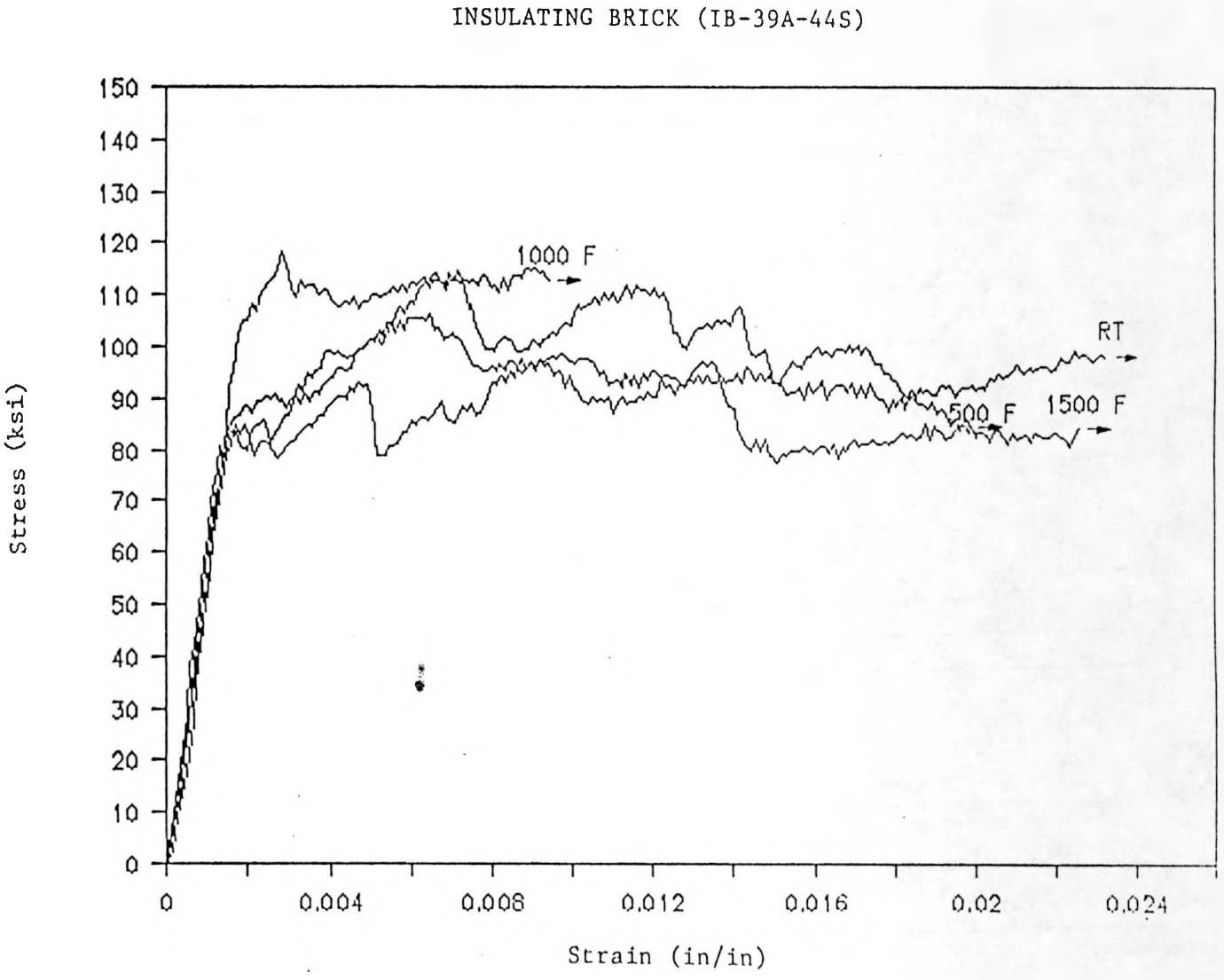

Figure 7-1: Stress-strain Curves for IB-39A-44S at Different Temperature Levels and a Constant Displacement Rate of 7.218×10^{-5} in/sec

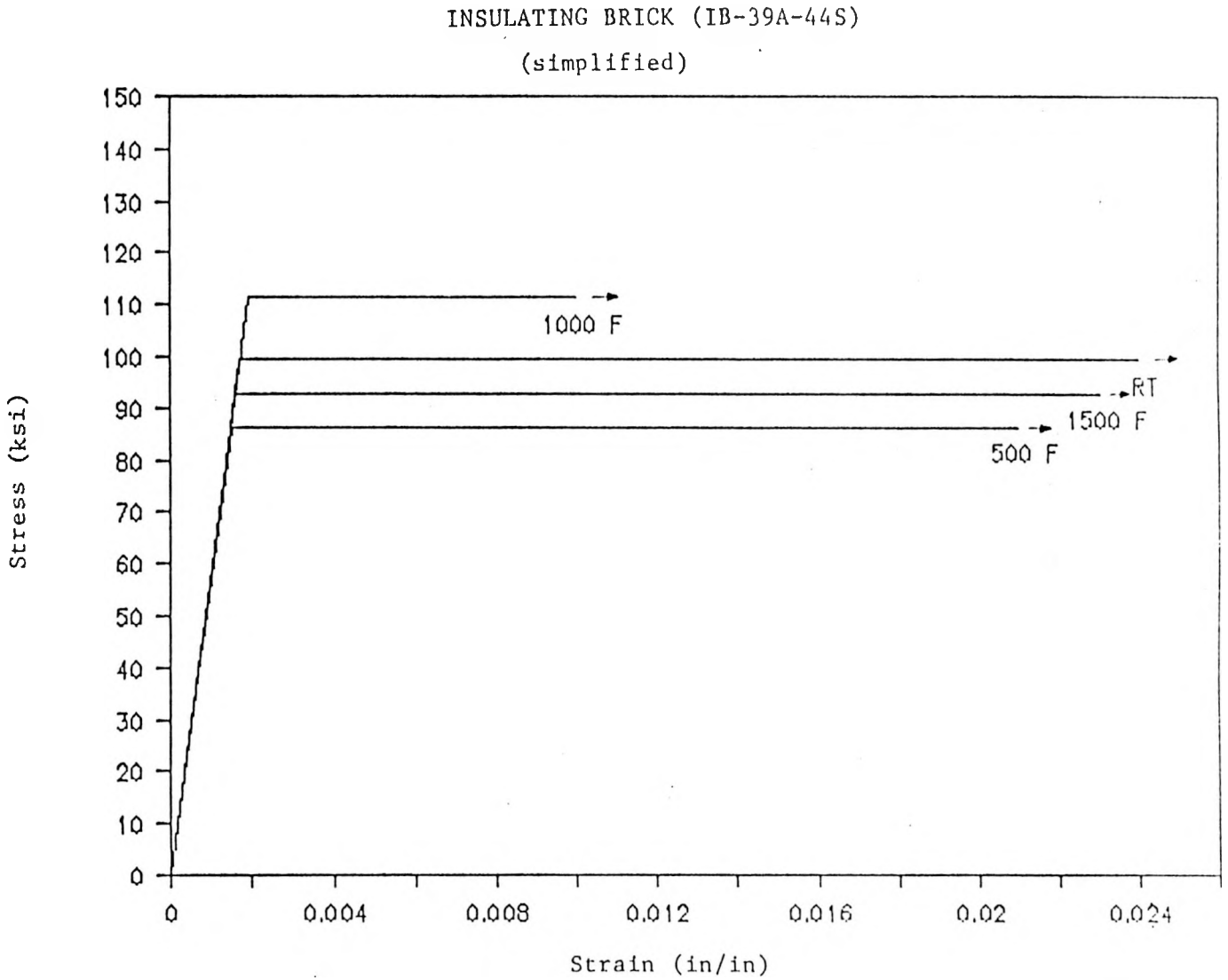

Figure 7-2: Simplified Stress-strain Curves for IB-39A-44S of Fig. 7.1

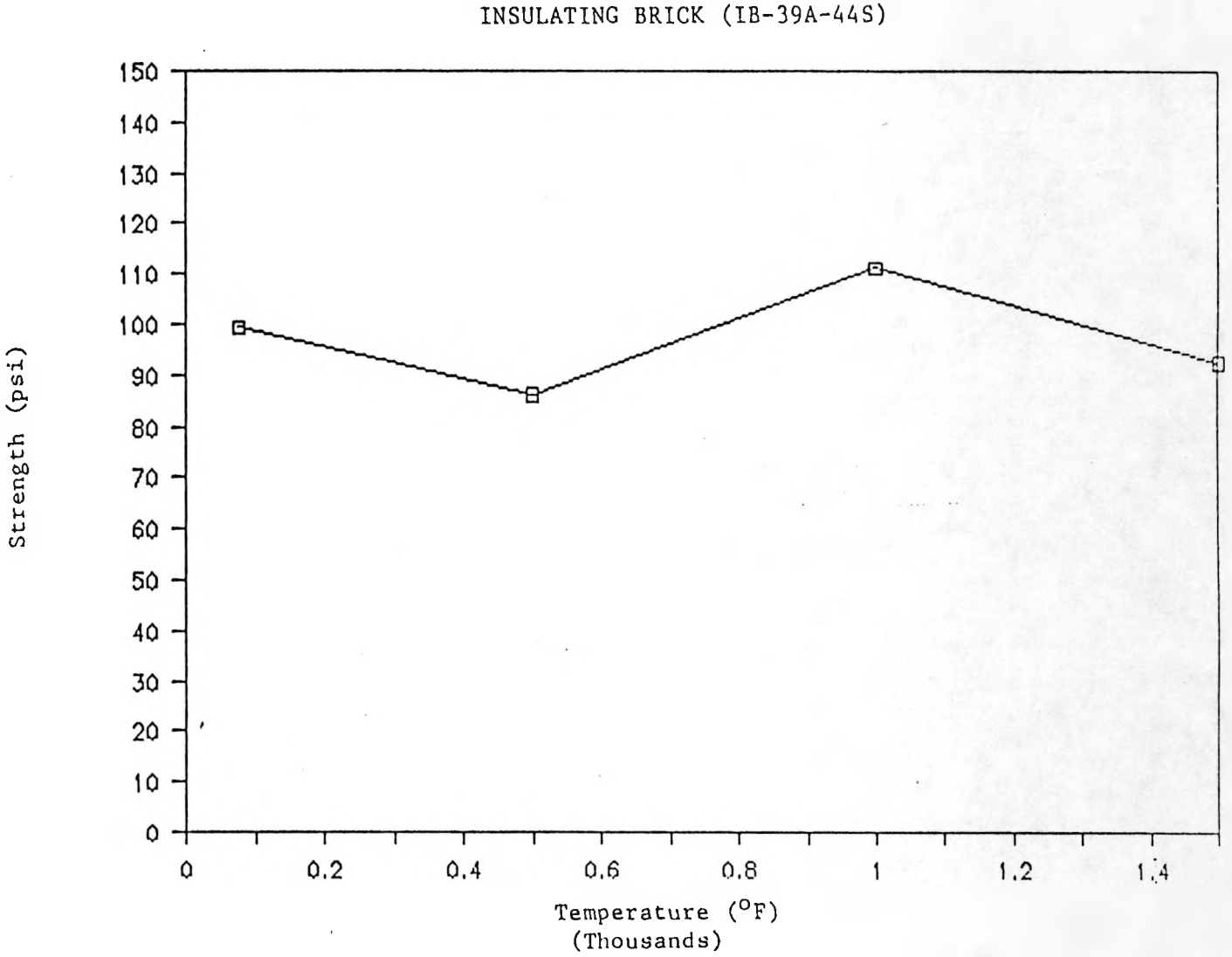

Figure 7-3: Strength Variation with Temperature for IB-39A-44S

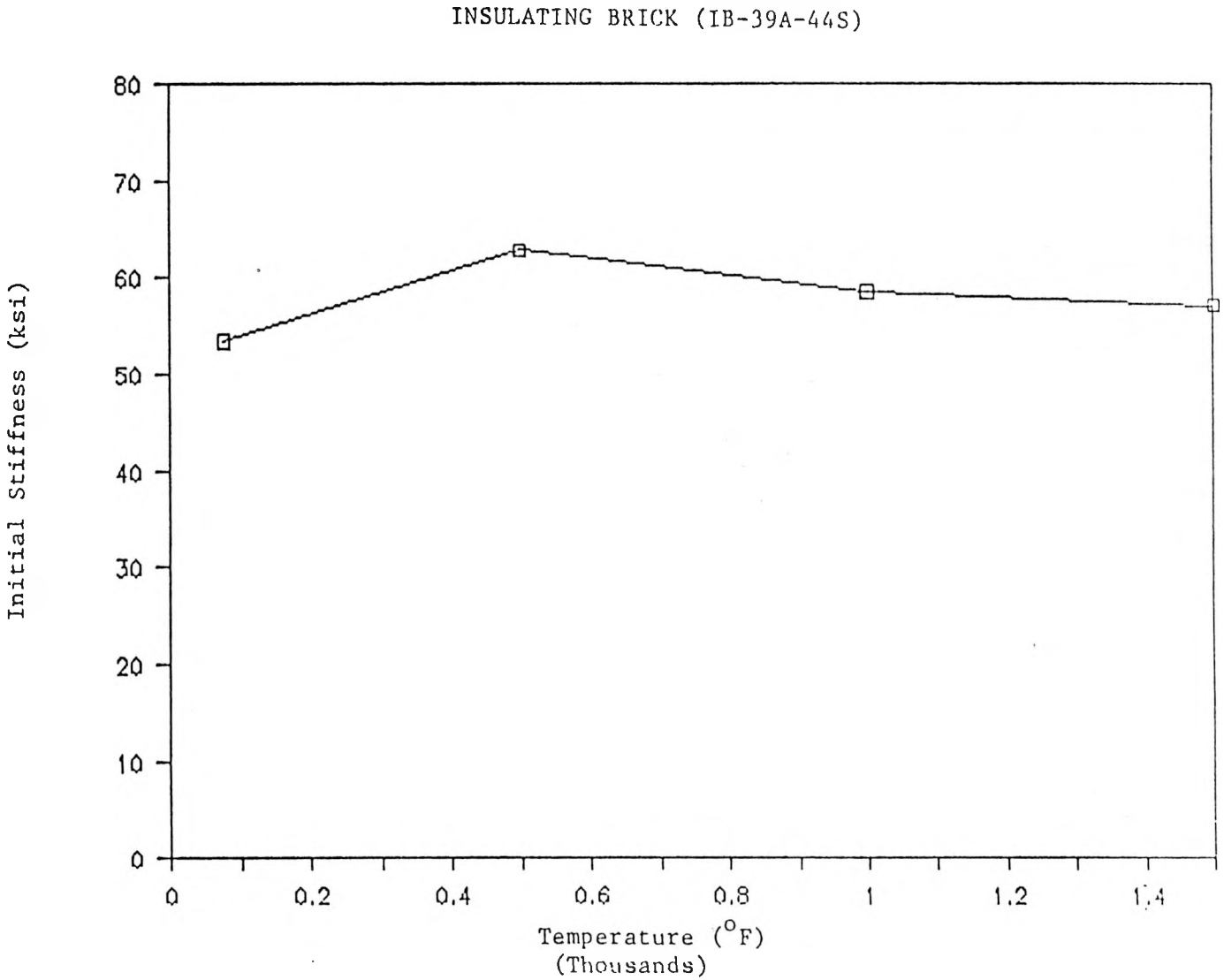

Figure 7-4: Variation of the Initial Stiffness with Temperature for IB-39A-44S

Chapter 8

MODELING OF CREEP BEHAVIOR

8.1 CREEP BEHAVIOR OF REFRACTORIES AT HIGH TEMPERATURE

One of the main problems in the nonlinear thermomechanical analysis of high temperature pressure vessels is the formulation of the creep behavior of refractory lining materials at high temperatures. This creep behavior may affect the overall stress-strain relationship of the refractories and the cracking behavior in refractory linings. Creep of concrete materials may be considered to be approximately linear for many types of response in the service stress range. Nevertheless, significant nonlinearities exist due to the several reasons as follows (Bazant, 1986):

1. nonlinearity due to humidity and temperature variation;
2. nonlinearity due to cracking or strain-softening;
3. nonlinearity due to cyclic loading;
4. nonlinearity at unloading and adaptation; and
5. nonlinearity at high stress and multiaxial viscoplasticity.

In most high temperature systems, creep becomes significant as temperature increases. Two main contingencies which must be avoided in the design of a high temprerature pressure vessel component operating within the creep range are: (1) the excessive deformation during operation and (2) the possibility of creep rupture (Findlay and Goodall, 1976).

For refractory lining materials, creep causes a significant stress redistribution in the refractory lining systems, since the magnitude of creep strain at high temperatrue is much larger than that of elastic strain. During the heating of the system under compressive stresses, creep tends to relax part of the local high compressive stresses, and these reduced compressive stresses show a critical effect at the beginning part of the holding period as shown in Fig. 8.1. These reduced compressive stresses cause tensile cracking during cooling. These redistributed stresses may cause damage on other areas, depending on the lining geometry, previous stress history, boundary conditions, and the heating/cooling process. From the observations, therefore, creep may be important at the initial stage of thermal cycles. This effects are well demonstrated in Fig. 8.1. This figure shows the analytical result for hoop, axial, and radial stresses in the center of the dense component with an 8 hours hold period (Pike et al., 1980). Because refractory materials have relatively low tensile strengths, and because the amount of the relaxation may be significant due to the high temperature effect, the cracking behavior of the refractory leading to the overall deterioration at early stages of operating may be accelerated. Other simulation runs with nonlinear finite element analysis programs under a constant temperature holding period have been carried out at M.I.T. (Tseng and Buyukozturk, 1982; Chen and Buyukozturk, 1984).

Generally a refractory material consists of a coarse material bonded by a second phase. The coarse material is usually a well-developed crystalline aggregate, while the second phase is often poorly developed with a lower degree of crystallinity, or is, in many cases, completely amorphous. A poorly developed second phase generally plays a major role in determining the properties, including creep (Bray, 1986). In refractory materials,

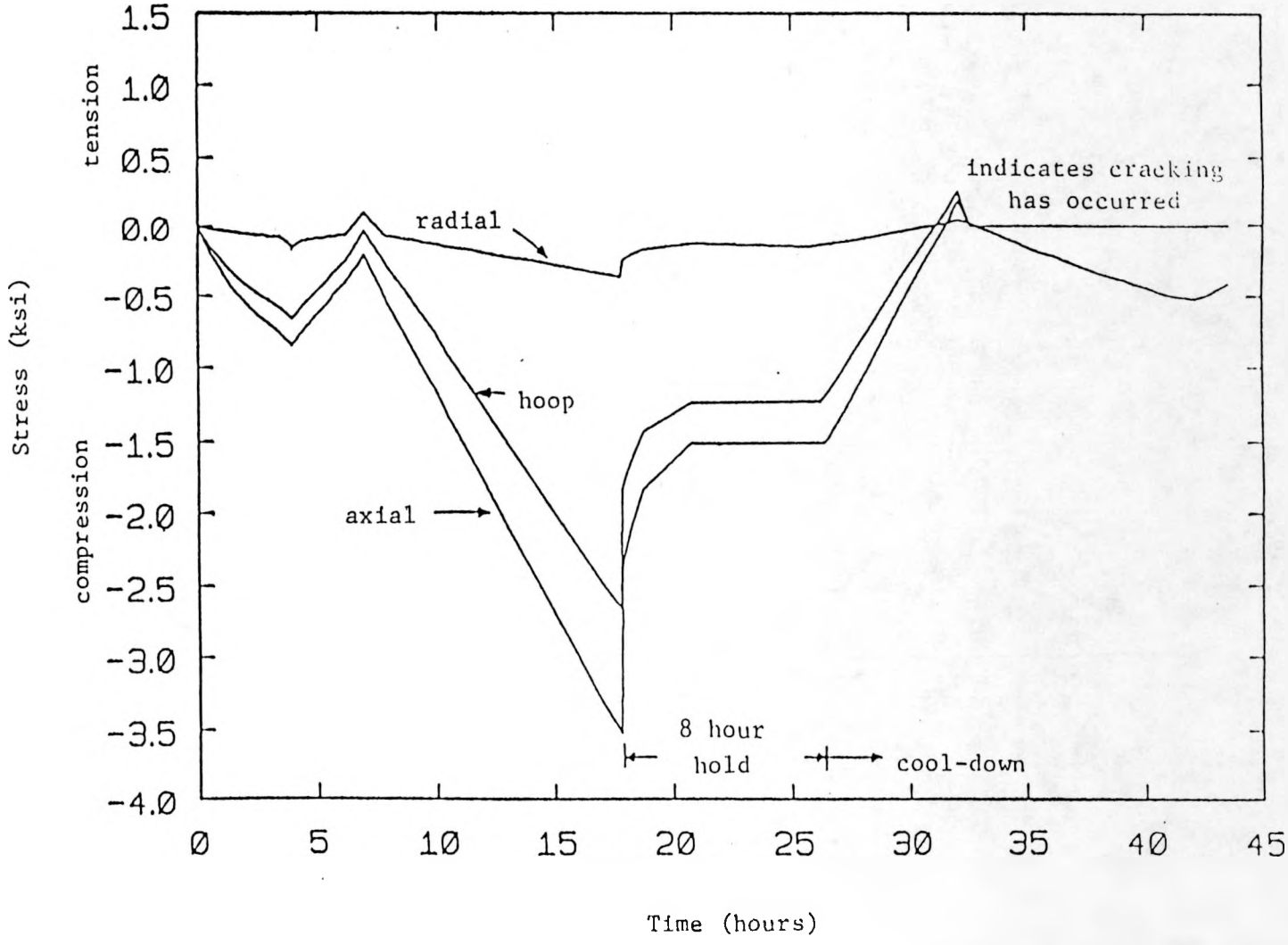

Figure 8-1: Hoop, Axial and Radial Stresses in the Center of the Dense Component with an 8 Hour Hold Period (Pike et al., 1980)

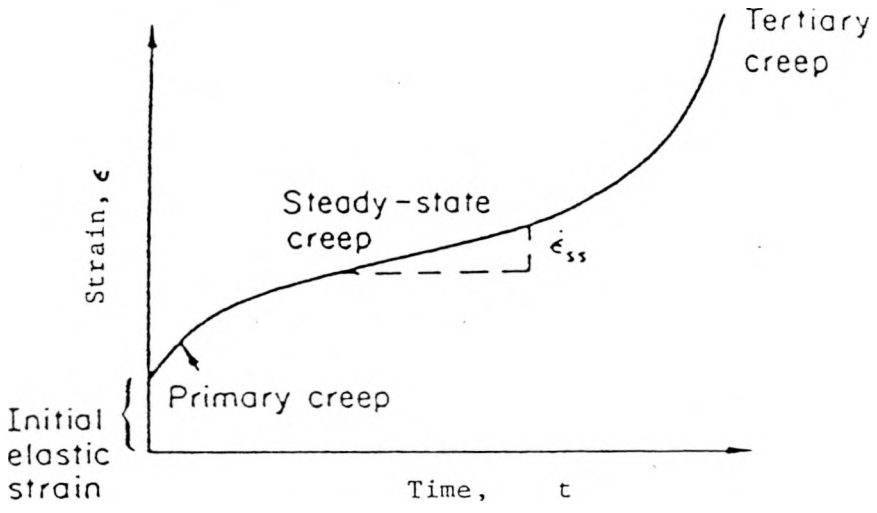

Figure 8-2: A Typical Creep Curve

creep is significant after the temperature goes over 0.4-0.5 T_M (where T_M is the melting point) under applied stresses. A typical creep curve (Fig. 8.2) can be divided into four stages:

1. initial elastic strain,

2. primary creep,

3. secondary (steady-state) creep, and

4. tertiary creep.

Primary creep occurs quickly compared with steady-state creep. The usual primary creep period of refractory materials may be between 5 and 30 hours depending on stress and temperature levels (Bray, 1986; Tamer and Buyukozturk, 1988). Since creep effects on the refractory lining systems are significant in early stages of temperature cycles,

this primary creep is important in analyzing the refractory system. In the secondary creep range, the strain increases steadily with time. In designing against creep, it is this steady accumulation of strain with time that concerns us most. Because it also leads to irrecoverable or permanent strains, which is one of the most typical properties of brittle materials, this steady-state creep is of engineering importance. Tertiary creep leads to the creep damage and/or creep fracture. Since creep damage, in the form of internal cavities, accumulates, creep rates go up even faster than stress does due to the cavity growth. Sometimes, for brittle materials, the ultimate strain is almost the same as the strain to enter the tertiary region; i.e. it is the stationary stress value which dictates failure (Findlay and Goodall, 1976). Creep rupture time (t_f) can be determined from Larson-Miller plot (Fig. 8.3). This figure is drawn with data for the time to onset of tertiary creep and/or for the failure. This allows correspondence between temperature and time to failure.

Creep strain of refractory materials depends on temperatue(T), stress(σ), and time(t). The time effect, or so-called aging effect, on refractories at high tempratures can be negelected because most of the inside moisture will be evaporated during heating.

General high-temperature creep mechanisms ($T \geq 0.4 - 0.5\ T_M$) can be categorized by (1) dislocation creep (which gives power-law creep) and (2) diffusional creep (which gives linear-viscous creep). The rate of both types of creep is usually limited by diffusion, so both follow Arrehnius' law. Diffusion becomes appreciable at about 0.3 T_M; that is why materials start to creep above this temperature.

Power-law creep occurs at high stress levels, and it is rate-dependent. With the microstructural consideration, this creep is associated with dislocation glide, disloaction climb-plus-glide, and grain boundary sliding (Ashby and Jones, 1980; Frost and Ashby, 1982) Power-law creep by glide alone may occur when the activation energy is so small that the thermally-activated glide leads to creep-like behavior above 0.3 T_M. The acti-

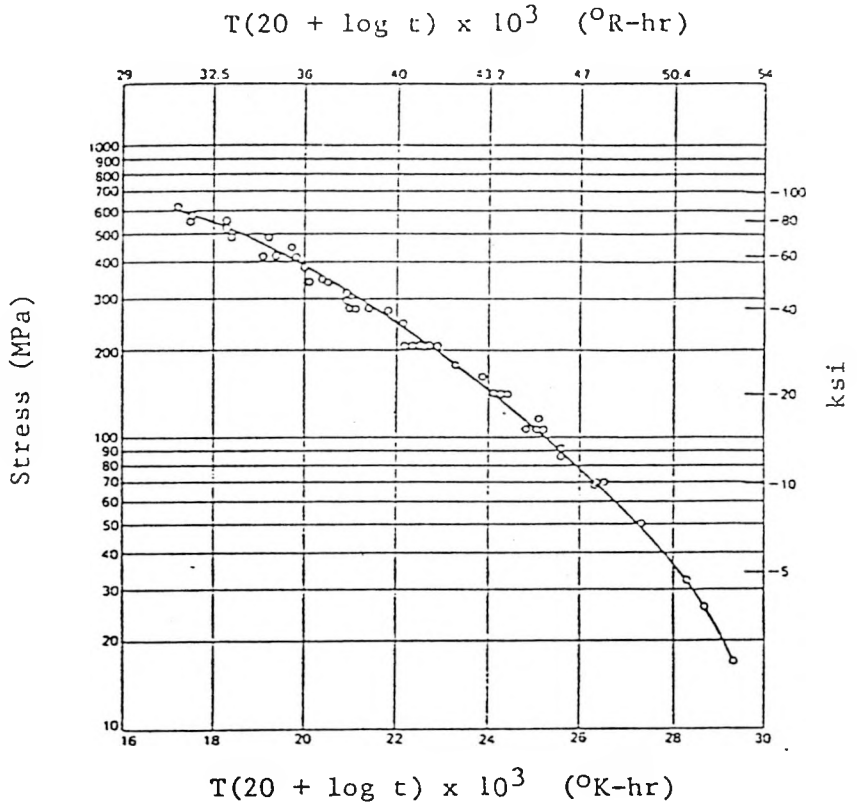

Figure 8-3: Larson-Miller Plot for Creep Rupture Time (t_f)

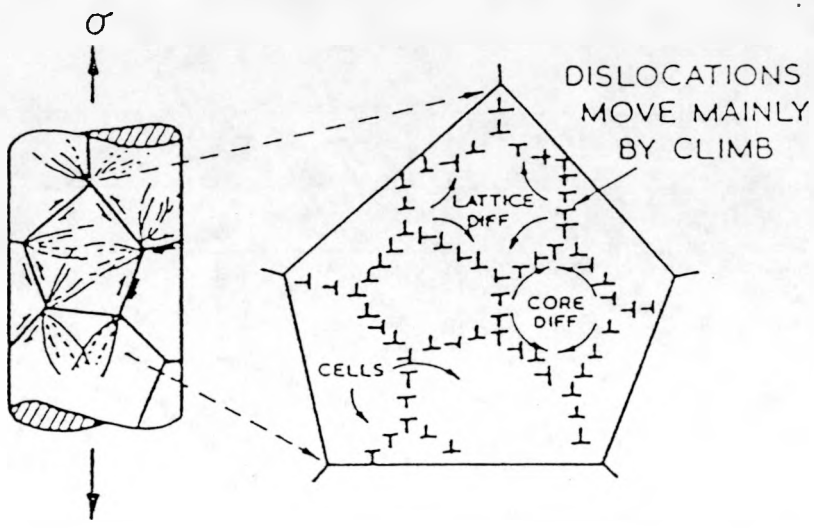

Figure 8-4: Power-law Creep by Dislocation Climb (Frost and Ashby, 1982)

vation of dislocation segements over obstacles leads to a drift velocity which approaches a linear dependence on stress. This glide-controlled creep may be important in ice and in certain ceramics, and in metals below 0.5 T_M.

At high temperature, dislocations acquire a new degree of freedom: they can climb as well as glide as shown in Fig. 8.4 & Fig. 8.5. Fig. 8.4 shows power-law creep involving cell formulation by climb, and Fig. 8.5 illustrates how the climb-glide sequence leads to creep. If a gliding dislocation is held up by discrete obstacles, a little climb may release it, allowing it to glide to the next set of obstacles where the process is repeated. The important feature which distinguishes these mechanisms from others is that the rate-controlling process, at an atomic level, is the diffusive motion of single ions or vacancies to or from the climbing dislocation, rather than the activated glide of the dislocation itself. At high stresses (above about $10^{-3}\mu$, where μ is shear modulus), the simple

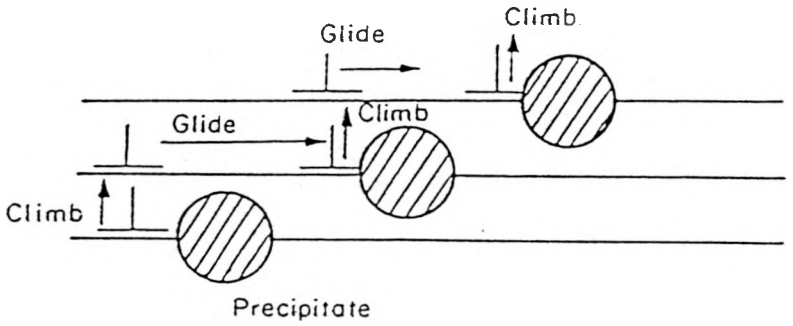

Figure 8-5: Graphical Illustration of the Climb-Glide Sequence (Ashby and Jones, 1980)

power-law breaks down so that the measured strain-rates are greater than expected. The process is evidently a transition from climb-controlled to glide-controlled flow as shown in Fig. 8.6.

At high temperatures (above 0.6 T_M) power-law creep may be accompanied by repeated wave recrystallization as shown in Fig. 8.7 (Nicholls and McCormick, 1970). Each wave removes or drastically changes the dislocation substructure, allowing a period of primary creep, so that the strain-rate (at constant load) accelerates.

Diffusional creep occurs at relatively low stress levels, and is controlled by the diffusion process. As the stress is reduced, the rate of power-law creep falls quickly. But creep does not stop; instead, an alternative mechanism takes over. As Fig. 8.8 shows, the applied stress, σ, can be relieved by grain elongation; here, σ acts again as a mechanical driving force, this time for diffusion from one side of the grain to the other. Diffusional flow by diffusional transport through and round the grains is illustrated in Fig. 8.9. The strain-rate may be limited by the rate of diffusion or by that of an interface interaction. At higher temperature ($T > 0.6\ T_M$) with this creep range, this diffusion is limited by

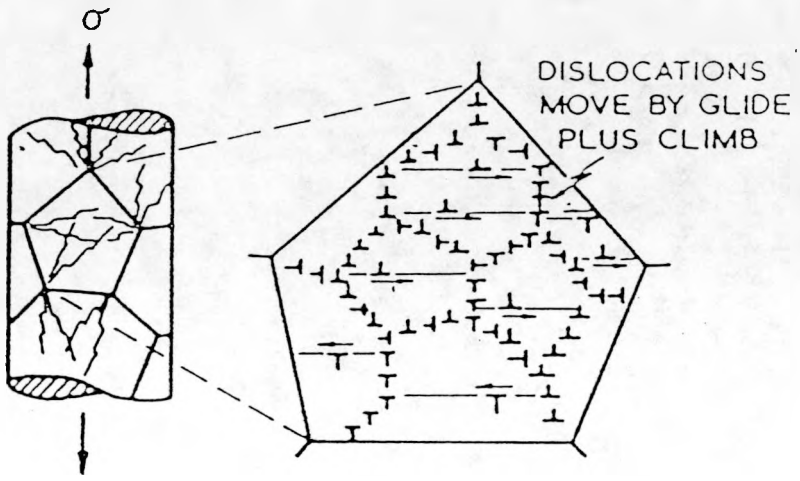

Figure 8-6: Power-law Breakdown (Frost and Ashby, 1982)

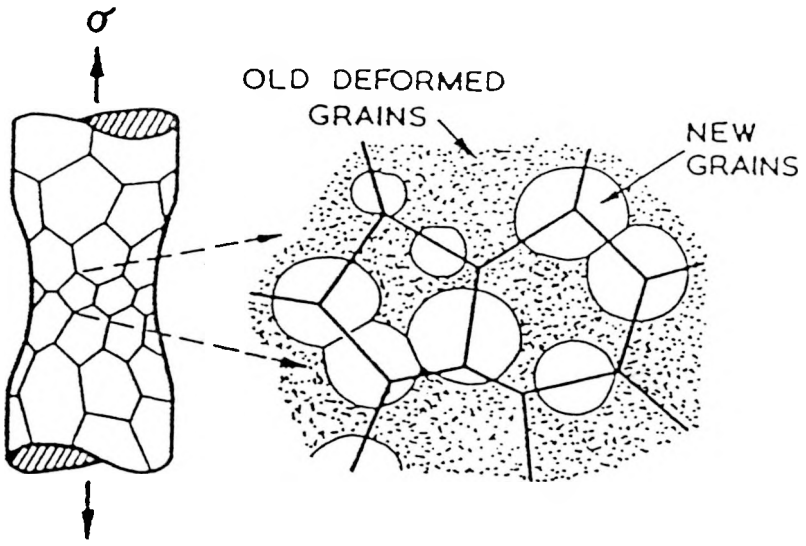

Figure 8-7: Dynamic Recrystallization of Power-law Creep (Frost and Ashby, 1982)

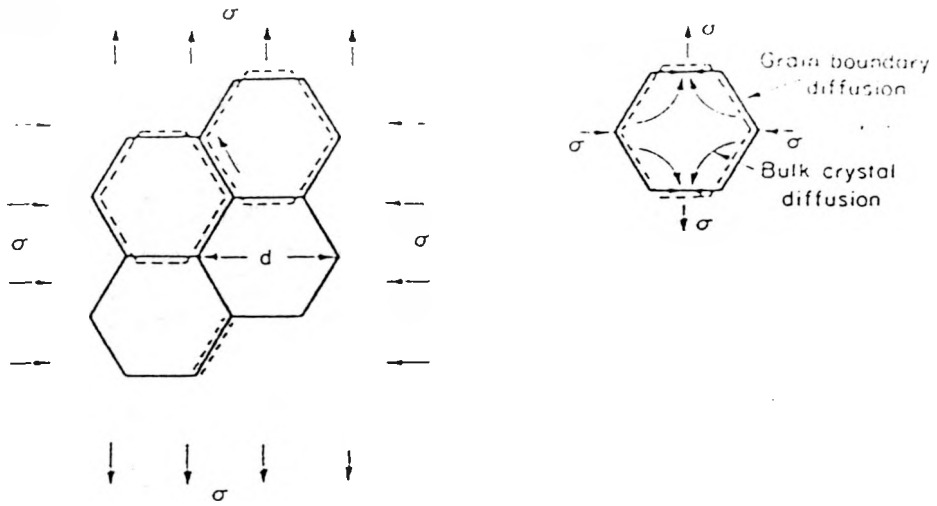

Figure 8-8: Mechanisms of Diffusional Creep (Ashby and Jones, 1980)

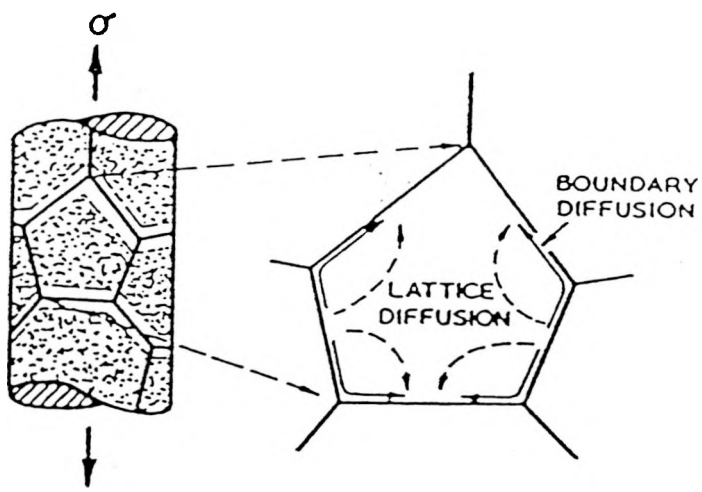

Figure 8-9: Diffusional Flow by Diffusional Transport Through and Round the Grains (Frost and Ashby (1982)

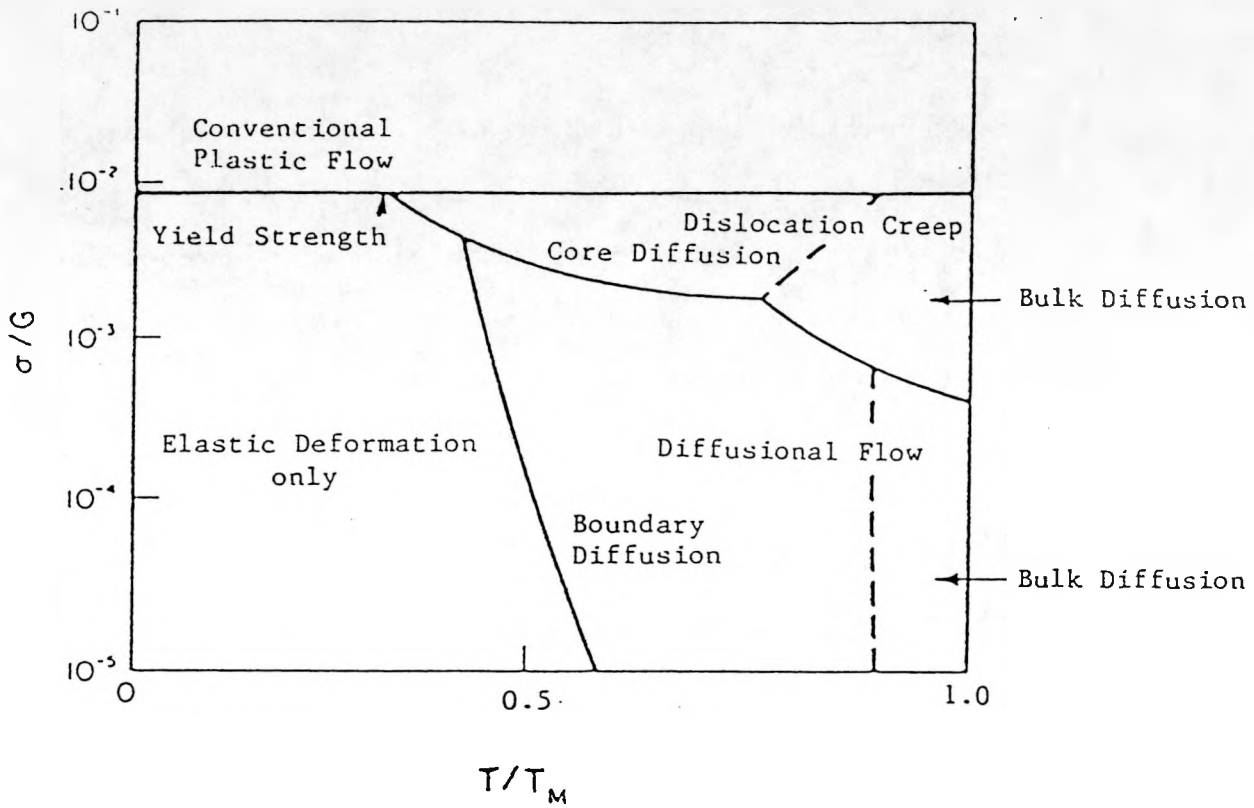

Figure 8-10: A Deformation Mechanism Map at Different Stresses and Temperatures

lattice diffusion (Nabarro-Herring creep: Nabarro, 1948; Herring, 1950). At lower T/T_M, when bulk diffusion is slow, grain-boundary diffusion (Coble creep: Coble, 1963) takes over, but the creep rate is still proportional to σ (Ashby and Jones, 1982: Tamer and Buyukozturk, 1988).

A deformation mechanism map, such as Fig. 8.10, is used as a useful way to represent the deformation behavior of the material with respect to temperature. It displays the relationship between the three variables; stress, temperature, and creep strain-rate, and gives a guideline to users and designers. Diargrams like these are available for many metals and ceramics, and are a useful summary of creep behavior, helpful in selecting a material for high-temperature applications.

8.2 REVIEW OF AVAILABLE CREEP MODELS FOR HIGH TEMPERATURE SYSTEMS

8.2.1 General Formulations

Many uniaxial and multiaxial constitutive models to describe the creep behavior are avilable in the literature (Wygant and Crowley, 1964; Snyder and Bathe, 1977; Pike et al., 1980; Tseng and Buyukozturk, 1982; Chen and Buyukozturk, 1984; Bray, 1986). Some of the basic 'simplified' uniaxial relations ingnoring the tertiary phase are well organized by Boyle and Spence(1983).

The most common form of nearly all approaches is to separate strain into the elastic and the inelastic parts:

$$\epsilon = \epsilon_E + \epsilon_C \tag{8.1}$$

where the inelastic strain may include only creep strain. The creep strain resulting from a constant load test may be written as a function of stress (σ), time (t), and temperature

(T):

$$\epsilon_C = f(\sigma, t, T) \tag{8.2}$$

which can be usually assumed to be separable as:

$$\epsilon_C = f_1(\sigma)\, f_2(t)\, f_3(T) \tag{8.3}$$

Some suggestions for the stress dependence ($f_1(\sigma)$) are:

- $f_1(\sigma) = B\sigma^n$ Norton
- $f_1(\sigma) = C sinh(\alpha\sigma)$ Prandtl
- $f_1(\sigma) = D exp(\beta\sigma)$ Dorn
- $f_1(\sigma) = A[sihn(\gamma\sigma)]^n$ Garofalo
- $f_1(\sigma) = B(\sigma - \sigma_o)^n$ Friction Stress

where sysmbols other than σ are material constants.

Suggestions for the time dependence ($f_2(t)$) are:

- $f_2(t) = t$ Secondary creep
- $f_2(t) = b\, t^m$ Bailey
- $f_2(t) = (1 + b\, t^{1/n})\, e^{kt}$ Andrade
- $f_2(t) = \sum_j a_j\, t^{m_j}$ Graham and Walls

Some functions for the temperature dependence ($f_3(T)$) are:

- $f_3(T) = A exp(-\frac{Q}{RT})$ Arrhenius' Law
- use temperature shift factor a_T.

where Q is the activation energy, R is Boltzmann's constant, and T is the absolute temperature.

For varying stresses, rate forms were examined with two different types of hardening rules for this kind of creep formulation. The hardening rules are (1) time-hardening and (2) strain-hardening. A simplest example of this type of creep model is:

$$\epsilon_C = B\sigma^n t^m \tag{8.4}$$

The time-hardening form of Eq. (8.4) for varying stresses is:

$$\dot{\epsilon_C} = \frac{d\epsilon_C}{dt} = mB\sigma^n t^{m-1} \tag{8.5}$$

This equation explains that the strain rate at any time depends on the elapsed time.

The strain-hardening form of Eq. (8.4) for varying stresses is:

$$\dot{\epsilon_C} = mB^{1/m}\sigma^{n/m}\epsilon^{1-1/m} \tag{8.6}$$

This equation indicates that strain-rate depends on the accumulated creep strain.

The comparison of these forms can be best understood graphically from Fig. 8.11. These two results are obviously the same for constant stress. For varying stress conditions, however, the strain-hardening form usually showed better agreement with the test results than the time-hardening rule as shown in Fig. 8.11. The choice of the rate form is an attempt to model the primary creep phase of decreasing creep strain rate and the secondary creep phase. They do not account for all the creep strain observed, and do not represent well the important recovery phenomenon for unloading. Two particular advantages of such formulations are:

1. they are capable of representing a wider range of material behavior including conventional plasticity and creep; and

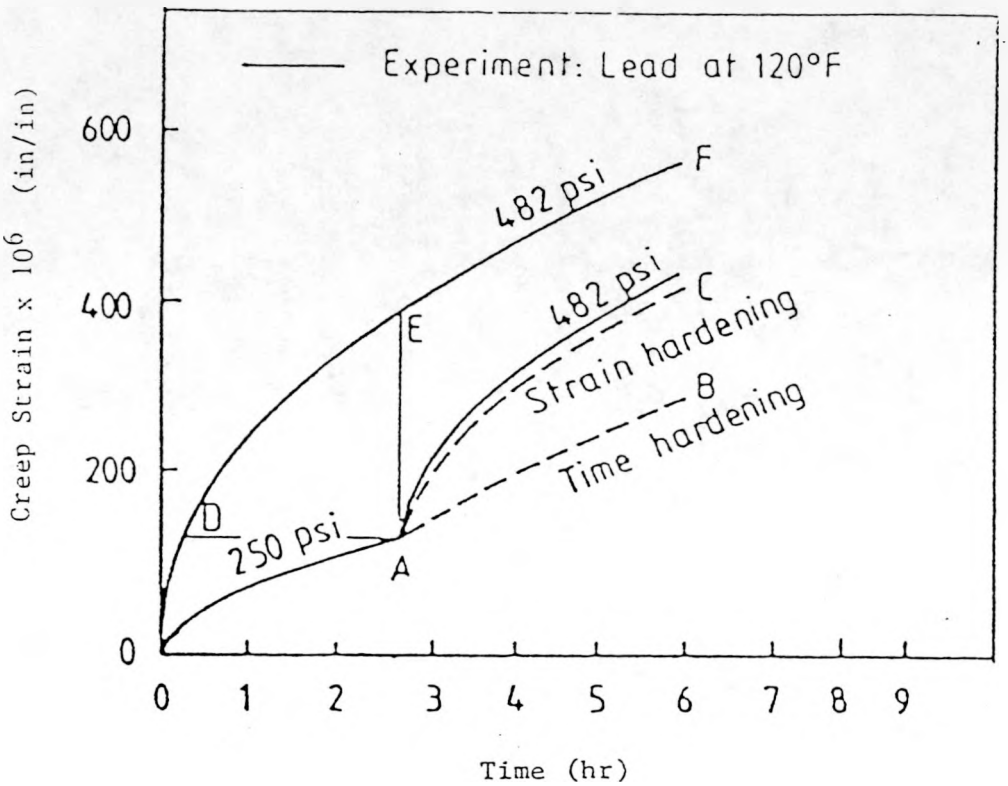

Figure 8-11: Experimental Comparison of Time- and Strain-hardening Theories (Boyle and Spence, 1983)

1. they are capable of representing a wider range of material behavior including conventional plasticity and creep.

2. they are useful in stress analysis.

Another common form to predict the creep behavior is from a visco-elastic or visco-plastic model. Some examples of those spring-dashpot models are shown in Fig. 8.12. For varying stresses, those models also used the stress-hardening rule. Some Finite Element analysis work with such visco-models were published (Zienkiewicz and Cormeau, 1974;

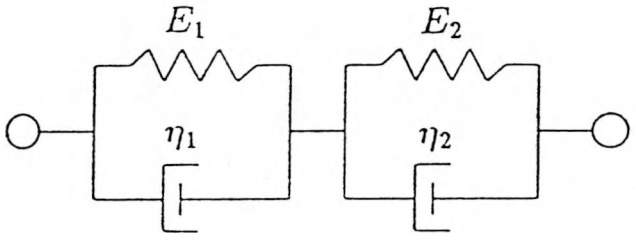

Figure 8-12a: Two Series of Kelvin Model (Pike et al., 1980)

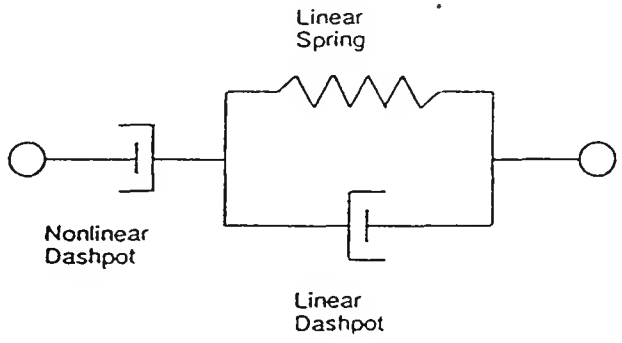

Figure 8-12b: Modified Visco-elastic Model (Tseng and Buyukozturk, 1982)

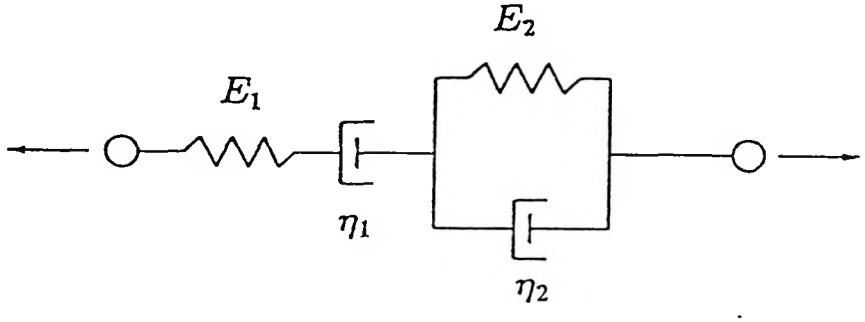

Figure 8-12c: Burger-body Model

8.2.2 Discussion on Incompressibility of Creep

Most multiaxial creep models for high temperature systems available in the literature were based on the concept of incompressible creep strain which depends only on deviatoric stress (S_{ij}), and were generalized by using effective stress($\overline{\sigma}$) and effective strain($\overline{\epsilon}$) concepts in the flow rules, such as:

$$\dot{\epsilon}^c_{ij} = \frac{3}{2}\frac{\dot{\overline{\epsilon}}^c}{\overline{\sigma}} S_{ij} \tag{8.7}$$

where $\overline{\sigma} = \sqrt{\frac{3}{2} S_{ij} S_{ij}}$, $\dot{\overline{\epsilon}} = \sqrt{\frac{2}{3}\dot{\epsilon}_{ij}\dot{\epsilon}_{ij}}$.
In this equation, the rate of creep strain is also easily found to be only a function of deviatoric stress. One typical example of this kind creep model can be found in the reference by Snyder and Bathe (1977).

This incompresibility restriction is only applicable for materials which show plastic behavior. Those materials preserve volumes and the hydraulic component of stress has no effect on creep. For brittle materials, however, this incompressible creep concept can not be applied, because the creep Poisson's ratio (ν_c) of the brittle materials are less than 0.5. Concrete materials, for example, were investigated to have 0.2 of creep Poisson's ratio even at high temperature (Blundell et al., 1976; Babcock & Wilcox, 1981; Bazant, 1986). Therefore, more complicated creep models, which can include the creep Poisson's ratio in its formulation, have been proposed (Pike et al., 1980; Tseng and Buyukozturk, 1982; Chen and Buyukozturk, 1984). One of the interesting ways to deal with this point was illustrated by Chen and Buyukozturk (1984). They decomposed the creep strain into a deviatoric component (e^c_{ij}) and a volumetric component (ϵ^c_v):

$$\Delta\epsilon^c_{ij} = (\dot{\epsilon}^c_{ij} + \frac{1}{3}\dot{\epsilon}^c_{ij}\delta_{ij})\,\Delta t$$

They defined the deviatoric creep strain as only a function of deviatoric stress, and

the volumetric creep strain as a function of volumetric stress. This means that they did not account for the volume changes due to shear stresses, i.e. shear-dilatation. Therefore, since the shear dilatation is known as one of the typical properties of brittle materials, a new model is required to include this phenomenon.

8.3 A GENERALIZED CREEP MODEL FOR HIGH TEMPERATURE SYSTEMS

8.3.1 Desirable Requirements For A Creep Model of Refractory Materials

From the review of section 8.2, some desirable features for high temperature creep behavior may be summarized. Even if they are essential in creep analysis of high temperature systems, however, none of the available models satisfied all of the following requirements. The creep model:

1. must be in the rate form (or incremental form) instead of total stress-strain formulation, to satisfy varying stress conditions;

2. should be able to follow the irrecoverable phenomena under unloading conditions;

3. must include temperature(T) and time(t) as variables in its formulation;

4. for refractory materials should be able to express the primary creep, because creep effects on refractory materials are significant in the early stages of thermal cycles (Some models often treat this primary creep in much the same way as elastic deformation is considered for in a structure);

5. must include creep Poisson's ratio (usually $\nu_c \simeq 0.2$) at high temperatures in a generalized multiaxial formulation; and

6. should be easily included in a computer program.

Among these requirements, the first two terms are for general creep behavior regardless of temperature, while the requirements 3-5 are for high temperature conditions.

8.3.2 Development of A Generalized Creep Model

The most widely used creep model at high temperature is a power-law equation. Creep strain rate $\dot{\epsilon}_{creep}$ is given by:

$$\dot{\epsilon}_{creep} = A\sigma^n e^{(-\frac{Q}{RT})} \tag{8.8}$$

where A is a constant, σ is the stress raised to a stress exponent n, Q is the activation energy, R is the molar gas constant ($= 8.31 J/moleK$), and T is the absolute temperature (K). Two types of tests are needed to determine A,n, and Q. The first is the constant stress tests under several different temperature levels. From Fig. 8.13(a) which is a plot of ln $\dot{\epsilon}_{ss}$ vs. 1/T (where $\dot{\epsilon}_{ss}$ is steady state creep rate), Q would be determined as the slope. The second is the constant temperature test under different stress levels. From the plot of ln $\dot{\epsilon}_{ss}$ vs. ln σ shown in Fig. 8.13(b), n and A can be obtained, and 'n' would be the slope.

The power-law creep equation is applicable to the steady-state (secondary) creep part in a uniaxial condition. However, for refractory systems, the creep effects from the primary creep part are also important as explained already. Therefore, this primary creep must be included in the formulation of a creep model, and be generalized to three dimensional stress states.

A usual way to include the primary creep has been suggested by Tseng and Buyukozturk (1984) and Bray (1986). In the proposed creep model, for the uniaxial case, creep strain is divided into two components such as the primary creep dominant term (ϵ^{1c}) and

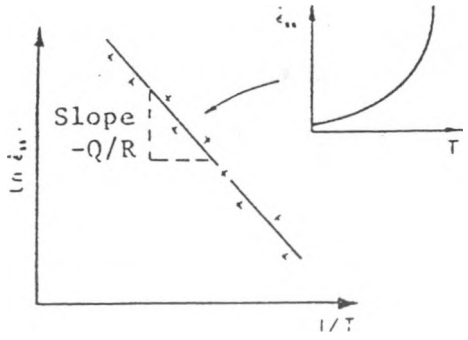

Figure 8-13a: Variation of Creep Strain Rate with Temperature (Ashby and Jones, 1980)

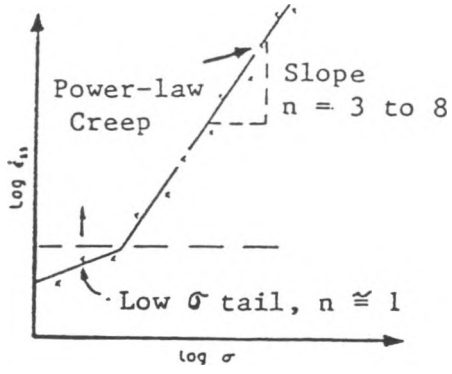

Figure 8-13b: Variation of Creep Strain Rate with Stress (Ashby and Jones, 1980)

the secondary creep dominant term (ϵ^{2c}):

$$\epsilon^c = \epsilon^{1c} + \epsilon^{2c} = B(\sigma)(1 - e^{-t/\lambda(T)}) + \dot{\epsilon}_{ss}\, t \tag{8.9}$$

where $\dot{\epsilon}_{ss} = A\sigma^n e^{(-\frac{Q}{RT})}$.

The Eq. (8.9) can be changed with the rate form:

$$\Delta\epsilon^{1c} = (1 - e^{-\Delta t/\lambda(T)})(B(\sigma) - \epsilon^{1c}) \tag{8.10}$$

$$\Delta\epsilon^{2c} = \dot{\epsilon}_{ss}\Delta t = A\sigma^n e^{(-\frac{Q}{RT})}\Delta t \tag{8.11}$$

These equations can be obtained from a viscoelastic model based on the combination of one Kelvin element and one Maxwell element as shown in Fig. 8.12(c). The temperature term is only included in the steady-state part ($\Delta\epsilon^{2c}$) with absolute temperature (K). Before doing multiaxial generalization, to simplify the mathematics, we define;

- $Ae^{(-\frac{Q}{RT})} = K$
- $B(\sigma) = \frac{\sigma}{E^c(T)}$
- $\lambda(T) = \alpha T + \beta \quad (\alpha, \beta = \text{constants})$

where $E^c(T)$ represents creep modulus depending on temperature.

Then, Eq. (8.10) and Eq. (8.11) reduced to

$$\Delta\epsilon^{1c} = (1 - e^{-\Delta t/\lambda(T)})(\frac{\sigma}{E^c(T)} - \epsilon^{1c}) \tag{8.12}$$

$$\Delta\epsilon^{2c} = K\sigma^n\Delta t \tag{8.13}$$

In the $\Delta\epsilon^{1c}$ formulaton, since the exponent of σ is 1, the generalized three dimensional

stress states can be developed by using a compliance matrix $\underline{B}$:

$$\Delta\underline{\epsilon}^{1c} = (1 - e^{-\Delta t/\lambda(T)})(\underline{B}\,\underline{\sigma} - \underline{\epsilon}^{1c}) \tag{8.14}$$

In the $\Delta\epsilon^{2c}$ formulaton, however, since the exponent of σ is an arbitrary number n (usually 3 - 8), another formulation, where the deviatoric and volumetric components of the creep strain tensor ϵ_{ij}^{2c} are elimenated, is required for generalized three dimensional conditions:

$$\epsilon_{ij}^{2c} = e_{ij}^{2c} + \frac{1}{3}\epsilon_v^{2c}\delta_{ij} \qquad\qquad i,j = 1,2,3 \tag{8.15}$$

where e_{ij}^{2c} = deviatoric strain component, ϵ_v^{2c} = volumetric strain component of ϵ_{ij}^{2c}.

Through time and temperature dependent creep functions J^D (deviatoric creep compliance function) and J^V (volumetric creep compliance function), deviatoric strain and volumetric strain components can then be related to deviatoric stress S_{ij} and volumetric stress σ_m, respectively.

$$e_{ij}^{2c} = J^D S_{ij} \tag{8.16}$$

$$\epsilon_v^{2c} = J^V \sigma_m \tag{8.17}$$

Since $J^V = \frac{3(1-2\nu_c)}{1+\nu_c} J^D$ and $\epsilon_{11} = K\sigma_{11}t$ in the uniaxial condition, J^D and J^V can be obtained for the uniaxial condition:

$$J^D = (1 + \nu_c)K\sigma_{11}^{n-1}t \tag{8.18}$$

$$J^V = 3(1 - 2\nu_c)K\sigma_{11}^{n-1}t \tag{8.19}$$

With Eq. (8.15) through Eq. (8.19), the final rate formulation for the multiaxial condition of a second creep dominant part could be obtained using an effective stress

concept:

$$\dot{\epsilon}_{ij}^{2c} = \dot{e}_{ij}^{2c} + \frac{1}{3}\dot{\epsilon}_{v}^{2c}\delta_{ij} \quad i,j = 1,2,3 \tag{8.20}$$

$$\dot{e}_{ij}^{2c} = (1+\nu_c)K\overline{\sigma}^{n-1}S_{ij} \tag{8.21}$$

$$\dot{\epsilon}_{v}^{2c} = 3(1-2\nu_c)K\overline{\sigma}^{n-1}\sigma_m \tag{8.22}$$

where $\overline{\sigma} = \sqrt{3/2 S_{ij}S_{ij}}$ (effective stress).

Therefore, the final matrix forms of high temperature creep behavior are;

$$\Delta\underline{\epsilon}^{2c} = \Delta\underline{e}^{2c} + \frac{1}{3}\Delta\epsilon_{v}^{2c}\ \underline{I} \tag{8.23}$$

where

$$\Delta\underline{e}^{1} = (1+\nu_c)K\overline{\sigma}^{n-1}\Delta t\ \underline{S} \tag{8.24}$$

$$\Delta\epsilon_{v}^{1} = 3(1-2\nu_c)K\overline{\sigma}^{n-1}\Delta t\ \sigma_m \tag{8.25}$$

In Eq. (8.23) the varying temperature effect is included in K (= A $e^{(-\frac{Q}{RT})}$). Since the effective stress ($\overline{\sigma}$) is a function of deviatoric stress (S_{ij}), Eq. (8.24) is a valuable form for deviatoric creep strain. The fact that the volumetric strain is also a function of deviatoric stess (S_{ij}) in addtion to the volumetric stress (σ_m) is verified by the shear-dilatation, as indicated in the section 8.2.2, Eq. (8.25) may be also a desirable form for volumetric creep strain.

This model is checked with reliable test data done at MIT (Tamer and Buyukozturk, 1988) and the test data obtained from the current research. The proposed model has been checked with test data of the materials CPS-90A-10C, DC-95A-5Ca, and IC-55A-36S. The Arrhenius plots and the comparison results are shown between Fig. 8.14 and Fig. 8.24. The parameters A, Q, and n in the power-law creep equation are determined from the Arrhenuis plots for each material. Creep modulus ($E^c(T)$)and the relaxation time ($\lambda(T)$) are obtained as linear functions of absolute temperature (K) by performing

a regression analysis of the least-squares method of function fitting. The functions of $E^c(T)$ and $\lambda(T)$, and the Arrhenius parameters are summarized in Table 8.1. The size of Δt can be determined from Eq. (8.12) & (8.13). The varying stress condition is checked with the creep data of the dense brick refractory material CPS-90A-10C in Fig. 8.16. The proposed creep model is observed to agree well with the creep test data of the material CPS-90A-10C. For the dense castable material DC-95A-5Ca, two series of tests were performed. One is creep test with constant stress level at different temperatures, and the other is the creep test with constant temperature under varying stresses. Those results are compared with the proposed model in Figs. 8.19 & 8.20. In Fig. 8.20, a recoverable creep phenomenon is checked with the creep test data obtained at 1500°F under 71% of the compressive strength at 1500°F. The propoed model is observed not to follow the test data well in the initial part of the unloading.

8.3.3 Discussion

A new creep model is proposed to satisfy all essectial requirements for high temperature creep characteristics of refractory materials. The proposed model was shown to agree well with data over the temperature and load ranges tested. Some more refinements in the proposed creep model are needed with more test data.

From the test results, the creep Possion's ratio is known as 0.2 at high temperatures (Blundell et al., 1976). However, the maximum temperature levels investigated are very limited (less than 500°F). Since the service temperature of refractory linings of interest is very high up to 3000°F, more refined tests for checking the real creep Poisson's ratio at high temperatures are needed. With this refined creep model, creep analyses for the high temperature high pressure coal gasifiers may be obtained.

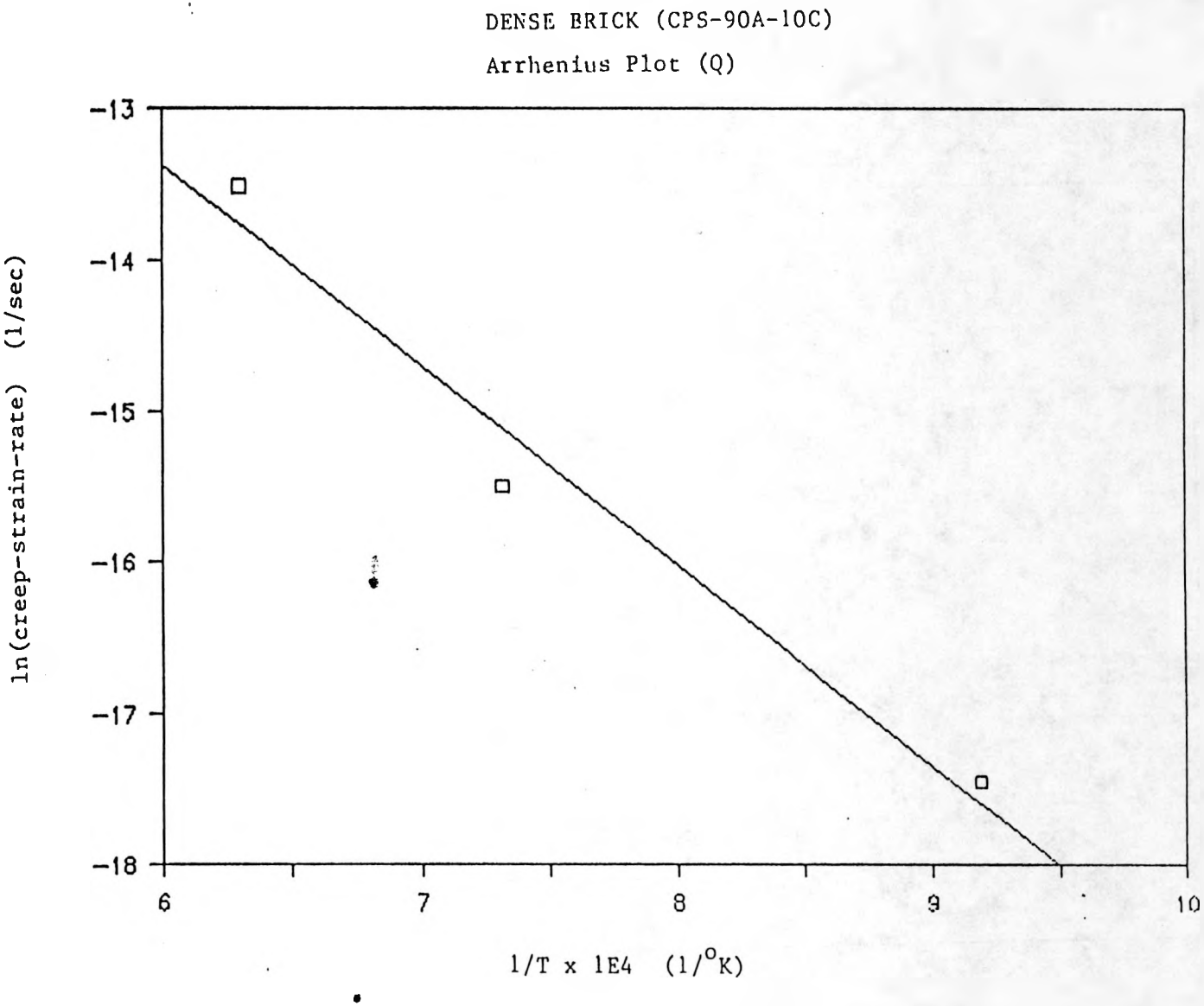

Figure 8-14: Calculation of Activation Energy 'Q' from Arrehnius Plot for the Dense Brick Refractory CPS-90A-10C

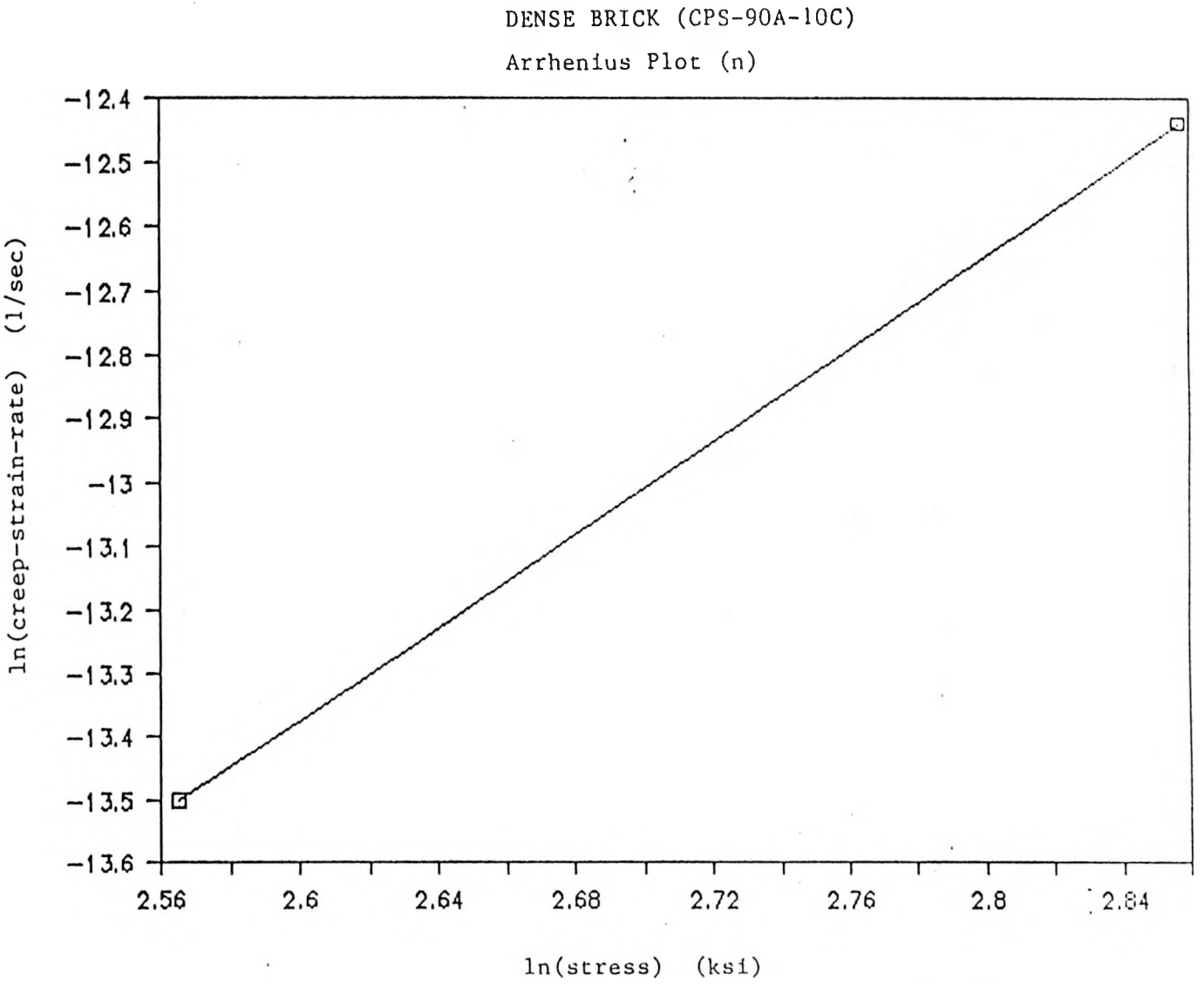

Figure 8-15: Calculation of Stress Exponent 'n' from Arrehnius Plot for the Dense Brick Refractory CPS-90A-10C

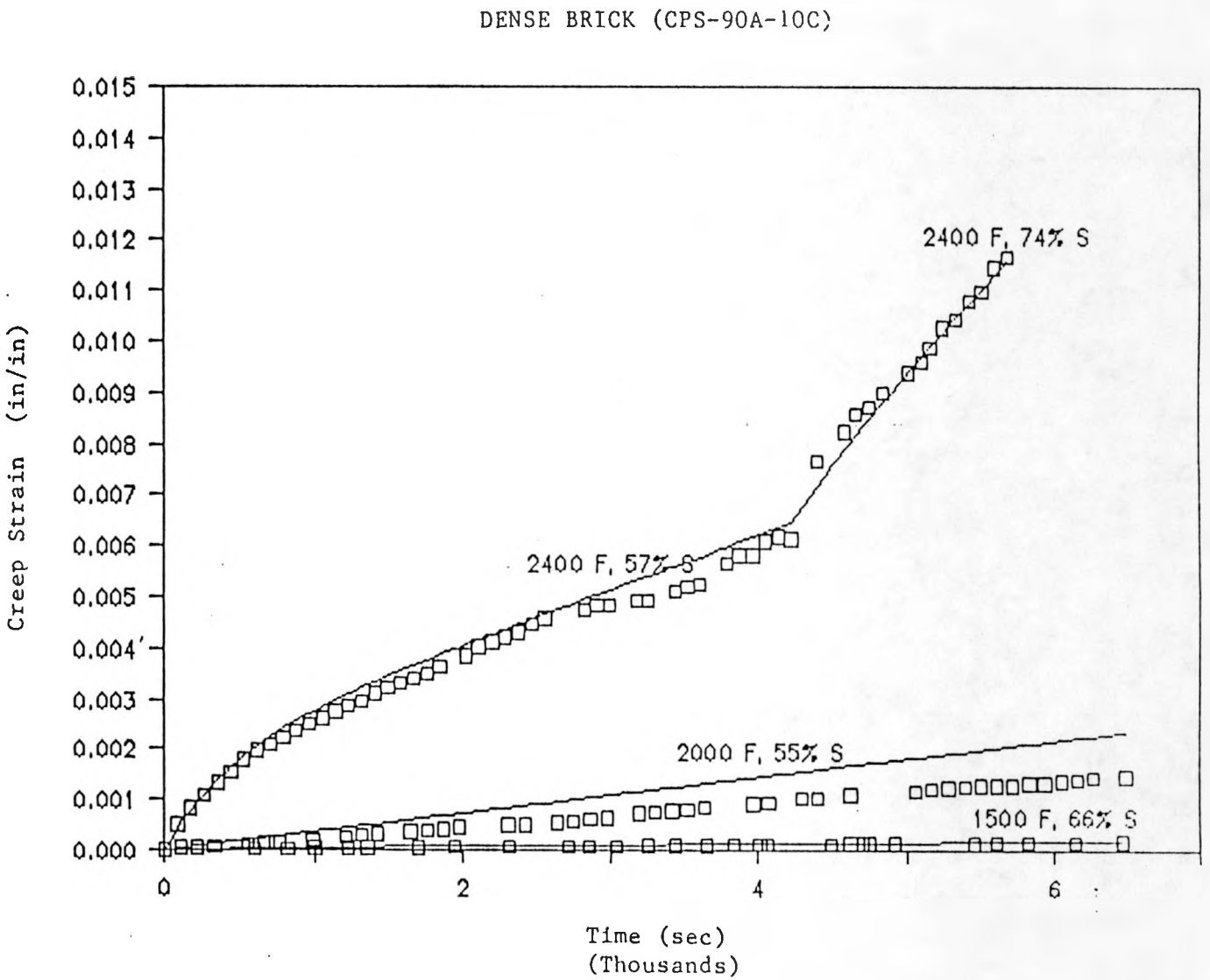

Figure 8-16: Comparison of the Proposed Model with a Creep Test Data of the Dense Brick Refractory CPS-90A-10C

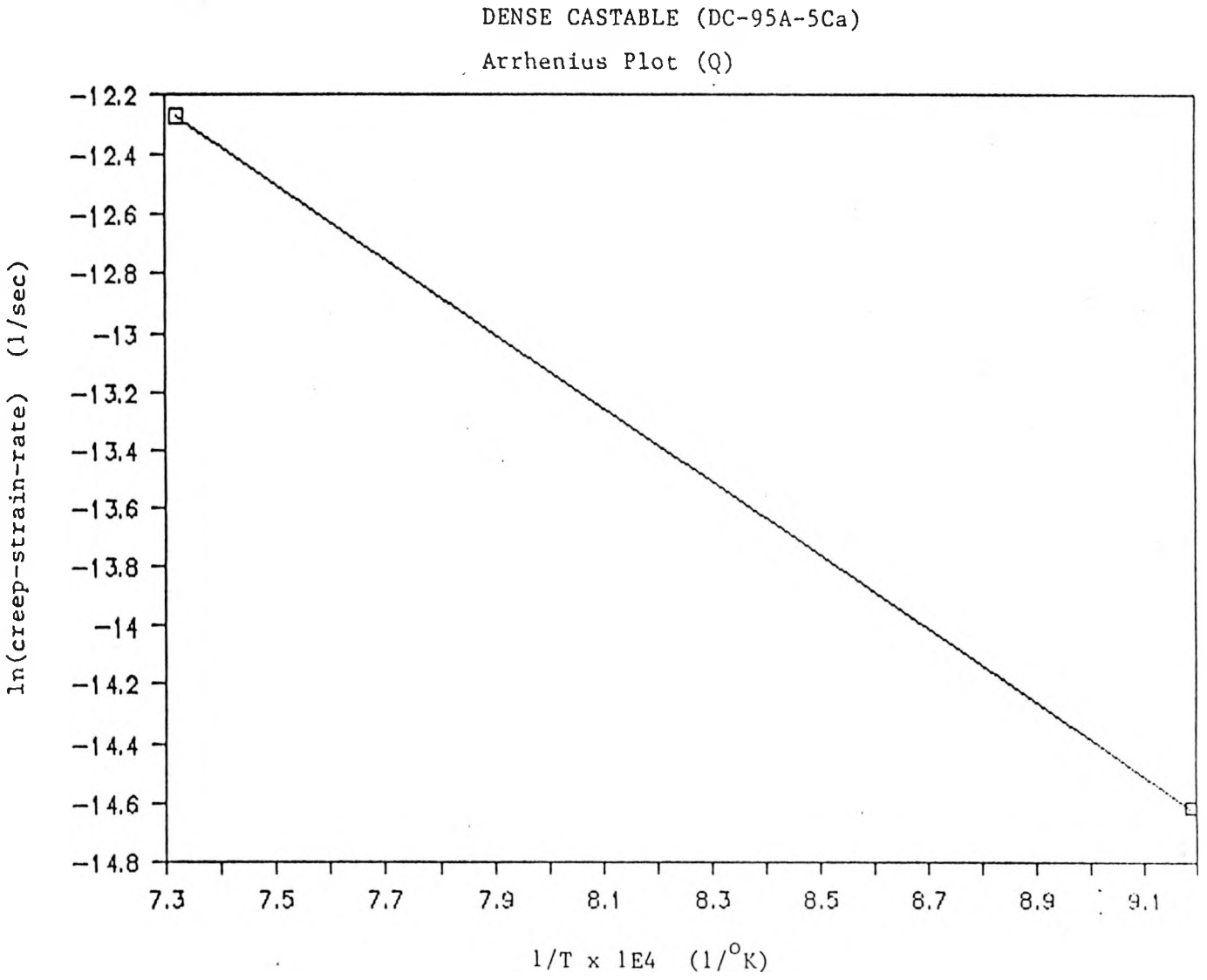

Figure 8-17: Calculation of Activation Energy 'Q' from Arrehnius Plot for the Dense Castable Refractory DC-95A-5Ca

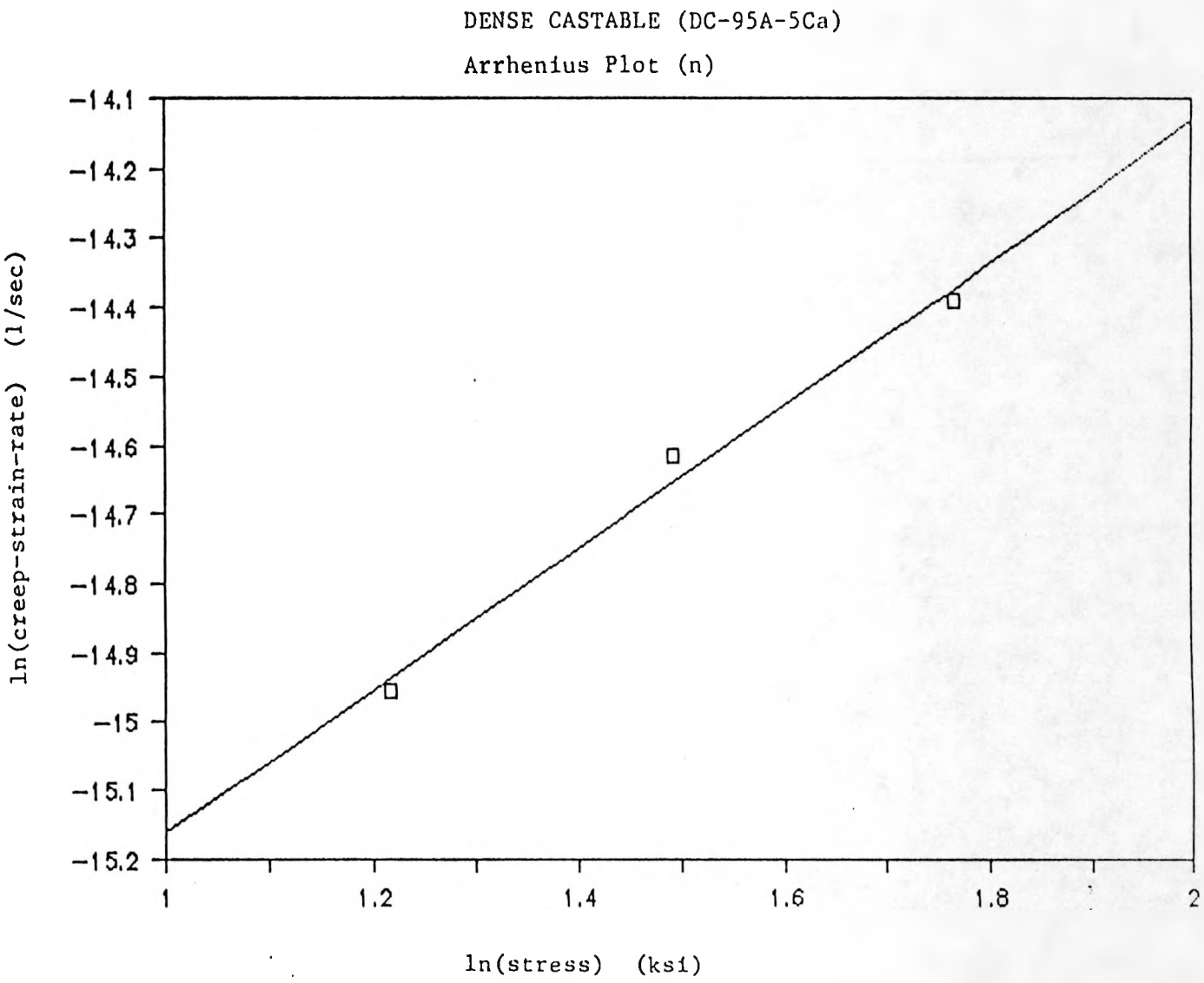

Figure 8-18: Calculation of Stress Exponent 'n' from Arrehnius Plot for the Dense Castable Refractory DC-95A-5Ca

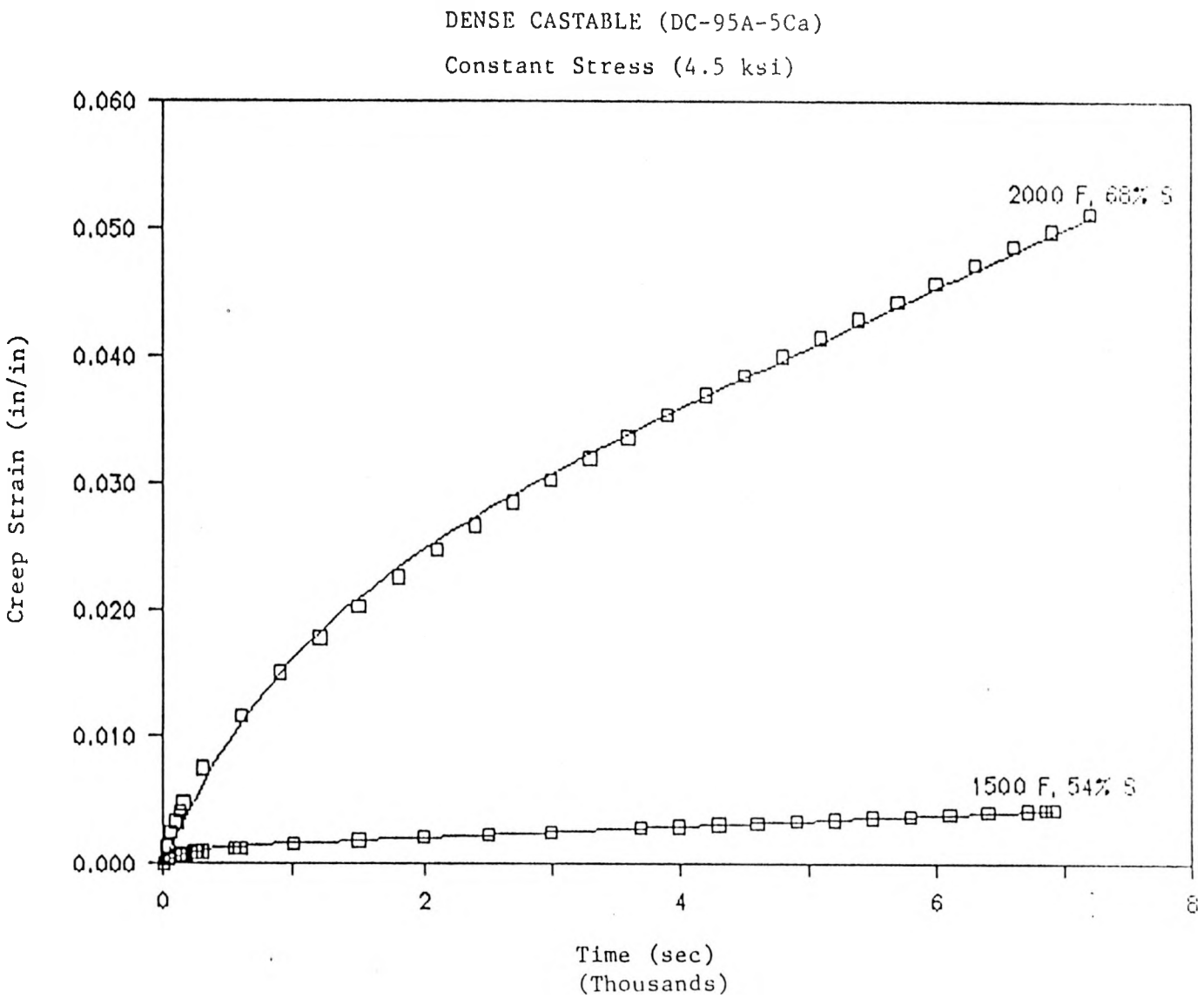

Figure 8-19: Comparison of the Proposed Model with a Creep Test Data of the Dense Castable Refractory DC-95A-5Ca under Constant Stress (4.5 ksi)

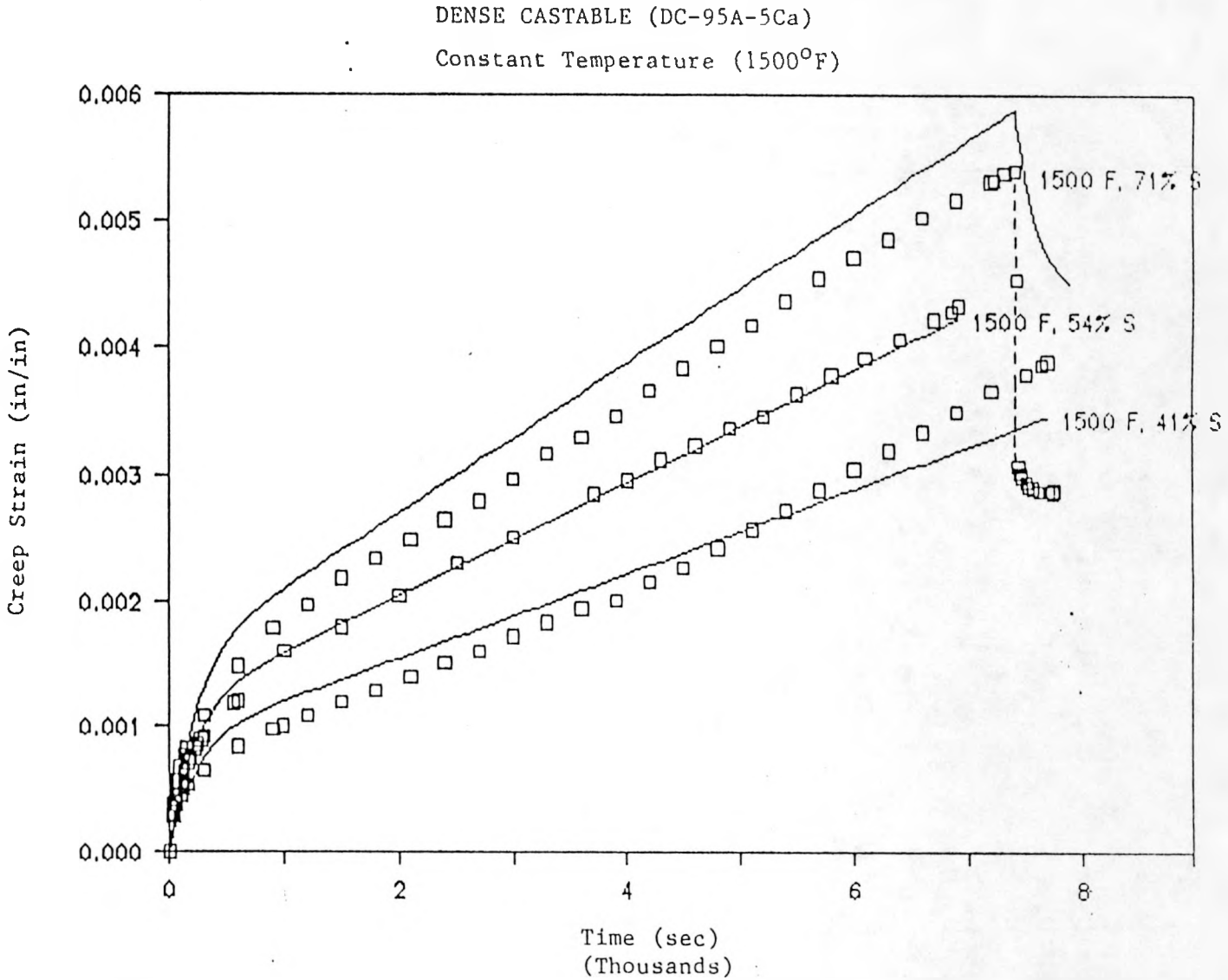

Figure 8-20: Comparison of the Proposed Model with a Creep Test Data of the Dense Castable Refractory DC-95A-5Ca under Constant Temperature (1500°F)

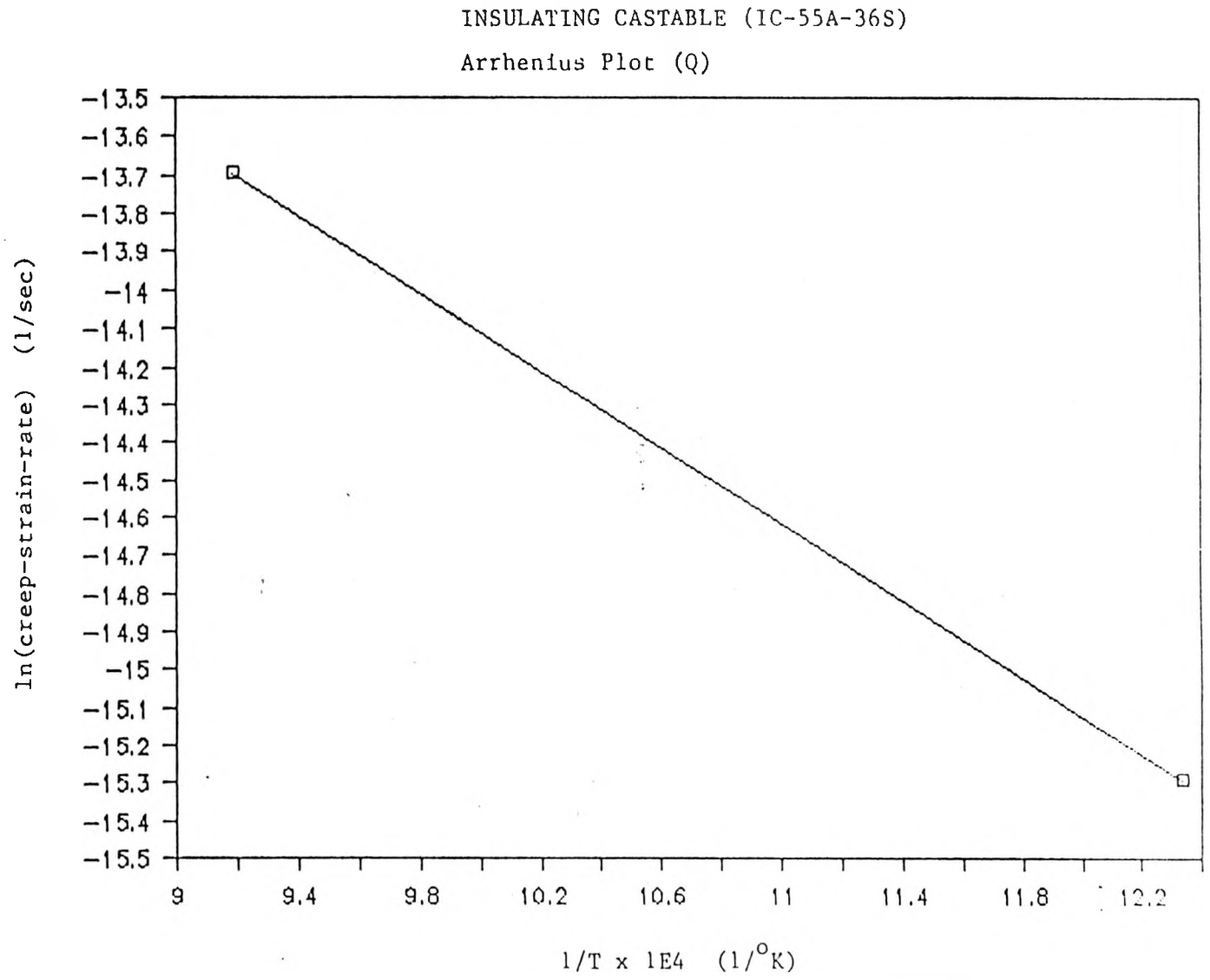

Figure 8-21: Calculation of Activation Energy 'Q' from Arrehnius Plot for the Insulating Castable Refractory IC-55A-36S

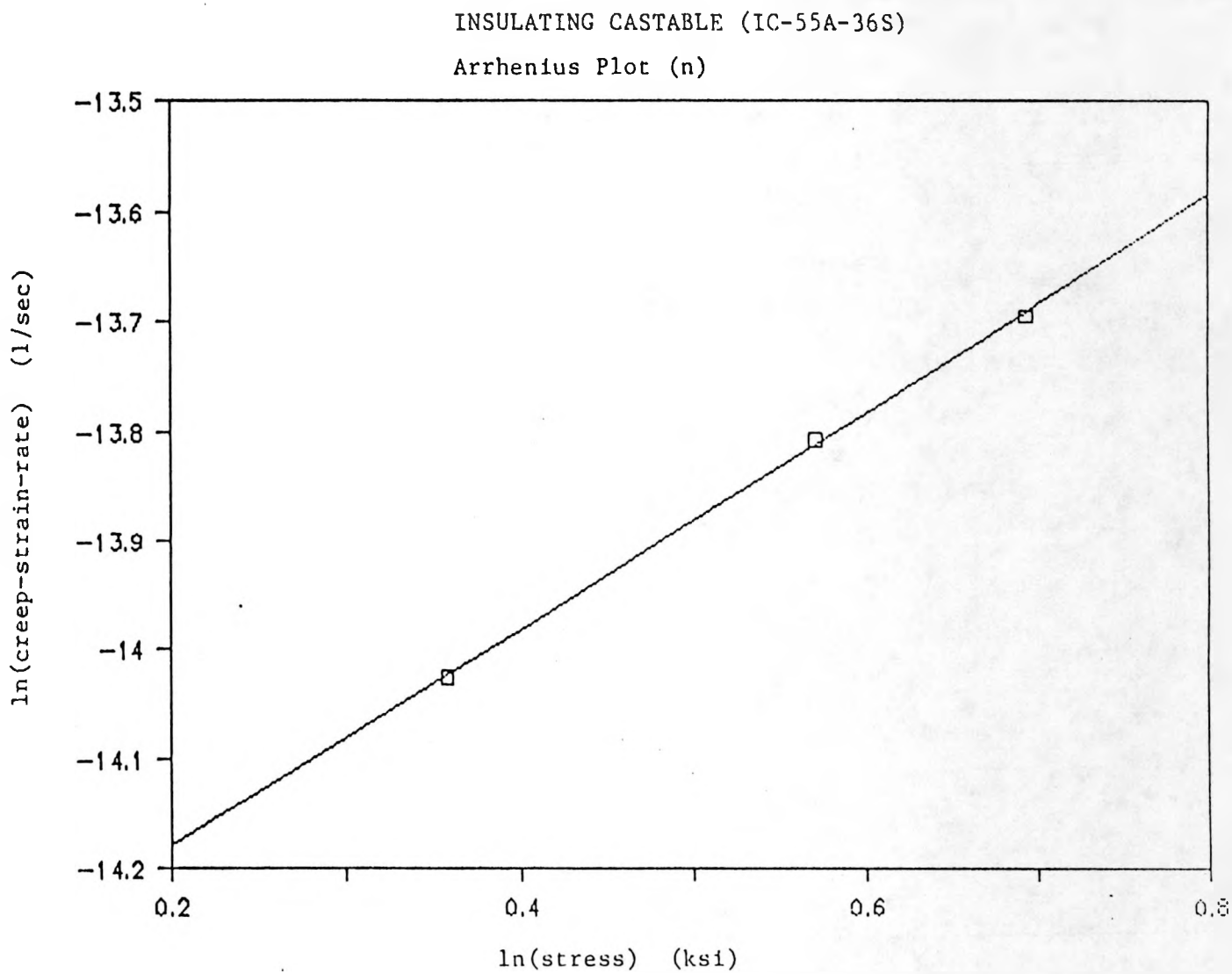

Figure 8-22: Calculation of Stress Exponent 'n' from Arrehnius Plot for the Insulating Castable Refractory IC-55A-36S

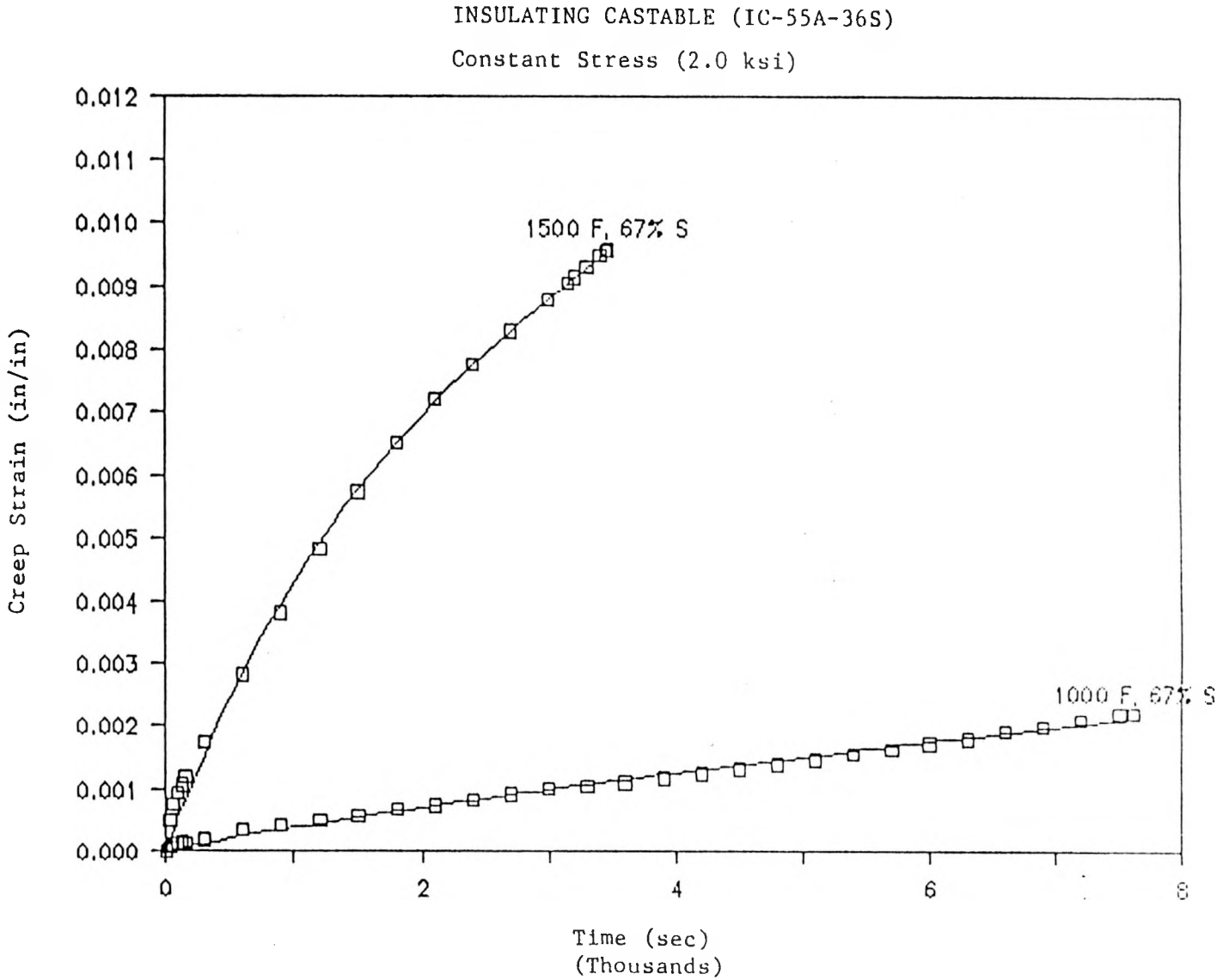

Figure 8-23: Comparison of the Proposed Model with a Creep Test Data of the Insulating Castable Refractory IC-55A-36S under Constant Stress (4.5 ksi)

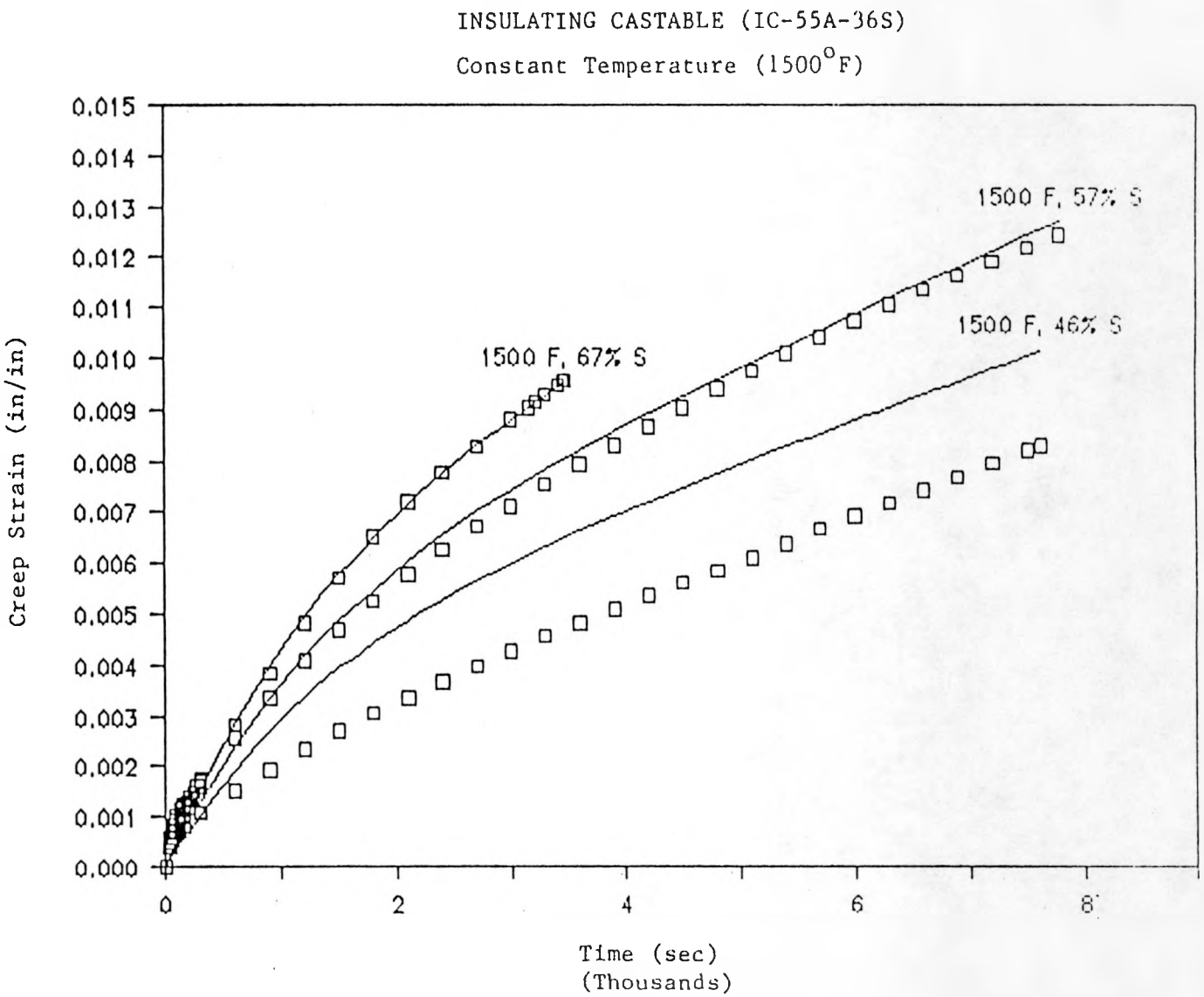

Figure 8-24: Comparison of the Proposed Model with a Creep Test Data of the Insulating Castable Refractory IC-55A-36S under Constant Temperature (1500°F)

Table 8.1: Parameters of the Proposed Creep Model Obtained for Each Material

	Dense Brick CPS-90A-10C	Dense Castable DC-95A-5Ca	Insulating Castable IC-55A-36S
Q (ksi)	110.57	104.39	42.15
n	3.645	1.030	0.993
A (ksi)	4.031×10^{-7}	9.822×10^{-3}	6.015×10^{-5}
Creep Modulus $E^c(T)$ (ksi) T(K)	-1215.178T + 1937044.430	-12.926T + 17921.736	-17.064T + 18935.923
Relaxation Time $\lambda(T)$ (sec) T(K)	-3.563T + 6140.023	2.537T - 2554.571	-2.738T + 4283.591

Chapter 9

SUMMARY, CONCLUSIONS, AND RECOMMENDATIONS

9.1 SYNOPSIS

This thesis has provided an overview of the thermomechanical behavior of refractory materials and a model for predicting creep behavior at elevated temperautres. Section 9.2 summarizes the objectives and the primary areas investigated. Section 9.3 provides the main conclusions from this research. Recommendations for future work are given in Section 9.4.

9.2 SUMMARY OF THE PRESENT RESEARCH

The application area of this research is the analysis and design for high temperature high pressure vessels, with a focus on slagging coal gasifiers. A review of previous work has indicated that there is a need to generate a fundamental understanding and characterization of the behavior of different refractory materials at elevated tempertures. Little research has concentrated on the thermomechanical behavior at high temperatur such as strength, modulus of rupture, creep behavior, etc.. Furthermore, no efforts have been made to collect available data in a systematic manner. The information mentioned above

has provided the incentive for the current research. The objectives of this research are (1) to characterize the short-term compressive behavior of refractories at elevated temperatures, (2) to expand and refine the existing data, and (3) to develop a model for predicting creep behavior of refractories at elevated temperatures. The focus was on refractory materials for slagging coal gasifier linings.

Four categories of refractory materials were chosen for examination. Those are dense brick, dense castable, insulating castable, and insulating firebrick refractories. Among these, brick refractories are used for high temperature brick lining systems as shown in Fig. 2.2. Castable refractory materials are used for high temperature monolithic lining systems (Fig. 2.1). The selected dense brick materials studied for thermomechanical properties were high alumina and high chromia refractories manufactured by cold-pressing and sintering (CPS). The cold-pressed and sintered high alumina refractory consists of 90% Al_2O_3 (A) and 10% Cr_2O_3 (C), denoted CPS-90A-10C, with an alumina-chromia solid solution and tabular alumina grains. The cold-pressed high chromia refractory consist of 82% Cr_2O_3 and 18% MgO (M), denoted CPS-82C-18M, with a picochromite ($MgCr_2O_4$) spinel matrix and fused pirochromite grains. The castable refractories for the thermomechanical properties studies were manufactureed by mixing them with water at room temperature. The dense castable (DC) refractory consists of 95% Al_2O_3 and 4.6% CaO (Ca), noted by DC-95A-5Ca. The insulating castable (IC) refractory consists of 54.5% Al_2O_3 and 36.3% SiO_2 (S), denoted IC-55A-36S. The selected insulating firebrick for the study of the thermomechanical behavior was manufactureed by firing it at high temperature. The insulating firebrick consists of 39% Al_2O_3 and 44% SiO_2, denoted IB-39A-44S. From the comparison of the chemical composition, insulating materials would be indicated that they have large percentages of SiO_2 compared with dense refractories.

In order to achieve all the objectives of the research, the following approaches have been taken:

1. Short-term uniaxial monotonic loading tests were performed on each selected refractory material at a predetermined constant temperature in the range from room temperature to 2400°F. Over 70 cylindrical specimens were made and tested.

2. Short-term uniaxial constant compressive loading tests were performed on each selected refractory material at a predetermined constant temperature level under constant stress. The range of temperature was between room temperature and 2400°F, and the range of applied stresses was between 40% and 75% of the compressive strength of the material. Over 20 cylindrical specimens were made and tested.

3. The thermomechanical data from the performed tests were collected and summarized in the figures and tables. Additional information of thermomechanical and thermophysical properties were also summarized.

4. A new creep model was proposed to predict different kinds of creep variation depending on different temperature and stress levels.

For the short-term monotonic loading and creep loading tests, cylindrical specimens of 1 inch diameter and 2.5-3.0 inches height were used. The specimens were cored out of the prefabricated bricks and prepared for tests by sawing both ends.

9.3 CONCLUSIONS

Based on the limited test results in the study with respect to the loading conditions and materials, the following conclusions were made.

9.3.1 Properties of Dense Brick Refractories (CPS-90A-10C and CPS-82C-18M)

1. A transition temperature roughly equal to one-half the melting temperature is observed to separate two different deformation behaviors.

2. Below the transition temperature, linear elastic deformations are observed with a sudden brittle fracture. The final strain is equal to the associated peak strain in this region.

3. Above the transition temperature the material behavior exhibits significant non-linearities in the post-peak region.

4. A slight decrease in strength below 0.5 T_M was observed for the high-chromia dense brick material CPS-82C-18M, followed by an increased rate of decrease in strength above 0.5 T_M (Fig. 4.3). For the dense brick material CPS-90A-10C, an increase in strength is observed above 0.5 T_M (Fig. 4.4).

5. The initial modulus decreases sharply with increased temperature (Fig. 4.5 & 4.6).

6. The associated peak strain increases slowly below 0.5 T_M, followed by a fast increase above 0.5 T_M (Fig. 4.7 & 4.8).

7. The equivalent toughness (defined as the area under the stress-strain curve) is approximately constant below 0.5 T_M, and increases significantly above 0.5 T_M (Fig. 4.9 & 4.10).

8. Below 2000°F, the contribution of the short-term creep deformation to the total deformation seems to be negligible (Fig. 4.11 & 4.13).

9. Different results of short-term creep are observed when different load histories are applied (Fig. 4.15).

9.3.2 Properties of Castable Refractories (DC-95A-5Ca and IC-55A-36S)

1. A global transition temperature roughly equal to 0.5 T_M exists.

2. Below 0.3 T_M, linear elastic deformations are observed with a sudden brittle fracture. The final strain is equal to the associated peak strain. Between 0.3-0.5 T_M, a small amount of stress-softening is observed with a brittle fracture. The final stress level is about 90% of the peak stress.

3. Above the transition temperature the deformation behavior is initially linear, but shows significant non-linearities in the post-peak region.

4. A slight increase in strength is observed between room temperature and 500°F. A slow decrease in strength with temperature is observed below 0.5 T_M, followed by a fast decrease in strength. Too low strength above 2000°F may limit the use of the castable materials to temparatures lower than 0.6-0.7 T_M (Fig. 5.2 & 6.2).

5. The initial modulus decreases sharply after a slight increase between room temperature and 500°F (Fig. 5.4 & 6.4).

6. The associated peak strain increases slowly below 0.5 T_M, followed by a fast increase above 0.5 T_M (Fig. 5.3 & 6.3).

7. The equivalent toughness (defined as the area under the stress-strain curve) is approximately constant below 0.5 T_M, and increases significantly between 0.5 and 0.6 T_M. For the temperature level above 0.6 T_M, the equivalent toughness drops remarkably (Fig. 5.5 & 6.5).

8. Below 0.4 T_M, the contribution of the short-term creep deformation to the total deformation seems to be negligible (Fig. 5.6 & 6.6).

9. Irrecoverable creep during unloading is observed (Fig. 5.8).

9.3.3 Properties of Insulating Firebrick (IB-39A-44S)

1. A perfect elastic-plastic behavior is observed. An almost constant strength level is observed with respect to temperature change (Figs. 7.1, 7.2, and 7.3).

2. The variation of the initial modulus with temperature is negligibly small (Fig. 7.4).

9.3.4 Modeling of Creep Behavior

1. A new creep model is proposed to incorporate the following main considerations:

   (a) Refractory materials have been observed to have certain values of creep Poisson's ratio ($\nu = 0.2$).

   (b) Irrecoverable creep behavior under unloading have been observed for brittle materials.

   (c) For the temperature high pressure vessels, the primary creep plays an important role because creep effects on refractory linings are critical in the early stages of thermal cycles.

2. The proposed model shows good agreement with test data over the temperature and load ranges tested (Fig. 8.16 for dense brick material CPS-90A-10C; Figs. 8.19 & 8.20 for dense castable material DC-95A-5Ca; Figs. 8.23 & 8.24 for insulating castable material IC-55A-36S).

9.4 RECOMMENDATIONS FOR FUTURE RESEARCH

Completion of Data-Base

The completion of the current research provided a new material data-base which provides insight into the understanding of the thermo-mechanical behavior of tested

refractories. Useful data for other kinds of refractory materials are available in the literature.

The information developed by the current research and obtained from other sources constructs a part of the data-base necessary for use in design purpose. However, misunderstanding due to the lack of well-defined summary of the refractory material data-base can lead to the poor design of lining systems. Therefore, a well-organized material data-base, which evaluates different materials under different conditions, is needed by users, designers, and namufacturers.

In order to construct a well-organized material data-base, the following is required:

1. A software capacity such as a knowledge-based expert system.

2. More precise thermomechanical and thermophysical data.

Modeling and Analysis of the Material Behavior

With the additional new information, the available models for predicting the thermomechanical behaviors need to be checked. Previous projects at MIT in this area led to the development of several models that are linked to a finite element capacity.

The re-evaluation of the available models with the finite element tool will lead to the new generation of the models, or the calibration of the exisiting models.

REFERENCES

1. ACI committee 547 (1979), "Refractory Concrete," *ACI Report 547R-79.*

2. ACI committee 318 (1983), "Building Code Requirements For Reinforced Concrete," *ACI 318R-83.*

3. Anderberg, Y. and S. Thelanderson (1976), "Stress and Deformation Characteristics of Concrete at High Temperature," *Lund Inst. of Tech.*, Lund, Sweden, *Division of Structural Mechanics and Concret Construction*, Bulletin, 54, August.

4. Ashby, M.F. and D.R.H. Jones (1980), *Engineering Materials I; An Introduction to their properties and applications*, Pergamon Press.

5. ASTM (1989), *Annual Book of ASTM Standards*, Vols. 4 & 15.

6. Babcock & Wilcox (1981), "Improvement of the Mechanical Reliability of Monolithic Refractory Linings for Coal Gasification Process Vessels," *DOE Report* Contract NO. DE-AC05-760R10434, LRC-5258, September.

7. Bakker, W.T. and J. Stringer (1981), "Materials for Coal Gasification Combined Cycle Power Plants," *Sixth Annual Conference on Materials for Coal Conversion and Utilization*, October.

8. Bakker, W.T. (1982), "Recent Advances in Refractory Concrete Technology," *MONOLITHIC REFRACTORIES*, ACI-SP-74-1, pp. 1-16.

9. Bakker, W.T., S. Greenberg, M. Trondt, and U. Gerhardus (1984), "Refractory Practice in Slagging Gasifiers," *American Ceramic Society Bulletin*, Vol. 63, No. 7.

10. Bandyopadhyay, G., J. Chen, C.R. Kennedy, and D.K. Diereks (1983), "Thermal-Shock Damage of Refractories for Application in Slagging Coal Gasifiers," *Journal of Materials for Energy Systems*, Vol. 4, No. 4, March.

11. Bazant, Z.P. (1986), "Creep and Shrinkage of Concrete: Mathematical Modeling," *Fourth RILEM International Symposium,* Aug. 26-29.

12. Blundell, R., C. Diamond, and R.G. Browne (1976), "The Properties of Concrete Subjected to Elevated Temperatures," *CIRIA Underwater Engineering Group, Technical Report*, June.

13. Bonnare, J.A., C.R. Kennedy, and R.G. Swaroop (1980), "Coal-Ash Slag Attack and Corrosion of Refractories," *American Ceramic Society Bulletin*, Vol. 59, No. 4.

14. Bortz, S.A., R.F. Firestone, and M.J. Greaves (1982), "Castable Refractory Design Requirements," *MONOLITHIC REFRACTORIES*, ACI-SP-74-2, pp. 17-31.

15. Boyle, J.T. and J. Spence (1983), "Stress Analysis for Creep," *Butterworth & Co.* Publication.

16. Bray, D.J. (1986), "Creep of Refractories: Mathematical Modeling," *Advanced Ceramics*, Vol. 13, *New Development in Monolithic Refractories, The American Ceramic Society.*

17. Brown, N.R. (1983), "Gaseous Corrosion Resistance of Refractories for Coal Gasifiers," *U.S. Bureau of Mines.*

18. Budnikov, P.P. (1964), "The Technology of Ceramics and Refractories," *The MIT Press*, Cambridge, MA.

19. Buyukozturk, O., A.H. Nilson, and F.O. Slate (1972), "Stress-Strain Response and Fracture of a Concrete Model in Biaxial Loading," *ACI*, Vol. 68, Aug., pp. 590-599.

20. Buyukozturk, O. and S.S. Shareef (1983), "Constitutive Modeling of Concrete in Finite Element Analysis," *Research Report R83-16, MIT*, Department of Civil Eng., December.

21. Chen, E.S. and O. Buyukozturk (1984), "Constitutive Modeling of Concrete in Finite Element Analysis," *MIT, Research Report*, Department of Civil Eng., June.

22. Chen, R.C., R.L. Carrasquillo, and D.W. Fowler (1985), "Behavior of High-Strength Concrete Under Uniaxial and Biaxial Compression," *ACI-SP-87, High-Strength Concrete*, pp. 251-273.

23. Clarke, D.R. (1983), "High Temperature Environmental Strength Degradation of a Hot-Pressed Silicon Nitride: An Experimental Test," *Journal of the American Ceramic Society*, Vol. 66, No. 2.

24. Coble, R.L. (1963), *J. Appl. Phys.*, 34, pp. 1679.

25. Crowley, M.S. and R.C. Johnson (1972), "Guidelines for Installing Refractory Linings in Cold Weather," *Ceramic Bulletin*, Vol. 51, No. 2.

26. Crowley, M.S. (1975), "Refractory Problems in Coal Gasification Reactors," *Ceramic Society Bulletin*, Vol.51, No. 12.

27. Crowley, M.S. (1984), "Refractory Usage in the Process Industries," *Standard Oil Company*, Indiana.

28. Cruz, C.R. (1966), "Elastic Properties of Concrete at High Temperatures," *Journal of the PCA Research and Development Lab.*, January.

29. Eibl, J. (1981), "Application and Experimental Verification of Advanced Mechnics in Reinforced Concrete," *IABSE-Colloquium, 'Advanced Mechanics of Reinforced Concrete'*, Delft, *Introductory Report*, pp. 135-156.

30. Evans A.G. and T.G. Langdon (1976), Structural Ceramics, *Progress in Materials Science*, Vol. 21, pp. 171-441.

31. Findlay, G.E. and I.W. Goodall (1976), "Some Observations on the Design of Pressure Vessel Operating in the Creep Range," *Failure of Components Operating in the Creep Range in IMechE Conference Publication*, 1974-6.

32. Folk, H.F. and W.C. Bohling (1968), "High Temperature Strength of High Alumina Refractories," *American Ceramic Society Bulletin*, Vol. 47, June.

33. Frost, H.J. and M.F. Ashby (1982), *Deformation Mechanism Maps,* Pergamon Press, Elmsford, N.Y.

34. Gentle, M., T. Sun, and J.J. Brown (1987), "Alkali Attack of Coal Gasifier Refractory Linings," *Department of Materials Engineering, Virginia Polytechnic Institute and State University, Report ORNL/85-43397*, prepared for Oak Ridge National Laboratory.

35. Gilchrist, J.D. (1977), *Fuels, Furnaces and Refractories*, Pergamon Press, Oxford, England.

36. Heindl, R.A. and Z.A. Post (1954), "Refractory Castables: SOme Properties, and Effects of Heat Treatments," *Journal of the American Ceramic Society*, Vol. 37, No. 5.

37. Herring, C. (1950), *Journal of Applied Physics*, 21, pp. 437.

38. Heuze, F.E. (1983), "High-temperature Mechanical, Physical and Thermal Properties of Granite Rocks - A Review," *Int. J. Rock Mech. Min. Sci. & Geomech.*, Abstract, Vol. 20, No. 1, pp. 3-10.

39. Huggett L.G. (1966), "Lining of Secondary Reformers," *Proc. Mat. Tech. Symposium,* Pergamon Press.

40. ISI Publication 116 (1968), *Blast-furnace Refractories Iron and Steel Institute*, London, England.

41. Iwano, Y. (1985), "An Efficient Numerical Method For Solving Creep Problems," *Nuclear Engineering and Design*, 88, pp. 333-339.

42. Johnson-Walls, D. and A.G. Evans (1986), "Residual Stresses in Machined Ceramics Surfaces," J. of the American Ceramics Society, Vol. 69, No. 1, January.

43. Katona, M.G. (1980), "Combo Viscoplasticity: An Introduction with Incremental Formulation," *Computer & Structures*, Vol. 11, pp. 217-224.

44. Kennedy, C.R. (1979), "Refractory for Application in Slagging Gasifiers", *Fourth Annual Conference on Materials for Coal Conversion and Utilization*, October.

45. Kenndey, C.R. (1980), "Compatibility of Water-Cooled Refractories with a Basic Coal-Ash Slag at 1500°C," *Journal of Materials for Energy Systems*, Vol. 2, Semptember.

46. Kingery, W.D., H.U. Bowen, abd D.R. Uhlmann (1976), *Introduction to Ceramic*, John Wiley & Sons, New York, NY.

47. Kotsovos, M.D. (1983), "Effect of Testing Techniques on the Post-Ultimate Behavior of Concrete in Compression," *Materiaux et Constructions*, Vol. 16, No. 91.

48. MacGregor, C.W. and J.C. Fisher (1946), "A Velocity Modified Temperature for the Plastic Flow of Metals," *Journal of Applied Mechanics,* March.

49. McCullough, J.M. and G.R. Rigby (1971), "Mechanical Properties of Refractory Castables," *Journal of British Ceramics Society*, Vol. 71, No. 7.

50. McGannon, E. (1964), "The Making, Sharping and Treating of Steel," *United States Steel Corporation*, eigth edtion.

51. McGee, T.D. (1984), "High Temperature Creep of Refractories for Coal Processing Vessels," *U.S. Department of Energy, Fossil Energy Advanced Research and Technology Development Report,* ONRL/FMP-83/3-5; ONRL/FMP-84/1.

52. McGee, T.D. and R. Konrady (1983-1987), "High Temperature Creep Behavior of Refractory Bricks," *Quarterly Reports pubished by the US DOE Fossil Energy Program.*

53. Megusar, J., A.S. Srgon, and N.J. Grant (1979), "Plastic Flow and Fracture in $Pd_{80}Si_{20}$ near T_g," *Material Science and Engineering,* 38, pp. 63-72.

54. Miller, E.D. and B. Davis (1966), "Modulus of Rupture of Alumina-Silica Refractories at Elevated Temperatures," *American Ceramic Society Bulletin*, Vol. 45, No. 8.

55. Nabbaro, F.R.N. (1948), *Report on a Conference on the Strength of Metals. Phys. Soc.*, London.

56. Newman, J.B. (1979), "Concrete under Complex Stress," *Development in Concrete Technology -1, ed.* by F.D. Lydon, *Applied Science Publishers ltd., London*, pp. 151-220.

57. Nicholls, J.H. and P.G. McCormick (1970), *Met. Trans.*, 1, 3469.

58. Pike, P.J., O. Buyukozturk, and J.J. Connor (1980), "Thermomechanical Analysis of Refractory Concrete-Lined Coal Gasification Vessels," *Research Report R80-2, MIT*, Department of Civil Eng., January.

59. Ruh, E. and A.L. Renkey (1963), "Thermal Conductivity of Refractory Castables," *Journal of the American Ceramic Society*, Vol. 46, No. 2.

60. Snyder, M.D. and K.J. Bathe (1977), "Formulation and Numerical Solution of Thermo-Elastic-Plastic and Creep Problems," *MIT, Report82448-3,* June.

61. Subrata Mukherjee (1982), "Boundary Element Method in Creep and Fracture," *Elsevier Science Publishing Co., INC.*

62. Sweeney, J. and M. Cross (1982), "Analysis of the Stress Response of Commercial Refractory Structure in Service at High Temperature: II, A Thermal Stress Model for Refractory Structures," *British Society Transactions and Journal*, Vol. 81, No. 1.

63. Tamer, F.G. and O. Buyukozturk (1988), "Material Characterization of Refractory Ceramics For High Temperature Linings," *Research Report R88-15, MIT*, Department of Civil Eng., October.

64. Tseng, T.M. and O. Buyukozturk (1982), "Thermomechanical Behavior of Refractory Concrete-Lined Vessels," *Research Report R82-44, MIT.* Department of Civil eng., August.

65. Van Mier, J.G.M. (1984), "Strain-Softening of Concrete Under Multiaxial Loading Conditions," *Ph.D. Thesis, Colorado University*, November.

66. Washburn, M.E. (1982), "Rotating Sample Slag Test For Refractories," *Seventh Annual Conference on Materials for Coal Conversion and Utilization*, November.

67. Wiederhorn, S.M. and R.F. Krause (1986), "Effect of Slag Penertration on the Mechanical Properties of Refractories," *NBS Final Report* prepared for the *DOE* under *ORNL contract* no. *DE-AI05-830R21349.*

68. Wygant, J.F. and W.L. Bulkley (1954), "Refractory Concrete for Refinery Vessel Linings," *American Ceramic Society Bulletin*, 33(1), pp. 233-239.

69. Wygant, J.F. and M.S. Crowley (1958), "Effects of High-Conductivity Gases on the thermal Conductivity of Insulating Refractory Concrete," *Journal of American Ceramic Society*, Vol. 41, No. 5.

70. Wygant, J.F. and M.S. Crowley (1964), "Designing Monolithic Refractory Vessel Linings," *American Ceramic Society Bulletin*, 43(3), pp. 233-239.

71. Zienkiewicz, O.C. and I.C. Cormeau (1974), "Visco-Plasticity-Plasticity and Creep in Elastic Solids - A Unified Numerical Solution Approach," *International Journal for Numerical Methods in Engineering*, Vol. 8, pp. 821-845.

Appendix A

MATERIAL DATA-BASE OF REFRACTORIES

Arrangements of Data-Base

1. Material Identification
2. Chemical Composition
3. Service Temperature / Melting Point
4. Thermomechanical Data :

   Hot Strength; Associated Peak Strain;
   Final Fracture Stress; Final Fracture Strain;
   Average Initial Stiffness; Toughness Measure;
   Displacement Rate; Creep; Shrinkage;
   Hot MOR; Cold MOR; Cold Crushing Strengh
5. Themophysical Data :

   Apparent Porosity; Density; Specific Heat;
   Thermal Conductivity;
   Themal Expansion and Thermal coefficient

A.1 MATERIAL DATA-BASE OF DENSE BRICKS (CPS-90A-10C & CPS-82C-18M)

CPS-90A-10C

Material Identification

class	: refractory
subclass	: dense brick
material name	: CPS-90A-10C
method of manufacturing	: cold-pressing, sintering
manufacturer's name	: Norton Co.

Chemical Compositon

Al_2O_3	: 90%
Cr_2O_3	: 10%

Service Temperature : 3450°F (1899°C)

Melting Temperature : -

Table A.1: Constant Temperature, Monotonic-Displacement Uniaxial Compression Tests for Material CPS-90A-10C

Temperature	Strength (ksi)	Associated Peak Strain (in/in) x 10^{-3}	Final Fracture Stress (ksi)	Final Fracture Strain (in/in) x 10^{-3}	Average Initial Stiffness (ksi) x 10^{3}	Toughness Measure (psi)	Displacement Rate (in/sec) x 10^{-5}
RT	19.36 ± 1.31	2.53 ± 0.07	19.36 ± 1.31	2.53 ± 0.07	7.64 ± 0.31	25.11 ± 3.31	7.218
500°F (260°C)	22.28	-	22.28	-	-	-	7.218
1000°F (538°C)	16.46	3.15	16.46	3.15	5.12	25.89	7.218
1500°F (816°C)	15.35 ± 0.7	3.39 ± 0.4	15.35 ± 0.7	3.39 ± 0.4	4.48 ± 0.42	28.64 ± 1.16	7.218
2000°F (1093°C)	14.73 ± 1.30	4.11 ± 0.3	14.73 ± 1.30	4.11 ± 0.3	3.73 ± 0.16	33.01 ± 3.05	7.218
2275°F (1246°C)	12.52	6.82	< 9.2	> 10.26	2.72	> 94.69	7.218
2400°F (1316°C)	7.40	6.16	< 5.9	> 10.29	2.02	> 59.24	7.218
2000°F (1093°C)	16.36	7.06	15.82	7.82	3.45	83.74	1.444
2275°F (1246°C)	8.72	9.49	< 0.7	> 24.28	1.59	> 138.51	1.444
2275°F (1246°C)	13.15	4.77	13.15	4.7	2.89	33.38	21.65

Table A.2: Variation of Short-term Creep Strain Rate of Material CPS-90A-10C

Temperature	Constant load as % of monotonic strength at corresponding temperature level	Strain rates corresponding to $time_c$ (in/in/sec)x10^8	$Time_c$ = time after reaching constant load level (sec)
RT	62		0
			2000
			4000
1500°F (816°C)	66	4.05	0
		1.99	2000
		1.95	4000
2000°F (1093°C)	55	23.32	0
		21.56	2000
		19.06	4000
2400°F (1316°C)	57	389.59	0
	57	171.94	2000
	57	146.79	4000
	74		> 4000
2400°F (1316°C)	74	611.64	0
		363.89	2000
		FAILURE	2310

Table A.3: Constant Load Tests at Varying Temperatures of Material CPS-90A-10C

Constant load % of monotonic strength	Temperature Variation (°F)	Creep Strain Variation (in/in)
Stress = 14021 psi 62% at 73°F	Increasing from 73°F to 2400°F at 250°F/hr	0 to 0.16 in 18100 sec Attains 0.034 at 2350°F
Stress = 14021 psi 62% at 73°F	Increasing from 73°F to 2400°F at 100°F/hr	0 to 0.015 in 44200 sec Attains 0.036 at 2300°F

Table A.4: Thermophysical Properties of Material CPS-90A-10C

Density (ρ)	206 lb/ft^3				
	500°F (260°C)	1000°F (538°C)	1500°F (816°C)	2000°F (1093°C)	2400°F (1316°C)
Product of Density and Specific Heat ($\rho\ C_p$) (B/in^3/°F)	.0304	.0334	.0350	.0360	.0369
Apparent Porosity	17 %				
	500°F (260°C)	1000°F (538°C)	1500°F (816°C)	2000°F (1093°C)	2400°F (1316°C)
Thermal Conductivity (k_s) (B.in/hr/ft^2/°F)	0.302	0.248	0.184	0.133	0.115
Coefficient of Thermal Expansion (α) (in/in/°F)	5.007 x 10^{-6}				

CPS-82C-18M

Material Identification

class	: refractory
subclass	: dense brick
material name	: CPS-82C-18M
method of manufacturing	: cold-pressing, sintering
manufacturer's name	: Norton Co.

Chemical Composition

Cr_2O_3	: 82%
MgO	: 18%

Service Temperature : 3272°F (1800°C)

Melting Temperature : -

Table A.5: Constant Temperature, Monotonic-Displacement Uniaxial Compression Tests for Material CPS-82C-18M

Temperature	Strength (ksi)	Associated Peak Strain (in/in) x 10^{-3}	Final Fracture Stress (ksi)	Final Fracture Strain (in/in) x 10^{-3}	Average Initial Stiffness (ksi) x 10^{3}	Equivalent Toughness (psi)	Displacement Rate (in/sec) x 10^{-5}
RT	22.76 ± 2.96	2.38 ± 0.47	22.76 ± 2.96	2.38 ± 0.47	10.98 ± 0.35	30.18 ± 9.95	7.218
500°F (260°C)	23.67	-	23.67	-	-	-	7.218
1000°F (538°C)	21.52 ± 2.30	3.00 ± 0.07	21.52 ± 2.30	3.00 ± 0.07	7.74 ± 0.59	41.86 ± 8.73	7.218
1500°F (816°C)	19.29 ± 0.05	3.37 ± 0.44	19.29 ± 0.05	3.37 ± 0.44	6.25 ± 1.16	37.12 ± 0.06	7.218
2000°F (1093°C)	25.39 ± 0.3	4.86 ± 0.33	25.39 ± 0.3	4.86 ± 0.33	5.27 ± 0.53	63.04 ± 0.95	7.218
2200°F (1204°C)	24.46	8.34	23.58	9.28	5.03	163.27	7.218
2440°F (1338°C)	22.74	13.62	< 21.5	> 16.45	3.91	> 287.19	7.218
2440°F (1338°C)	22.85	6.56	22.85	6.56	4.67	67.54	21.65
1500°F (816°C)	18.29	3.09	17.63	3.34	8.00	41.41	1.444

Table A.6: Variation of Short-term Creep Strain Rate of Material CPS-82C-18M

Temperature	Constant load as % of monotonic strength	Strain rates corresponding to $time_c$ (in/in/sec)x10^8	$Time_c$ = time after reaching constant load level (sec)
RT	67%		0 2000 4000
1500°F (816°C)	84%	23.4 21.3 18.8	0 2000 4000
2300°F (1260°C)	55% 55% 68% 68%	368.25 153.08 522.82 FAILURE	0 1000 2000 2142

Table A.7: Thermal Cycling at Zero Load, followed by Monotonic-Displacement Uniaxial Compressive Load Tests

Condition	Average Initial Stiffness Variaton	Displacement Rate (in/sec)
One themal cycle at no load between 73°F (23°C), and 2200°F (1204°C)	Reduced by 3.5%	7.218 x 10^{-5}

Table A.8: Thermophysical Properties of Material CPS-82C-18M

Density (ρ)	235 lb/ft^3				
	500°F (260°C)	1000°F (538°C)	1500°F (816°C)	2000°F (1093°C)	2400°F (1316°C)
Product of Density and Specific Heat ($\rho\ C_p$) (B/in^3/°F)	.0809	.0829	.0842	.0853	.0862
Apparent Porosity	12 %				
	500°F (260°C)	1000°F (538°C)	1500°F (816°C)	2000°F (1093°C)	2400°F (1316°C)
Thermal Conductivity (k_s) (B.in/hr/ft^2/°F)	0.258	0.246	0.237	0.230	0.226
Coefficient of Thermal Expansion (α) (in/in/°F)x10^6	5.280	4.125	2.970	1.815	0.891

A.2 MATERIAL DATA-BASE OF DENSE CASTABLE DC-95A-5Ca

Material Identification

class	: refractory
subclass	: dense castable
material name	: DC-95A-5Ca
method of manufacturing	: mix with water
manufacturer's name	: Thermal Ceramics Co.

Chemical Composition

Al_2O_3	: 95%
CaO	: 4.6%
SiO_2	: 0.1%
Fe_2O_3	: 0.1%
Na_2O	: 0.1%
TiO_2	: trace
MgO	: trace

Service Temperature : 3400°F (1871°C)

Melting Temperature : 3500°F (1927°C)

Table A.9: Constant Temperature, Monotonic Displacement Uniaxial Compression Tests for Matrial DC-95A-5Ca

Temperature	Strength (ksi)	Associated Peak Strain (in/in) x 10^{-3}	Final Fracture Stress (ksi)	Final Fracture Strain (in/in) x 10^{-3}	Average Initial Stiffness (ksi) x 10^{3}	Toughness Measure (psi)
RT	9.837	2.385	9.837	2.385	6.421	10.98
500°F (260°C)	11.373	2.426	11.373	2.426	7.915	13.03
1000°F (538°C)	8.141	5.823	7.887	6.255	1.795	30.17
1500°F (816°C)	8.245	12.036	7.804	12.896	0.859	64.13
2000°F (1093°C)	6.601	32.896	< 6.310	> 41.306	0.559	204.37
2400°F (1316°C)	0.860	43.419	< 0.834	> 45.070	0.104	23.99

Table A.10: Variation of Short-term Creep Strain Rate of Material DC-95A-5Ca

Temperature	Constant load as % of monotonic strength	Strain rates corresponding to time$_c$ (in/in/sec)x10^8	Time$_c$ = time after reaching constant load level (sec)
1500°F (816°C)	40%	1237	0
		51.2	5000
		51.8	7000
1500°F (816°C)	50%	1526	0
		52.4	3000
		44.2	5000
		42.5	7000
1500°F (816°C)	70%	1590	0
		55.9	3000
		61.9	5000
		52.9	6000
2000°F (1093°C)	68%	4999	0
		581.6	3000
		493.3	5000
		471.8	7000
1000°F (538oC)	56.5%	150.0	0
		42.79	3000
		43.92	5000
		44.82	6000

Table A.11: Cold Modulus of Rupture and Cold Crushing Strength

Temperature	MOR (ksi)	Cold Crushing Strength (ksi)
220°F (104°C)	1.3-1.8	5.1-6.0
1500°F (816°C)	0.7-1.6	4.8-10.0
3200°F (1760°C)	1.6-1.9	4.0-4.5

Table A.12: Thermophysical Properties of Material DC-95A-5Ca

Density (ρ)	166 lb/ft^3			
Specific Heat (C_p)	-			
Apparent Porosity	-			
Thermal Conductivity (B-in/hr.ft^2.°F)	500°F (260°C)	1000°F (538°C)	1500°F (816°C)	2000°F (1093°C)
	20.20	15.68	15.16	13.10
	* Test Method: ASTM C417-84			
Permanent Linear Expansion	220°F (104°C)	1500°F (816°C)	3200°F (1760°C)	
	0.0	-0.2	-0.2	
	* Test Method: ASTM C133-74			
Coefficient of Thermal Expansion (α)	1 cycle, RT-1875°F (1024°C): 3.84 x 10^{-6}			

A.3 MATERIAL DATA-BASE OF INSULATING CASTABLE IC-55A-36S

Material Identification

class	: refractory
subclass	: insulating castable
material name	: IC-55A-36S
method of manufacturing	: mix with water
manufacturer's name	: General Refractories

Chemical Composition

Al_2O_3	: 54.5%
SiO_2	: 36.3%
CaO	: 4.8%
Fe_2O_3	: 1.1%
TiO_2	: 1.1%
Alkalies	: 0.8%
MgO	: 0.1%

Service Temperature : 2800°F (1538°C)

Melting Temperature : -

Table A.13: Constant Temperature, Monotonic Displacement Uniaxial Compression Tests for Material IC-55A-36S

Temperature	Strength (ksi)	Associated Peak Strain (in/in) x 10^{-3}	Final Fracture Stress (ksi)	Final Fracture Strain (in/in) x 10^{-3}	Average Initial Stiffness (ksi) x 10^{3}	Toughness Measure (psi)
RT	3.778	3.668	3.778	3.668	1.104	7.36
500°F (260°C)	4.279	3.835	4.279	3.835	1.325	8.60
1000°F (538°C)	3.798	5.849	3.742	5.849	0.743	11.66
1500°F (816°C)	3.096	10.041	2.585	11.899	0.373	21.08
1750°F (954°C)	1.775	34.792	< 1.567	> 44.824	0.321	61.63
2000°F (1093°C)	0.498	45	< 0.432	> 45.401	0.288	17.92

Table A.14: Variation of Short-term Creep Strain Rate of Material IC-55A-36S

Temperature	Constant load as % of monotonic strength	Strain rates corresponding to $time_c$ (in/in/sec)x10^8	$Time_c$ = time after reaching constant load level (sec)
1500°F (816°C)	46%	1973.	0
		101.9	3000
		84.44	5000
		81.57	7000
1500°F (816°C)	57%	2733.	0
		141.7	3000
		119.0	5000
		101.3	7000
1500°F (816°C)	67%	1953.	0
		228.1	2000
		164.6	3000
		FAILURE	3450
1000°F (538°C)	53%	2400.	0
		17.50	3000
		23.73	5000
		21.50	7000

Table A.15: Hot Modulus of Rupture of IC-55A-36S

Temperature	RT	500°F	1000°F	1250°F	1500°F
Hot M.O.R. (psi)	570 ± 65	320 ± 30	225 ± 55	220 ± 25	185 ± 11.5

Table A.16: Linear Shrinkage of IC-55A-36S

Temperature	200°F	1000°F	1500°F
Linear Shrinkage (%)	0.3	0.4	0.4

Table A.17: Themophysical properties of Material IC-55A-36S

Density (ρ)	85 lb/ft^3	
Specific Heat (C_p)	0.83	
Apparent Porosity	-	
Thermal Conductivity (k_s) (B.in/hr/ft^2/°F)	2.8	
Coefficient of Thermal Expansition	1st Cycle RT-1875°F	2.61 x 10^{-6}
	700-1875°F	4.04 x 10^{-6}
	2nd Cycle RT-1875°F	4.10 x 10^{-6}

A.4 MATERIAL DATA-BASE OF INSULATING FIRE-BRICK IB-39A-44S

Material Identification

class	: refractory
subclass	: insulating firebrick
material name	: IB-39A-44S
method of manufacturing	: fired
manufacturer's name	: Thermal Ceramics Co.

Chemical Composition

Al_2O_3	: 39%
SiO_2	: 44%
CaO	: 14.4%
TiO_2	: 1.1%
Fe_2O_3	: 0.6%
Na_2O	: 0.4%
MgO	: 0.1%

Service Temperature : 2300°F (1260°C)

Melting Temperature : 2750°F (1510°C)

Table A.18: Constant Temperature, Monotonic-Displacement Uniaxial Compression Tests for Material IB-39A-44S

Temperature	Strength (psi)	Average Initial Stiffness (ksi)
RT	99.357	53.396
500°F (260°C)	86.271	62.853
1000°F (538°C)	111.360	58.464
1500°F (816°C)	92.688	57.120
Average Value	97.419	57.958

Modulus of Rupture (ASTM C93-83) : 110 psi

Cold Crushing Strength (ASTM C93-83) : 110 psi

Table A.19: Thermophysical Properties of Material IB-39A-44S

Density (ρ)	31 lb/ft^3			
Specific Heat (C_p)	-			
Apparent Porosity	-			
Thermal Conductivity (k_s) (B.in/hr/ft^2/°F)	500°F	1000°F	1500°F	2000°F
	0.9	1.1	1.3	1.5
Coefficient of Reverse Thermal Expansion	3.0x10^{-6} in/in/°F			
Permanent Linear Change	Fired at 2250°F: 0			
	* Test Method: ASTM C210-68			

DISTRIBUTION

A.P. GREEN REFRACTORIES COMPANY
Green Blvd.
Mexico, MO 65265
J. L. Hill

AIR PRODUCTS AND CHEMICALS
P.O. Box 538
Allentown, PA 18105
S. W. Dean
S. C. Weiner

ARGONNE NATIONAL LABORATORY
9700 S. Cass Avenue
Argonne, IL 60439
W. A. Ellingson
K. Natesan
J. P. Singh

AVCO RESEARCH LABORATORY
2385 Revere Beach Parkway
Everett, MA 02149
R. J. Pollina

BABCOCK & WILCOX
1562 Beeson St.
Alliance, OH 44601
T. I. Johnson

BABCOCK & WILCOX
Domestic Fossil Operations
20 South Van Buren Avenue
Barberton, OH 44023
M. Gold

BABCOCK & WILCOX
Lynchburg Research Center
P.O. Box 11165
Lynchburg, VA 24506
H. Moeller

BATTELLE-COLUMBUS LABORATORIES
505 King Avenue
Columbus, OH 43201
V. K. Sethi

BRITISH COAL CORPORATION
Coal Research Establishment
Stoke Orchard, Cheltenham
Glochester, England GL52 4RZ
M. Arnold
C. Bower
A. Twigg

BRITISH GAS CORPORATION
Westfield Development Centre
Cardenden, Fife
Scotland KY5OHP
J. E. Scott

BROOKHAVEN NATIONAL LABORATORY
Department of Applied Science
Upton, Long Island, NY 11973
T. E. O'Hare

COMBUSTION ENGINEERING
911 W. Main Street
Chattanooga, TN 37402
D. A. Canonico

CONSOLIDATION COAL COMPANY
4000 Brownsville Road
Library, PA 15129
S. Harding

DOW CORNING CORPORATION
3901 S. Saginaw Road
Midland, MI 48686-0995
W. H. Atwell

ELECTRIC POWER RESEARCH INSTITUTE
P.O. Box 10412
3412 Hillview Avenue
Palo Alto, CA 94303
S. B. Alpert
R. L. S. Chang
W. T. Bakker
J. T. Stringer

EUROPEAN COMMUNITIES JOINT RESEARCH CENTRE
Petten Establishment
P.O. Box 2
1755 ZG Petten
The Netherlands
M. Van de Voorde

FOSTER WHEELER DEVELOPMENT CORPORATION
Materials Technology Department
John Blizard Research Center
12 Peach Tree Hill Road
Livingston, NJ 07039
J. L. Blough

IDAHO NATIONAL ENGINEERING LABORATORY
P.O.Box 1625
Idaho Falls, ID 83415
D. W. Keefer

LANXIDE CORPORATION
1 Tralee Industrial Park
Newark, DE 19711
E. M. Anderson

LAVA CRUCIBLE-REFRACTORIES CO.
P.O. Box 278
Zelienople, PA 16063
T. Mulholland

LAWRENCE LIVERMORE LABORATORY
P.O. Box 808, L-325
Livermore, CA 94550
W. A. Steele

LOS ALAMOS NATIONAL LABORATORY
P.O. Box 1663
Los Alamos, NM 87545
P. D. Shalek
S. R. Skaggs

MOBIL RESEARCH & DEVELOPMENT CORPORATION
P. O. Box 1026
Princeton, NJ 08540
R. C. Searles

NATIONAL INSTITUTE OF STANDARDS AND TECHNOLOGY
Materials Building
Gaithersburg, MD 20899
S. J. Dapkunas

NEW ENERGY DEVELOPMENT ORGANIZATION
Sunshine 60 Bldg.
P.O. Box 1151,
1-1 Higashi-Ikebukuro 3-chrome
Toshima-Ku, Tokyo, 170
Japan
S. Ueda

OAK RIDGE NATIONAL LABORATORY
P.O. Box 2008
Oak Ridge, TN 37831
P. T. Carlson
R. R. Judkins
J. L. Langford (8 copies)

RESEARCH TRIANGLE INSTITUTE
P.O. Box 12194
Research Triangle Park, NC 27709
T. W. Sigmon

RISOE NATIONAL LABORATORY
P.O. Box 49
DK-4000, Roskilde
Denmark
Aksel Olsen

SHELL DEVELOPMENT COMPANY
P. O. Box 1380
Houston, TX 77251-1380
L. W. R. Dicks

TENNESSEE VALLEY AUTHORITY
1101 Market Street
MR 3N57A
Chattanooga, TN 37402
R. Q. Vincent

UNIVERSITY OF TENNESSEE AT KNOXVILLE
Materials Science and Engineering Department
Knoxville, TN 37996
C. D. Lundin

UNIVERSITY OF TENNESSEE SPACE INSTITUTE
Tullahoma, TN 37388
J. W. Muehlhauser

VIRGINIA POLYTECHNIC INSTITUTE & STATE UNIVERSITY
Department of Materials Engineering
Blackburg, VA 24061
J. J. Brown, Jr.

WESTINGHOUSE HANFORD COMPANY
P.O. Box 1970
W/A-65
Richland, WA 99352
R. N. Johnson

DOE
OAK RIDGE OPERATIONS OFFICE
P. O. Box E
Oak Ridge, TN 37831
Assistant Manager for Energy Research and Development

DOE
OAK RIDGE OPERATIONS OFFICE
Oak Ridge National Laboratory
P. O. Box 2008
Building 4500N, MS 6269
Oak Ridge, TN 37831
E. E. Hoffman

DOE
OFFICE OF BASIC ENERGY SCIENCES
Materials Sciences Division
ER-131, GTN
Washington, DC 20545
J. B. Darby

DOE
OFFICE OF CONSERVATION AND
RENEWABLE ENERGY
Energy Conversion and Utilization Technologies
Division
CE-12, Forrestal Building
Washington, DC 20545
J. J. Eberhardt

DOE
OFFICE OF FOSSIL ENERGY
Washington, DC 20545
D. J. Beecy (FE-14) GTN
J. P. Carr (FE-14) GTN
F. M. Glaser (FE-14) GTN

DOE
MORGANTOWN ENERGY TECHNOLOGY
CENTER
P.O. Box 880
Morgantown, WV 26505
R. A. Bajura
R. C. Bedick
F. W. Crouse, Jr.
N. T. Holcombe
W. J. Huber
M. J. Mayfield
J. E. Notestein
J. S. Wilson

DOE
PITTSBURGH ENERGY TECHNOLOGY
CENTER
P.O. Box 10940
Pittsburgh, PA 15236
S. Akhtar
T. C. Rupel
R. Santore
T. M. Torkos